Alma Mater Studiorum - Università di Bologna

DOTTORATO DI RICERCA IN

CHIMICA

Ciclo 35

Settore Concorsuale: 03/C2 - CHIMICA INDUSTRIALE

Settore Scientifico Disciplinare: CHIM/04 - CHIMICA INDUSTRIALE

DEVELOPMENT AND CHARACTERIZATION OF INNOVATIVE GRAPHENE-BASED COMPOSITES

Presentata da: Filippo Valorosi

Coordinatore Dottorato

Luca Prodi

Supervisore

Loris Giorgini

Co-supervisori

Vincenzo Palermo

Emanuele Treossi

Esame finale anno 2023

Summary

Abstract

Over the last decade, graphene and related materials (GRM) have drawn significant interest and resources for their development into the next generation of composite materials. This is because these nanoparticles have the ability to operate as reinforcing additives capable of imparting considerable mechanical property increases while also embedding multi-functional advantages on the host matrix. Because graphene and 2D materials are still in their early stages, the relative maturity of different types of composite systems varies. As a result, certain nanocomposite systems are currently commercially accessible, while others are not yet sufficiently developed to enter the market. A substantial emphasis has been placed on developing thermoplastic and thermosetting materials that combine a variety of mechanical and functional qualities. These include higher strength and stiffness, increased thermal and electrical conductivity, improved barrier properties, fire retardancy, and others, with the ultimate goal of providing multifunctionality to already employed composites.

The work presented in this thesis investigates the use and benefits that GRM could bring to composites for a variety of applications, with the goal of realizing multifunctional components with improved properties that leads to lightweight and, as a result, energy and cost savings and pollution reduction in the environment. In particular, we worked on the following topics:

- Benchmarking of commercial GRM-based master batches;
- GRM-coatings for water uptake reduction;
- GRM as thermo-electrical anti-icing /de-icing system;
- GRM for Out of Oven curing of composites.

Introduction

Graphene is a breakthrough recently discovered material at the nanoscale with very good properties, which is going through a very good momentum in terms of evaluation and exploiting its potential, in fact it is being considered for a wide number of applications.

Graphene, one-atom-thick planar sheet of carbon atoms densely packed in a honeycomb crystal lattice, has attracted great interest due to its exceptional electronic and optoelectronic properties. It has a large theoretical specific surface area, high intrinsic electron mobility (200 000 $cm^2v^{-1}s^{-1}$), high Young's modulus (≈1.0 TPa), thermal conductivity (≈5000 W/(m*K)), optical transmittance (≈97.7%), good electrical conductivity a low density. These properties have opened up new opportunities for the future applications. Graphene and related materials (GRM) are nowadays found everywhere, from fundamental research to market products.

This work concerns the production and characterization of multifunctional GRM-based composite materials: Chapter 1 briefly introduces graphene and graphene-related materials, focusing on the main production methods employed at industrial level and their application in different sectors. Chapter 2 describes in detail the use of GRM in the composite world underlying the potential applications in aerospace and automotive industry, pointing out the main challenges. In this chapter we reported the full text of the article published on Composites Science and Technology: Valorosi et al, “Graphene and related materials in hierarchical fiber composites: Production techniques and key industrial benefits”, Composites Science and Technology, Volume 185, 2020, 107848.

The benchmarking of commercial GRM-based master batch produced by industrial companies is presented in the Chapter 3, evaluating the advantages that GRM could bring from a morphological, thermal and electrical point of view.

Chapter 4 and 5 are dedicated to the employment of GRM for two specific aerospace application, for the reduction of the water uptake and as anti/de-icing system in aircraft structures, respectively.

The last Chapter (6) investigates the potential use of GRM as a heating element incorporated in a CFRP mold for the out-of-oven (OoO): we performed a comparison of the physical and thermal characteristics of OoO cured Vs Oven-cured composites.

1. Graphene and Related Materials (GRM)

In this Chapter, the basic information on graphene and its related materials is given; moreover, the structure, the intrinsic properties of pristine graphene, the production methods and applications are discussed.

1.1 Graphene

Carbon is the foundation of organic chemistry, and hence of life on Earth: this unique importance is due to carbon's chemical diversity, which results in a wide range of physical and chemical characteristics.

Atomic carbon occurs in three bonding states with distinct geometry, form, and size, corresponding to atomic orbital hybridization states sp^3, sp^2, and sp. These various linkages result in a wide range of carbon allotrope structures, including diamond, graphite, carbyne, fullerenes, nanotubes, polyaromatic hydrocarbons, graphene, and amorphous carbon, to name a few.

Graphene is the first isolated two-dimensional (2-D) material; it has a thickness of one atom and may be considered the unit cell of other carbon materials such as graphite (3-D), carbon nanotubes (1-D), and buckyballs or fullerenes (0-D) due to its sp^2-carbon atoms grouped in a hexagonal pattern.

It has the highest modulus of elasticity ever measured (1 TPa) and a breaking strength of approximately 120 GPa (200 times higher than steel), combined with high carrier mobility at room temperature (10.000 $cm^2\ V^{-1}\ s^{-1}$), high thermal conductivity (up to 5000 $W\ m^{-1}\ K^{-1}$), high specific surface area (2630 $m^2 g^{-1}$) and optical transparency (97.7%) [1].

	Graphene	Carbon nanotube	Fullerene	Graphite
Dimensions	2	1	0	3
Hybridization	sp^2	Mostly sp^2	Mostly sp^2	sp^2
Hardness	Highest (for single layer)	High	High	High
Tenacity	Flexible, elastic	Flexible, elastic	Elastic	Flexible, non-elastic
Experimental SSA ($m^2\ g^{-1}$)	~1,500	~1,300	80–90	~10–20
Electrical conductivity ($S\ cm^{-1}$)	~2,000	Structure-dependent	10^{-10}	Anisotropic: $2–3 \times 10^4$*, 6†
Thermal conductivity ($W\ m^{-1}\ K^{-1}$)	4,840–5,300	3,500	0.4	Anisotropic: 1,500–2,000*, 5–10†

*a direction, †c direction.

Table 1.1: Graphene properties compared with other carbonaceous materials [2].

As previously stated, there are numerous types of carbon nanofiller known as GRM. Graphene is the fundamental structure of all graphenic nanomaterials. This nanomaterial is characterized as a one-atom-thick planar sheet made of carbon atoms with sp^2 hybridization. These carbon atoms are arranged in a honeycomb lattice, as seen in figure 1.1. Two single and one double covalent bond connect the carbon atoms to the three neighboring atoms.

The graphitic structure is made up of multi-layered graphene sheets, and GRM is thought to exist in a variety of configurations, including graphene monolayers, graphene nanosheets, and graphene nanoplatelets (GNPs) [3].

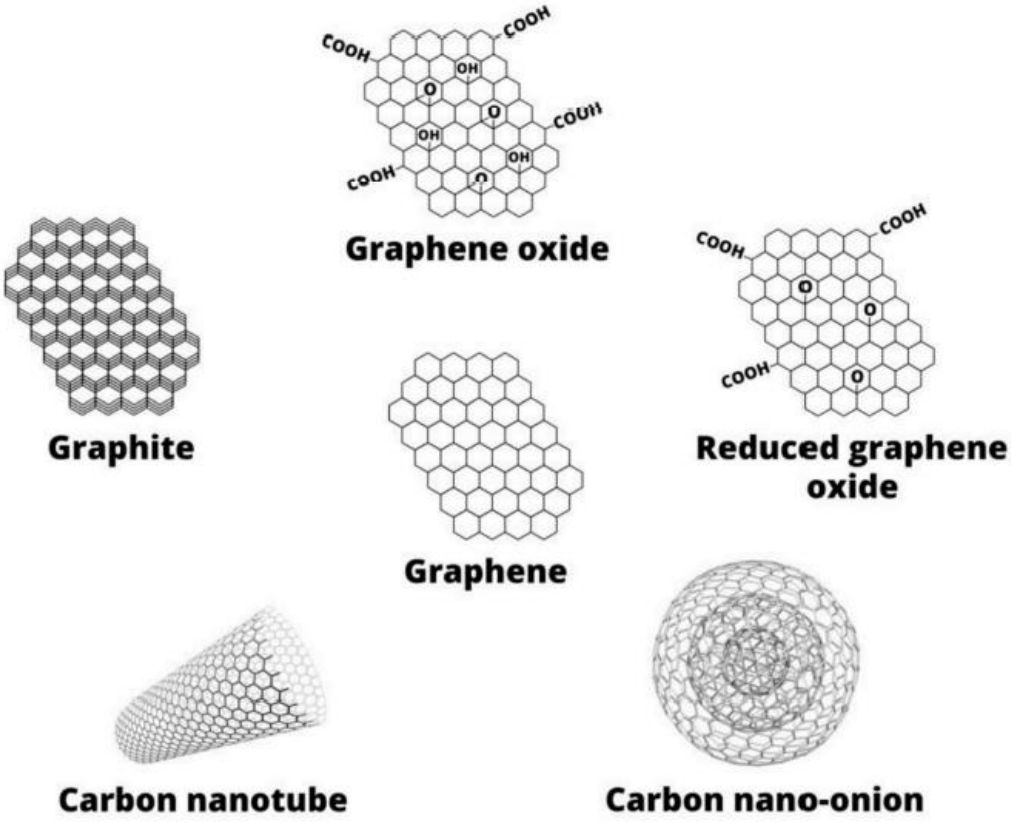

Figure 1.1: Mother of all graphitic forms: Graphene is a 2D building material for carbon materials of all other dimensionalities. Structures of the most common graphenic nanofillers [3].

1.2 Graphene main production methods

Graphene should be produced at a competitive cost to that of current materials in order to be successfully applied in industry. Developing synthetic methods, which are cost-effective, efficient and flexible at the same time, with good product yield and performance, is a great challenge. According to ref. [1], [4]–[6], the synthesis of graphene can be performed by two main approaches: top-down and bottom-up methods as illustrated in figure 1.2.

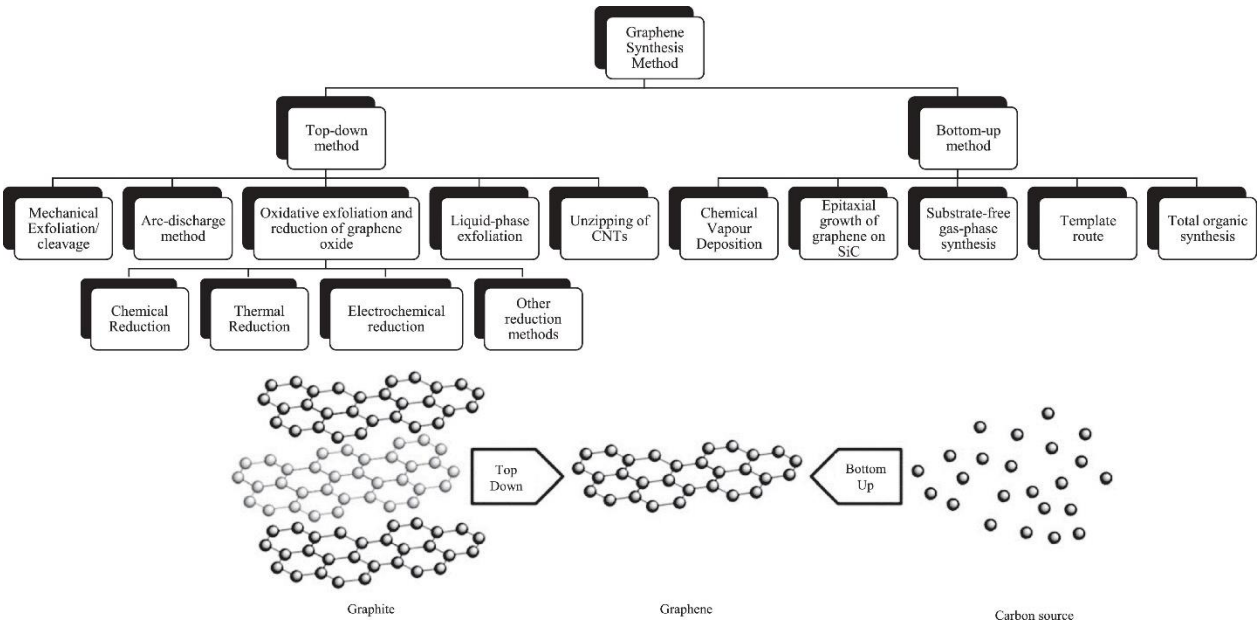

Figure 1.2: Synthesis method of graphene [5].

The top-down methods such as mechanical exfoliation, arc discharge, oxidative exfoliation-reduction, liquid-phase exfoliation (LPE) and unzipping of CNT usually separate the layers of graphite into single-, bi- and few-layer graphene. These methods dismantle larger precursors (such as graphite or other carbon-based materials) to form nano-sized graphene.

Generally, top-down approaches are highly scalable and can obtain products of high quality but there are still technical issues in producing products with consistent properties on large scale. The drawback of these methods is the low yield and the strongly dependence on the quality of the graphite precursor.

The bottom-up methods synthesize graphene and its derivatives using other carbon sources apart from graphite, typically carbon-based gas molecules. The bottom-up methods include chemical vapour deposition (CVD), epitaxial growth, substrate-free gas-phase synthesis (SFGP), template route and total organic synthesis. Although the bottom-up methods manufacture graphene products

with an almost defect-free and large surface area, they also have high production costs and complex functional configuration [5], [6].

The Institution of Chemical Engineers Sustainable Development Progress Metrics (IChemE SDPM) evaluated the different graphene synthesis methods based on their potential industrial implementation [5]. In order to assess the most promising synthesis method for commercialization, a preference score was assigned to each key indicator (based on the IChemE) for each synthesis method, having different characteristics in terms of cost (precursor cost and operating cost), scalability potential, product quality, process condition (process safety and complexity), yield and environment (use of hazardous chemicals) indicators.

Based on the overall preference score, oxidative exfoliation-reduction, CVD and LPE showed high scaling-up potential due to their relatively high graphene yield and product quality, as evidenced by the widespread use of graphene produced by these methods in different research fields such as wastewater treatment, polymer reinforcement, energy storage and biosensors.

In the next sections these methods will be discussed in details.

1.2.1 Oxidative exfoliation-reduction

The majority of GO are produced by oxidative exfoliation of graphite followed by reduction to graphene sheets or rGO. There are four major pathways for GO synthesis: Brodie, Staudenmaier, Hofmann, and Hummers [5], [7]. To keep manufacturing costs low, a relatively moderate synthesis temperature is preferred. These processes, however, produce hazardous gases such as nitrogen dioxide (NO_2) and dinitrogen tetroxide (N_2O_4).

As a result, during process scaling-up, process safety and environmental costs must be addressed. The Hummers technique is currently commonly utilized for GO synthesis since it is a very quick and safe procedure. Furthermore, because potassium permanganate ($KMnO_4$) and sodium nitrate ($NaNO_3$) are used instead of potassium perchlorate ($KClO_4$) and nitric acid, it does not produce explosive gases such as chlorine dioxide (ClO_2) and acidic fog (HNO_3).

The Hummers process has been modified throughout the years to produce GO in a more environmentally friendly manner. For example, the enhanced Hummers technique eliminates the use of $NaNO_3$ in the synthesis of GO, lowering manufacturing costs and environmental protection costs. Because of the inclusion of graphite intercalation chemicals, graphite oxidation increases the spacing between graphite layers from 0.335 to 0.625 nm or larger.

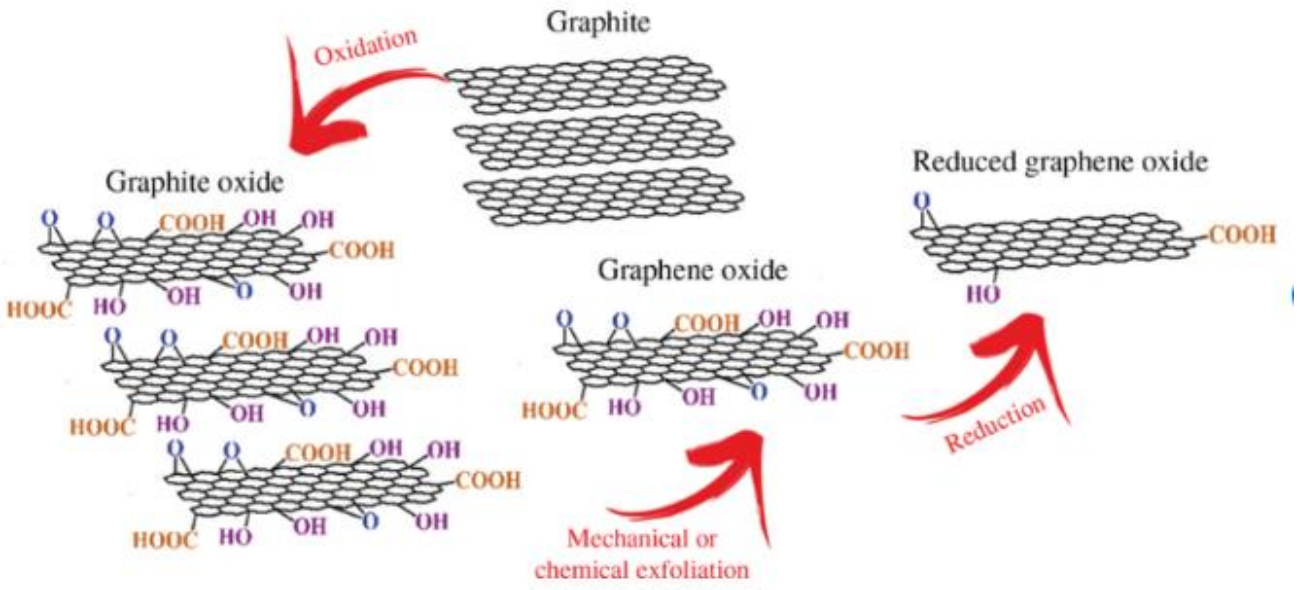

Figure 1.3: Schematic representation of the reduced graphene oxide production by the mechanical or chemical exfoliation method [8].

As a result of the interlayer van der Waals force being decreased during carbon sheet displacement, further exfoliation by sonication in appropriate solvents can yield well distributed single-, bi-, and few-layer GO. Because of the presence of oxygenous functional groups, GO is very hydrophilic and may be distributed in a variety of solutions including water, ethylene glycol, N-methyl-2-pyrrolidone (NMP), and tetrahydrofuran (THF). Because GO has a damaged sp^2 bonding, reduction procedures are frequently used to restore its honeycomb lattice.

The primary techniques for GO reduction include chemical, thermal, and electrochemical procedures. During reduction, most of the oxygenous functional groups in GO, such as carbonyl, hydroxyl, and carboxylic, are removed. However, total GO reduction to generate pure graphene is still not possible. The resultant rGO is typically quite similar to pure graphene, although with certain defects and size changes. Reductant type and process factors such as reduction duration, temperature, pressure, and voltage influence rGO quality.

Furthermore, the C/O ratio indicates the reducing agent's potential for GO reduction. Boronhydrides, aluminum hydride, hydrohalic acid, sulfur-based reagents, nitrogen-based reagents, oxygen-based reagents, metal-acid, metal-alkaline, amino acid, plant extracts, microbes, proteins, and hormones were all employed as reduction agents.

Although the chemical reduction produced high C/O using zinc/hydrochloric acid, benzyl alcohol, thionyl chloride, caffeic acid, sodium borohydride, and baker's yeast, safety concerns, additional chemical costs, environmental pollution, and a lengthy synthesis time must be considered during process scale-up. As a result, researchers are actively looking at other techniques of reducing GO, such as thermal reduction and hydrothermal reduction.

The biggest concerns with thermal reduction are high temperatures, which result in high operating costs, and the emission of CO_2, a well-known greenhouse gas. Hydrothermal reduction, on the other hand, has been proven to decrease GO to rGO at lower temperatures and hence requires less energy. Electrochemical reduction of GO has gained popularity because to its speed, cost efficiency, environmental friendliness, and ease of usage. More importantly, it uses less harmful reductants than chemical reduction. Microwave, photothermal, photocatalytic, sono-chemical, laser, and plasma treatment are some of the additional GO reduction techniques mentioned in the literature.

The synthesis of GO through oxidative exfoliation of graphite and subsequent reduction to rGO has a cheap production cost and a high yield. However, the rGO has a low surface area, weak electrical conductivity, limited solubility, and irreversible sheet restacking due to van der Waals attraction. There are further uncertainties in the synthesis process, such as chemical composition change from the oxidation and reduction processes, batch-to-batch repeatability, and the formation of permanent defects during the oxidation phase. Nonetheless, the benefits of great scalability and cheap operating costs exceed the drawbacks of this technology [5], [9], [10].

1.2.2 Chemical Vapor Deposition (CVD)

CVD uses hydrocarbon gases (such as CH_4, acetylene (C_2H_2), ethylene (C_2H_4), and hexane (C_6H_{14}) and other biomass materials to build graphene sheets on metallic catalysts (such as Cu and Ni films) at high temperatures (650-1000 °C).

When the carbon precursor comes into contact with the heated surface of a metal catalyst, it dissociates into free carbon and hydrogen atoms. When the carbon solubility limit is reached, the carbon atom diffuses across the surface and bulk of the metal catalyst, forming a graphene sheet on the metal surface.

CVD is capable of producing high-quality graphene with very few defects, a highly linked structure, and a huge surface area. However, it has drawbacks such as high manufacturing costs,

poor throughput, further purification to eliminate leftover catalyst, and graphene transfer to other substrates.

To overcome these challenges, several researchers have worked on refining the synthesis conditions at lower temperatures and ambient pressures while maintaining graphene quality. CVD alone is currently considered immature for commercialization due to the need for significant improvements in the synthesis process in terms of manufacturing cost and yield.

CVD should be developed further in conjunction with other technologies such as thermal-based and plasma-based CVD in order to be commercially viable [5], [9], [10].

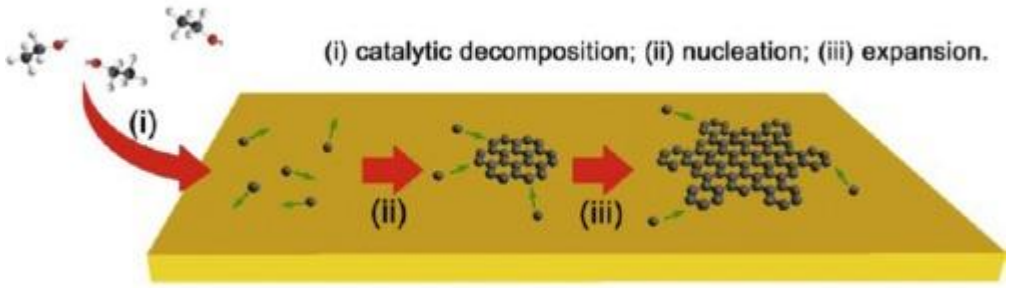

Figure 1.4: Schematics of CVD graphene grown on Cu foil [11].

1.2.3 Liquid Phase Exfoliation (LPE)

LPE is one of the most extensively used graphene manufacturing techniques and consists of three major steps: (i) disperse graphite in a suitable solvent, (ii) exfoliate, and (iii) purify the end products. Because LPE exfoliates graphite by overcoming van der Waals force, the liquid properties such as surface energy, surface tension, Hildebrand solubility, and Hansen solubility factors must be considered while choosing a solvent. For graphite exfoliation, aqueous or non-aqueous solvents with surface energies of 70-80 mJ/m^2 or surface tensions of 40-50 mJ/m^2 are optimal. This is because they have similar surface energies to graphite, resulting in a lower mixing enthalpy and hence an easier exfoliation process.

Aside from solvent selection, sonication modulation is critical for providing suitable cavitation effects for graphite exfoliation to form single-layer graphene. Ultrasound at low frequencies (20-100 kHz) can generate physical changes in graphite solids such as fragmentation, shock wave, well-mixing, and mass movement.

Despite the fact that LPE is a promising approach for graphene production, various investigations have shown that sonication can cause flaws on its edges and basal planes. Defects in graphene products might be prevented by optimizing the effects of sonication duration, temperature, and intensity, which is an area of study that is currently underfunded. These details are critical for the design of a sonication reactor. While LPE has several drawbacks, it is a very flexible technique for product synthesis and functionalization that yields high-quality graphene [5], [9], [10].

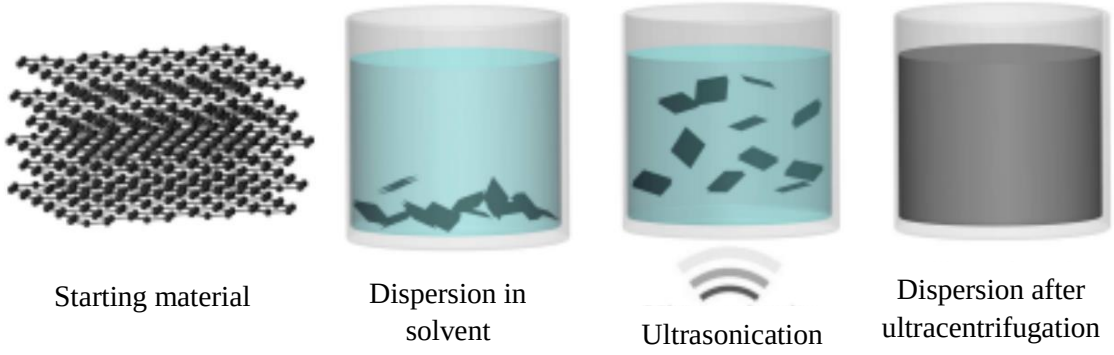

Figure 1.5: Liquid phase exfoliation of 2D materials. (a) Starting material (e.g., graphite), (b) chemical wet dispersion, (c) ultrasonication and (d) final dispersion after the ultracentrifugation process [12].

1.3 Classification of GRM

The name "graphene" is often used generically by scientists to characterize several graphene-based materials that they have manufactured and researched. The nomenclature contradiction stems not only from the usage of graphene for isolated single atom-thick sheets, but also from its reference to comparable two-dimensional sheet-like and flake carbon structures.

As a result, a clear, consistent, and widely acknowledged method for characterizing and identifying graphene derivatives remains to be created. In past years many works have been done to solve these issues [13]–[16]. Here we report the definitions of 2D materials and the most common GRM according to [16] published in 2017:

- **2D material**: material, consisting of one or several layers with the atoms in each layer strongly bonded to neighbouring atoms in the same layer, which has one dimension, its thickness, in the nanoscale or smaller and the other two dimensions generally at larger scales. The number of layers when a two-dimensional material becomes a bulk material

varies depending on both the material being measured and its properties. In the case of graphene layers, it is a two-dimensional material up to 10 layers thick for electrical measurements, beyond which the electrical properties of the material are not distinct from those for the bulk (also known as graphite);

- **Graphene graphene layer/single-layer graphene/monolayer graphene**: single layer of carbon atoms with each atom bound to three neighbours in a honeycomb structure. As graphene is a single layer, it is also sometimes called monolayer graphene or single- layer graphene and abbreviated as **1LG** to distinguish it from bilayer graphene (2LG) and few-layered graphene (FLG);
- **Bilayer graphene (2LG)**: two-dimensional material consisting of two well-defined stacked graphene layers;
- **Trilayer graphene (3LG)**: two-dimensional material consisting of three well-defined stacked graphene layers;
- **Few-layer graphene (FLG)**: two-dimensional material consisting of three to ten well-defined stacked graphene layers;
- **Graphene nanoplate/graphene nanoplatelet (GNP)**: nanoplate consisting of graphene layers. GNPs typically have thickness of between 1 nm to 3 nm and lateral dimensions ranging from approximately 100 nm to 100 μm;
- **Graphene oxide (GO)**: chemically modified graphene prepared by oxidation and exfoliation of graphite, causing extensive oxidative modification of the basal plane. Graphene oxide is a single-layer material with a high oxygen content, typically characterized by C/O atomic ratios of approximately 2,0 depending on the method of synthesis;
- **Reduced graphene oxide (rGO)**: reduced oxygen content form of graphene oxide. This can be produced by chemical, thermal, microwave, photo-chemical, photo-thermal or microbial/bacterial methods or by exfoliating reduced graphite oxide. If graphene oxide was fully reduced, then graphene would be the product. However, in practice, some oxygen containing functional groups will remain and not all sp^3 bonds will return back to sp^2 configuration. Different reducing agents will lead to different carbon to oxygen ratios and different chemical compositions in reduced graphene oxide. It can take the form of several morphological variations such as platelets and worm-like structures.

Moreover, according to a simple model [14] (figure 1.6) the different graphene materials can be classified using the number of graphene layers, the average lateral size, and the carbon-to-oxygen (C/O) atomic ratio as the three fundamental properties that cover the largest set of current graphene materials. In this way, it is possible to recognize several graphene based materials as single-layer graphene but also few-layer graphene (i.e.,2–10 layers), graphene oxide (GO, typically attainable as a single layer), reduced graphene oxide (rGO, typically attainable as a single layer), graphene nanosheets, ultrafine graphite (i.e., thicker than graphene sheets but below 100 nm in thickness), graphene ribbons, and graphene dots.

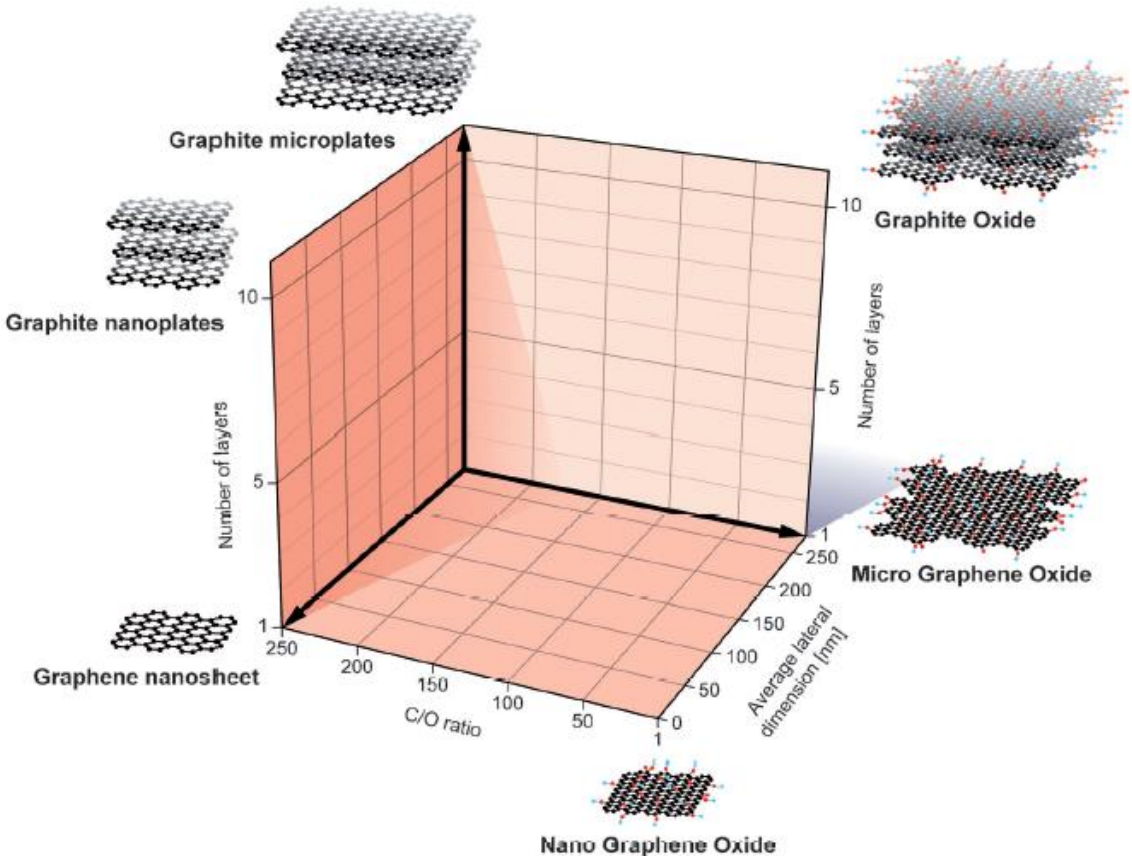

Figure 1.6: Classification grid for the categorization of various graphene-based materials (GBM) according to three fundamental properties: number of graphene layers, average lateral dimensions, and carbon/oxygen atomic ratio [14].

A graphical representation for different GRM products is proposed by [15], where in the 2D plot, each X or Y semi-axis corresponds to a GRM property (figure 1.7).

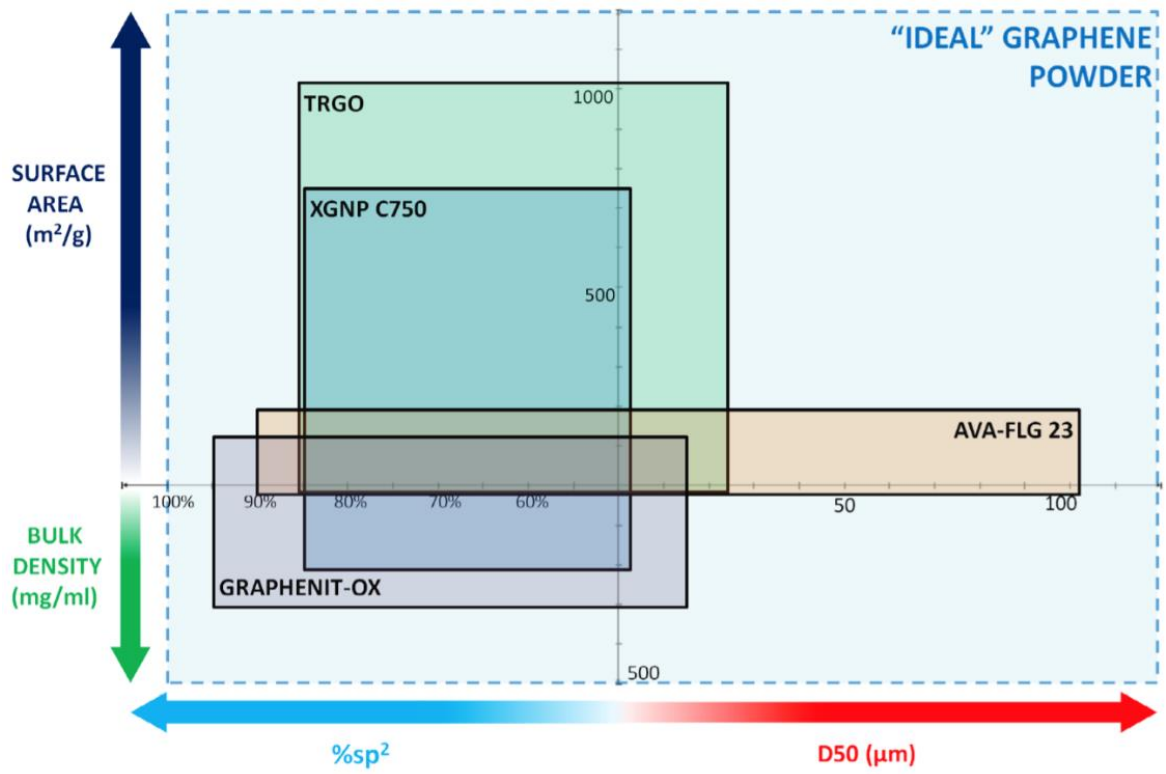

Figure 1.7: Composite graph using four axes to represent the different key properties of GRM. The positive and negative branches of X and Y axis indicate lateral size, % of sp2, specific surface area and density. Selected GRM products, with a high value in one or more of the selected properties, are shown for clarity. A large light-blue rectangle indicates the properties of an 'ideal' graphene [15].

Each rectangle is specific to a GRM, and crosses the axes in 4 points corresponding to the specific values of the material properties. The rectangles give the opportunity to better visualize the properties of each material and allow a rapid comparison between different products. For example, it is possible to see the differences between a material highly exfoliated like TRGO—with high surface area, low bulk density and a high level of defects- and AVAFLG 23, a material that is less exfoliated (low surface area), but with higher lateral size and bulk density and a much lower number of defects compared to TRGO. A material approaching the 'perfect' graphene mentioned above would be represented as the dashed light blue rectangle in figure 1.7, with a large overall area and high values along all four semi-axes [15].

It's important to underline that graphene should not be considered as one single material but as a family of materials where each constituent has its own target application.

1.4 Application of GRM

Because of their exceptional structural and functional features, GRM are currently being employed in a wide range of applications, from agriculture to aerospace, as a consequence of years of intense research.

Solar cells, super capacitors, Li-ion batteries, microbial fuel cells, sensors, and nanomembranes for wastewater treatment are just a few of the astonishing applications for graphene-based materials. Graphene nanomaterials are also being employed in a variety of key medical applications, including drug delivery systems, gene therapy, DNA sequencing, tissue engineering and artificial bones, bio-imaging, and possible cancer therapeutics.

Furthermore, due to their high strength-to-weight ratio qualities, graphene-incorporated fiber-reinforced composites are gaining prominence in the automotive, marine, and aerospace industries [1], [6], [17].

Figure 1.8: Overview of applications of Graphene in different sectors ranging from conductive ink to chemical sensors, light emitting devices, composites, energy, touch panels and high frequency electronics [1].

1.4.1 Energy storage and conversion

Graphene-based materials are employed in the production of renewable energy, which is one of the world's most pressing challenges today. Graphene is used to make many sorts of solar cells that convert solar energy into different forms of energy. Graphene-based solar cells, for example, are employed for solar-thermal or solar-electrical conversion, as well as photo catalysis applications.

Among graphene's remarkable properties, which include its 2D structure, excellent electrical and thermal conductivity, high transparency, flexibility, exceptional mechanical strength, and very large specific surface area, the improved electrical conductivity without affecting optical transmittance is the most important reason for its success in solar cells. Furthermore, graphene's hydrophobic characteristic is anticipated to prevent undesired reactions from inhibiting breakdown. Graphene/polymer composites are increasingly being employed as electrodes in dye-sensitised solar cells (DSSC) to convert solar energy into electrical energy. Because of their bigger surface area, high porosity, superior conductivity, and relatively excellent chemical stability, this type of electrode has significantly enhanced energy conversion efficiency.

Graphene-based conducting polymer composites are utilized in super capacitors or ultra-capacitors and have been shown to outperform traditional batteries. By filtering, an ultrathin (100 nm) graphene sheet may be created, which can then be converted onto a flexible substrate such as polyethylene terephthalate (PET). As a result, graphene is a promising contender for usage in the electrode of super capacitors designed for flexible and wearable energy storage device. In addition, graphene can compensate for the limits of insulating polymers when combined with a polymer binder. However, it improves the mechanical characteristics of the polymer framework, resulting in a remarkable improvement in cycle ability and specific capacitance of conductive polymers. Polyaniline (PANI) is one of the most often employed conducting polymers in the fabrication of high-performance capacitors using graphene oxide or reduced graphene oxide.

Another widely utilized storage method is the lithium-ion battery (LiB). The anode and cathode materials, on the other hand, have a short life due to the continual volume expansion and contraction generated by the lithiation/de-lithiation process. Furthermore, due to the poor electron conductivity qualities of the present electrodes, Li-ion batteries fail to operate as planned. In Li-batteries, the problem was overcome by employing graphene-based anodes and cathodes. Because graphene-based electrodes have outstanding electrical conductivity and relatively high porosity architectures, Li-ion batteries performed exceptionally well [1], [6], [17].

1.4.2 Wearable Technology

Graphene-based materials are gaining popularity in the realm of wearable devices. The goal is to build flexible fiber-based super capacitors with excellent electrochemical characteristics. Super capacitors, for example, are a prominent example of wearable storage and conversion devices and are widely employed in hybrid electric cars, energy management, backup memory devices, and industrial power. Different ways have been tried to develop super capacitors for energy storage and wearable technology using graphene-based fibers.

According to [17], an asymmetric super capacitor with great flexibility, outstanding cycling ability, and mechanical stability stands out among them. Furthermore, because of its greater volumetric energy density, it could be reversibly cycled at a high voltage of 1.6 V thanks to the employment of transition metal oxide nanorods and reduced graphene oxide hybrid fibers.

Significant electrochemical capabilities were also identified in an all-solid-state symmetric super capacitor due to the increased electron transportation of the conductive graphene network, even under bending and stretching circumstances, indicating the material's feasibility for usage in wearable technology.

Graphene is a natural candidate for flexible electrical devices since it is a thin flexible ultra-strong sheet and a very excellent conductor. It offers various distinct electrical, mechanical, and optical features that may enable innovative and unexpected applications as well as improved performance. Because of its inherent flexibility, graphene is perfect for sensors and gadgets that will stick to and interact with the human body, allowing revolutionary consumer and medical applications that are not now possible [1], [17].

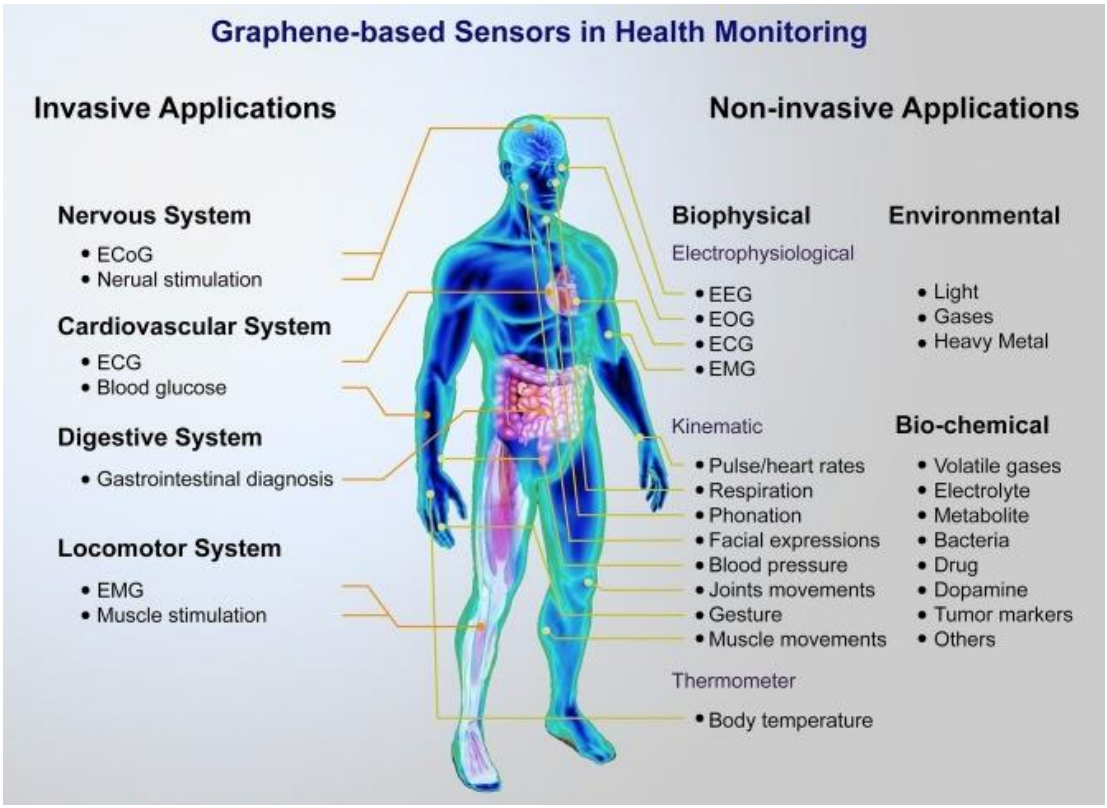

Figure 1.9: Brief of a graphene-based sensor platform for health monitoring [17].

1.4.3 Agriculture and Wastewater Management

Water pollution with numerous harmful compounds originating from both organic and inorganic sources, such as industry, agriculture, and domestic concerns, is a concerning issue in terms of environmental sustainability. Aquatic creatures are on the edge of extinction as a result of widespread water poisoning.

Despite the fact that water covers more than 70% of the Earth's surface, finding clean, useable water is getting increasingly challenging. As a result, a variety of measures are being employed to reduce water contamination. Graphene-based nano porous membranes are now employed as an effective technology to remove many types of contaminants [17], [18]. The nanomembranes serve as an effective barrier for both liquid and gaseous molecules.

1.4.4 Biomedical

The extraordinary qualities of graphene have provided the groundwork for a new horizon of possibilities for a variety of applications, one of which is the use of graphene/polymer nanocomposites in the healthcare industry. Much study has been done on graphene's adaptability since the initial report on its usage in the medical area in 2008. As shown in figure 1.10, the large surface area, strong affinity for hydrophobic drugs, stable chemical properties of graphene, and enhanced mechanical properties of graphene-based polymer composites made it suitable for a wide range of biomedical applications such as drug delivery, DNA sequencing, gene therapy, tissue engineering, cancer therapies, and artificial muscles. Moreover, graphene is widely employed in bioimaging materials due to its atomic thickness and extraordinarily high conductivity capabilities [1], [17], [19]. Figure 1.10 summarizes the possible biological uses of graphene/polymer composites. Although graphene and graphene-based composites have gained remarkable interest in the medical community, additional study on the long-term implications of graphene incorporation in the human body is required.

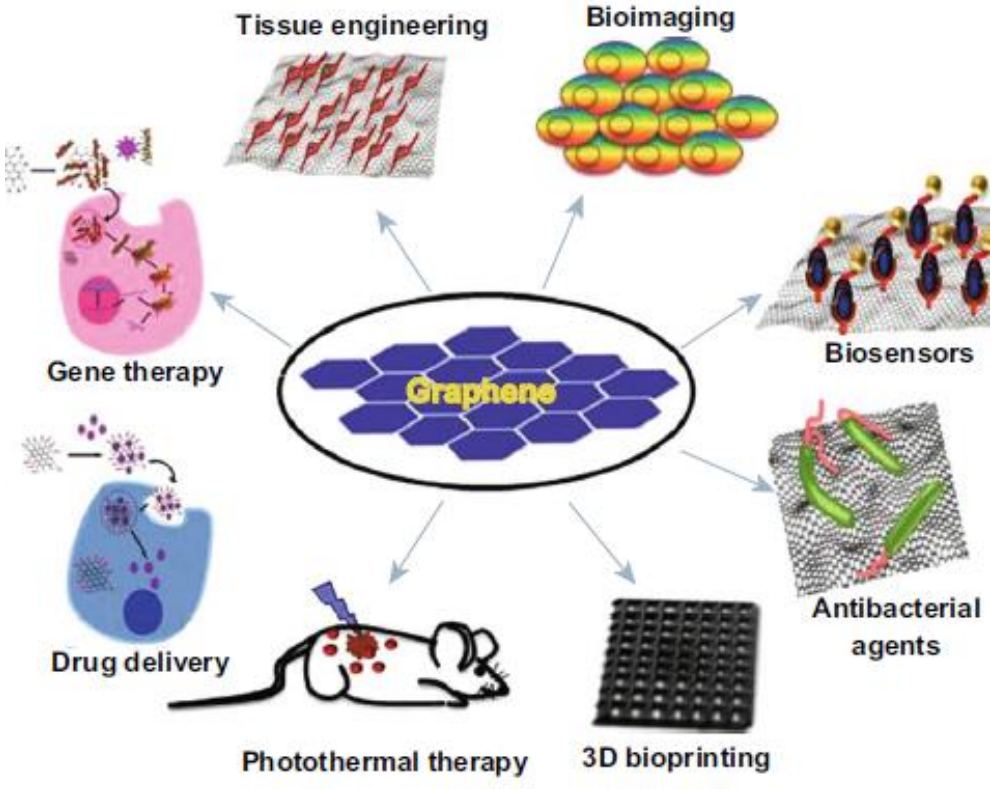

Figure 1.10: Applications of graphene-based materials in medical and healthcare [19].

1.4.5 Automobile, Marine and Aerospace Industry

Currently, the emphasis is on the use of lightweight but robust materials in a variety of structural engineering industries, including the automotive, aerospace, and marine industries. This requirement minimizes the weight of the parts and the quantity of fuel used, resulting in significant cost and fuel consumption savings. Less fuel use results in lower CO_2 emissions and pollution of the environment. Because of their lightweight and outstanding specific strength/stiffness qualities, fiber-reinforced composite materials are replacing heavy steel components.

As textile reinforcement, many forms of high strength and high modulus fiber, such as glass fiber, carbon fiber, and para-aramid fiber, are employed. Because they are chemically inert, thermally stable, and easy to work with, thermosetting polymer resins are widely utilized as the polymer matrix in the fabrication of fiber-reinforced composites.

Although fiber/polymer composites (FPCs) increase in-plane characteristics significantly, they cannot improve through-the-thickness qualities as required. Furthermore, under cyclic loading circumstances, thermosetting polymer resins are highly prone to cracking. To address these issues, graphene nanoparticles are currently used as alternative reinforcing agent in FPCs, demonstrating considerable improvements in both in-plane and out-of-plane characteristics for having a high strength-to-weight ratio and good mechanical capabilities [1], [6], [17], [20].

In the next section the use of GRM in FRC will be discussed in detail, with a particular focus on the advantage that it can bring on the aerospace and automotive sectors.

1.5 References

[1] A. C. Ferrari *et al.*, "Science and technology roadmap for graphene, related two-dimensional crystals, and hybrid systems," *Nanoscale*, vol. 7, no. 11, pp. 4598–4810, 2015, doi: 10.1039/c4nr01600a.

[2] R. Raccichini, A. Varzi, S. Passerini, and B. Scrosati, "The role of graphene for electrochemical energy storage," *Nat. Mater.*, vol. 14, no. 3, pp. 271–279, 2015, doi: 10.1038/nmat4170.

[3] J. Sanes, C. Sánchez, R. Pamies, M. D. Avilés, and M. D. Bermúdez, "Extrusion of polymer nanocomposites with graphene and graphene derivative nanofillers: An overview of recent developments," *Materials (Basel).*, vol. 13, no. 3, 2020, doi: 10.3390/ma13030549.

[4] Y. Xu, H. Cao, Y. Xue, B. Li, and W. Cai, "Liquid-phase exfoliation of graphene: An overview on exfoliation media, techniques, and challenges," *Nanomaterials*, vol. 8, no. 11, 2018, doi: 10.3390/nano8110942.

[5] X. J. Lee *et al.*, "Review on graphene and its derivatives: Synthesis methods and potential industrial implementation," *J. Taiwan Inst. Chem. Eng.*, vol. 98, pp. 163–180, 2019, doi: 10.1016/j.jtice.2018.10.028.

[6] V. B. Mohan, K. tak Lau, D. Hui, and D. Bhattacharyya, "Graphene-based materials and their composites: A review on production, applications and product limitations," *Compos. Part B Eng.*, vol. 142, no. January, pp. 200–220, 2018, doi: 10.1016/j.compositesb.2018.01.013.

[7] T. M. Magne *et al.*, *Graphene and its derivatives: understanding the main chemical and medicinal chemistry roles for biomedical applications*, no. 0123456789. Springer Berlin Heidelberg, 2021. doi: 10.1007/s40097-021-00444-3.

[8] L. S. Porto, D. N. Silva, A. E. F. de Oliveira, A. C. Pereira, and K. B. Borges, "Carbon nanomaterials: Synthesis and applications to development of electrochemical sensors in determination of drugs and compounds of clinical interest," *Rev. Anal. Chem.*, vol. 38, no. 3, pp. 1–16, 2020, doi: 10.1515/revac-2019-0017.

[9] B. et Al, "Production and processing of graphene and related materials," *2D Mater.*, vol. 7, no. 2, 2020, doi: 10.1088/2053-1583/ab1e0a.

[10] A. Santhiran, P. Iyngaran, P. Abiman, and N. Kuganathan, "Graphene Synthesis and Its Recent Advances in Applications—A Review," *C*, vol. 7, no. 4, p. 76, 2021, doi: 10.3390/c7040076.

[11] X. Chen, L. Zhang, and S. Chen, "Large area CVD growth of graphene," *Synth. Met.*, vol. 210, pp. 95–108, 2015, doi: 10.1016/j.synthmet.2015.07.005.

[12] B. T. Hogan, E. Kovalska, M. F. Craciun, and A. Baldycheva, "2D material liquid crystals for optoelectronics and photonics," *J. Mater. Chem. C*, vol. 5, no. 43, pp. 11185–11195, 2017, doi: 10.1039/c7tc02549a.

[13] A. Bianco *et al.*, "All in the graphene family - A recommended nomenclature for two-dimensional carbon materials," *Carbon N. Y.*, vol. 65, pp. 1–6, 2013, doi: 10.1016/j.carbon.2013.08.038.

[14] P. Wick *et al.*, "Classification framework for graphene-based materials," *Angew. Chemie - Int. Ed.*, vol. 53, no. 30, pp. 7714–7718, 2014, doi: 10.1002/anie.201403335.

[15] A. Kovtun *et al.*, "Benchmarking of graphene-based materials: Real commercial products versus ideal graphene," *2D Mater.*, vol. 6, no. 2, 2019, doi: 10.1088/2053-1583/aafc6e.

[16] "ISO/TS 80004-13".

[17] M. A. Al Faruque, M. Syduzzaman, J. Sarkar, K. Bilisik, and M. Naebe, "A review on the production methods

and applications of graphene-based materials," *Nanomaterials*, vol. 11, no. 9, 2021, doi: 10.3390/nano11092414.

[18] A. Kovtun *et al.*, "Graphene oxide-polysulfone filters for tap water purification, obtained by fast microwave oven treatment," *Nanoscale*, vol. 11, no. 47, pp. 22780–22787, 2019, doi: 10.1039/c9nr06897j.

[19] S. Syama and P. V. Mohanan, *Comprehensive Application of Graphene: Emphasis on Biomedical Concerns*, vol. 11, no. 1. Springer Berlin Heidelberg, 2019. doi: 10.1007/s40820-019-0237-5.

[20] F. Valorosi *et al.*, "Graphene and related materials in hierarchical fiber composites: Production techniques and key industrial benefits," *Compos. Sci. Technol.*, vol. 185, no. July 2019, p. 107848, 2020, doi: 10.1016/j.compscitech.2019.107848.

2. Graphene and related materials in hierarchical fiber composites: Production techniques and key industrial benefits

2.1 Introduction

Fiber-reinforced composites (FRC) are increasingly used in sport cars, airplanes, boats, sporting tools, building components and a large number of high-tech fashionable products need to have at least some part made of FRC, in particular made of carbon fiber reinforced composites (CFRC). These fibers composed mainly of carbon have already replaced the state-of-the-art metal alloys in many parts of commercial airplanes and in most of the structural parts of high-level sport cars. The current trend to electrification of mainstream cars will also push for lower weight and thus wider use of CFRC in mass-produced vehicles.

Historically it was Thomas Alva Edison who produced the first car- bon fibers during the development of the incandescent electric bulb, in year 1879. In his search for a filament able to withstand electric current, Edison treated cotton threads or bamboo slivers at high temperature, in absence of oxygen, obtaining a carbonized filament that could glow for hours in vacuum inside a glass bulb. Carbon was soon replaced in the lamps by tungsten wires; though, ca. 80 years afterward, researchers from Union Carbide discovered how to exploit the outstanding mechanical properties of carbon fibers obtained by high-temperature treatments of textiles or other carbon-based precursors [1]. Such microscopic fibers could be added to thermoplastic or thermosets polymers to obtain materials as stiff and strong as metals, but much lighter.

Today CFRC are mature commercial products, but still present a number of technical challenges that limit their use to high-cost/high performance applications. In particular, they exhibit high anisotropy between axial and radial directions and they have to be oxidized in order to be fully wetted and bonded to polymer matrices. The strength of that interaction has also to be tailored to specific applications as strong interfacial bonding leads to brittle behavior whereas weak bonding leads to delamination and poor off-axis properties. Finally, conventional carbon fiber production processes involve toxic solvents and high temperatures and that adds to high production costs and adverse environ- mental impact. In recent years, results obtained in the scientific community indicate that the performance of CFRC can be improved by addition of graphene or related 2-dimensional materials (GRM).

In the following sections, we summarize the main technological challenges of FRC use and recent, state-of-the-art examples of how GRM can help to solve such challenges. In section 2.1, we will

introduce briefly how and why CF and GRM are useful in composites. Section 2.2 will discuss the best ways to process GRM into composites, and the beneficial effect that GRM can have to improve the performance of the composite at nanoscopic and mesoscopic scale. In section 2.3 we will describe what are the major issues limiting wider use of CF for applications in key industrial sectors, and how GRM can help to solve such issues. Finally, section 2.4 will briefly describe FRC-GRM composites that are already available commercially.

2.1.1 Use of carbon and glass fibers for mechanical reinforcement

Both glass fibers (GF) and carbon fibers (CF) are widely used at the commercial level, with the former being cheaper but heavier, and the latter being stronger, lighter but more brittle and expensive. The mechanical properties of carbon fibers are strongly dependent upon processing conditions that control fiber microstructure [2–4]. Although there are many types of carbon fibers available, those used in engineering applications fall into two broad categories: high strength fibers with relative low or intermediate level of Young's modulus and high modulus fibers that exhibit a relative low or intermediate tensile strength. Carbon fibers are inert and have good electrical and thermal conductivities depending on modulus and degree of crystallinity. As mentioned below, however, the fibers exhibit a turbostratic structure and anisotropic physical properties with a much lower Young's modulus and worse general properties transverse to the fiber axis [3]. The main method now employed in the manufacture of carbon fibers is through the pyrolysis of the polymer polyacrylonitrile (PAN). The PAN is spun into fibers in which the molecules are aligned along the fiber axis. The fibers are then heated and the PAN becomes converted into a ladder polymer. Increasing the temperature and heating the fibers under tension in an oxygen-containing atmosphere causes further reaction in which the ladder molecules form crosslinks with each other. The material is then reduced and heated at high temperatures to give a 'turbostratic' graphitic structure [5]. This is an allotropic form of carbon, in which the graphene basal planes are not packed regularly as in a graphite single crystal. The basal planes are, however, aligned approximately parallel to each other along the fiber axis, leading to fibers with high levels of axial stiffness and strength. A different type of CF is obtained by spinning of pitch, a viscoelastic material coming from distillation of crude oil, coal or plants. Pitch fibers are often more rigid than PAN fibers (higher tensile modulus), while PAN fibers have higher strength and lower density than pitch fibers. Glass fibers have been for long time the most commonly-used type of fiber, employed in a range

of applications due to their low cost and good mechanical properties. They are inorganic fibers based upon silica mixed with other oxides and a number of different types of glass fibers are used. The most common kind of fiber is E-glass and other types of silica-based fibers with somewhat different compositions are employed; the more expensive S-glass for higher modulus and strength, and C-glass for better corrosion resistance in acids and water [5]. Impressive levels of reinforcement in polymer composites are obtained through the use of high-performance fibers. This reinforcement is controlled by the geometry of fiber packing, the mechanical properties of the fibers and matrix polymer, along with the properties of the fiber/ matrix interface [6]. One of the advantages of using fiber-reinforced composites is that it is possible to tailor different fiber arrangements to take advantage of the anisotropic properties of the fiber reinforcement [5,6]. It is also possible to stack layers of continuous fibers in unidirectional (stacked parallel), angle-ply (stacked at angles) and cross-ply (stacked at 90°) arrangements. FRC with the highest axial stiffness and strength are obtained with unidirectional fibers in all plies whereas angle-ply or cross-ply configurations yield quasi-isotropic composites that exhibit, however, lower mechanical property values than unidirectional composites in the fiber direction. Other arrangements of continuous fibers include knitted or woven structures that can be draped into complex shapes and then impregnated with a thermosetting resin. The off-axis fibers tend to reduce the reinforcement efficiency and reduce the composite modulus compared with composites containing straight fibers. As mentioned also above, such composites tend to have more uniform properties and the interlacing of the fibers leads to composites with better impact and penetration resistance [5]. Table 2.1 shows an indicative comparison of the properties of typical fibers used in FRC and typical GRM.

Table 2.1: Mechanical properties of mesoscopic fibers vs. typical GRM. All data are indicative and should be considered as order-of-magnitude estimation, varying greatly with preparation technique and producer.

		Density ($g\ cm^{-3}$)	**Tensile Strength (GPa)**	**Young's modulus (GPa)**
Mesoscopic additives	Carbon fiber (PAN Std. Mod.)	1800	4.9	230
	Glass fiber	2460	4.8	87
Nanoscopic additives	Graphene	n.d.[a]	130	1 050
	Graphene oxide	n.d.[a]	30	200

[a] Not defined. Density of nano-materials is not defined univocally, depends on packing and exfoliation grade. Perfectly packed graphene sheets (graphite) have a macroscopic density of 2.2 g cm^{-3}. For a list of measured density of commercial graphene-based materials, see Ref. [7].

2.1.2 Use of graphene nanosheets for nanoscale mechanical reinforcement

Carbon fibers have typical sizes at the micron range (typically 5–10 μm in diameter), thus only reinforce the structure of the composite at a mesoscopic scale. One of the most promising developments in Materials Science over the past 40 years has been the identification and exploitation of new nano-sized allotropes of carbon in the form of different nanocarbons, starting with the discovery of C60 in the 1980s [8]. This was followed by the discovery of carbon nanotubes (CNT) (first multi-walled [9], then single-walled [10] and double-walled) in the 1990s. Carbon nanotubes were soon found to have interesting and exciting physical properties, in particular high levels of stiffness and strength [11,12]. Soon after these nanocarbon allotropes were first identified, researchers started to investigate the properties of nanocomposites produced by processing them in polymer matrices. It was anticipated that the high inherent values of stiffness and strength of the CNTs might be realised when reinforcing nanocomposites. Poor levels of reinforcement were obtained with C60 nanospheres [13] but it was soon demonstrated that CNTs could in certain cases provide good reinforcement of polymer matrices [14–20].

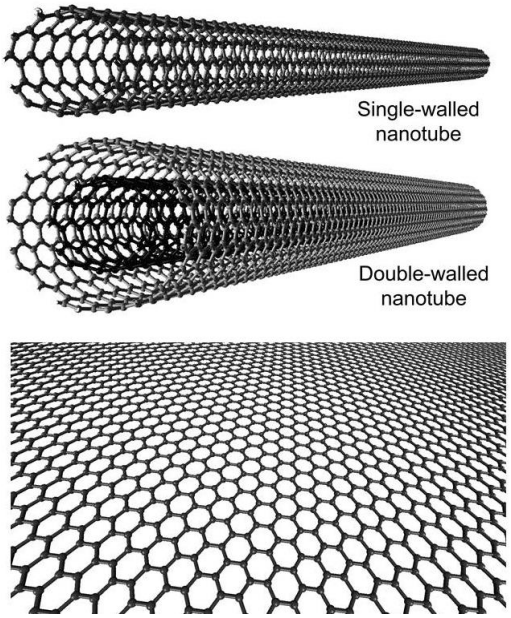

Figure 2.1: Carbon nanotubes and graphene (Courtesy of Professor Feng Ding)

The isolation and identification of graphene (Fig. 2.1) was first reported in 2004 [21] and over recent years a number of different forms of graphene have been identified [22]. The material of initial interest was mechanically-exfoliated by ‘scotch-tape’. A number of other different forms of graphene are now recognised [23], including mechanically-exfoliated (mono- and few-layer)

graphene, CVD graphene, graphene nanoplatelets, graphene oxide (GO) and reduced graphene oxide (rGO), that are usually termed GRM. The literature is full of papers that have used different terminologies to describe their materials and attempts now have been made to standardise the terminology of this range of different materials as can be seen in a number of publications [24,25]. The different forms of GRM have different physical properties with monolayer having perhaps the most unique mechanical properties of a Young's modulus up to 1050 GPa and strength values of up to 130 GPa [26]. Such mechanical properties have led to a high level of interest in both the academic and industrial communities, accompanied the rapid development of nanocomposites based upon GRM. Initial studies employed GO or rGO, the preparation of which can be readily upscaled to produce large enough quantities to make specimens that can be deformed on conventional mechanical testing machines. Differently from other nano-additives (e.g. fullerenes or CNT), graphene can be prepared at low temperature, with no need of metal catalysts, by exfoliation of bulk graphite using ultrasonic methods [27], high-speed mixing [28], or water-jet milling [29]. The current situation after nearly two decades of research upon nanocomposites reinforced with carbon nanotubes and graphene has recently been reviewed by Kinloch and co-workers [30]. They pointed out questions which still remain about the practical impact of such materials and suggested that this uncertainly stems from factors that include poor load transfer, interfacial engineering, dispersion, and viscosity-related issues that lead to challenges with processing the nanocomposites. One major issue is that CNTs form bundles and individual GRM can agglomerate such that their ability to reinforce nanocomposites is compromised. Such factors make the effective aspect ratio of the nanofillers smaller which reduces the efficiency of load transfer, similar to the behaviour of short fiber composites [6]. Secondly, the surfaces of both CNT and graphene are devoid of any dangling bonds or defects that make strong matrix-filler bonds difficult to achieve. It is possible to remedy the situation to a certain extent for CNTs and graphene or graphene nanoplatelets (GNP) through chemical functionalization, although care must be taken to avoid compromising their intrinsic properties [31]. Moreover, such surface treatments may also help to reduce problems with agglomeration or restacking. The situation is somewhat different with GO and rGO, whose surface functionality can be easily tuned to improve the interfacial strength in nanocomposites [32].

2.2 Preparation and properties of FRC-GRM composites

2.2.1 Production techniques

While both CF and GRM have exceptional properties, they also share difficulties in processing, being complicated or even impossible to simply process in a solvent. Combining them in a hierarchical composite with the appropriate structure is thus a major challenge. In standard GRM-polymer composites, the objective is to disperse GRM as uniformly as possible. In FRC, conversely, different approaches are possible, being often preferable to include the nanosheets in the polymer matrix or on the fiber surface, in the pre-peg, in between different FRC layers. Fig. 2.2 shows a cartoon depicting all possible approaches which illustrates the challenges encountered for the efficient decoration of FRC with GRM.

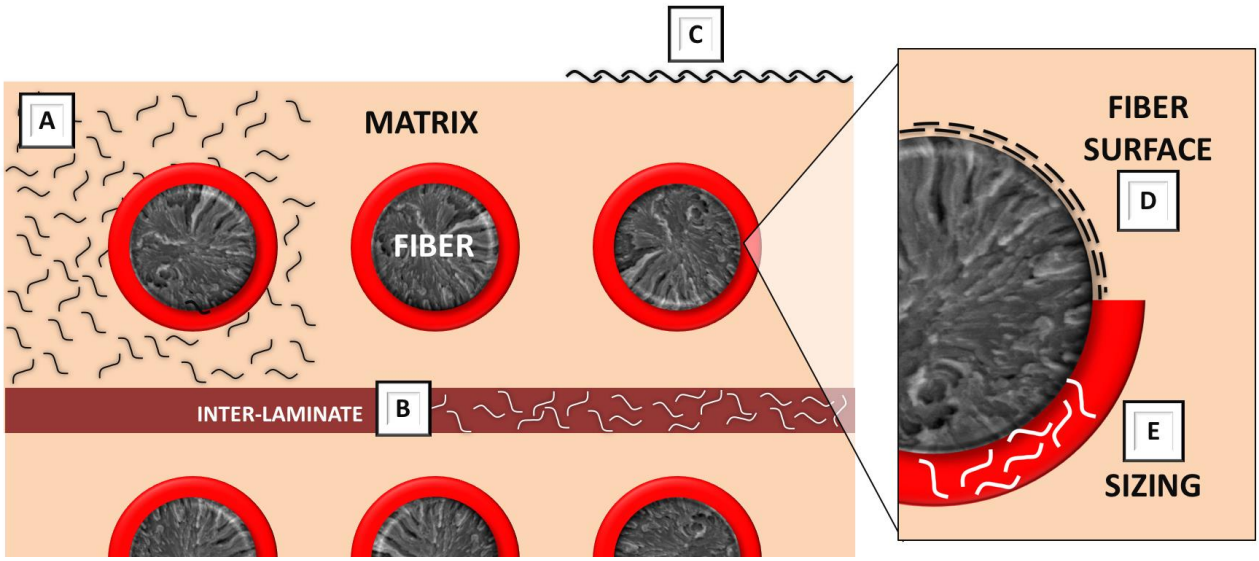

Figure 2.2: Schematic representation of the different ways to include GRM into FRC: A) dispersion in the polymer matrix [33,34]; B) at the interface between different laminate layers [35]; C) on the surface, as gas and moisture barrier [36]; D) on the bare fiber surface [37–41]; E) in the sizing (pre-peg) layer [42].

There are, in general, two main approaches to fabricate FRC containing GRM. One method involves simply adding the GRM to the matrix and processing the nanocomposite in a conventional way. The other approach ensures that the GRM are positioned at the interface between the fibers and matrix in order to optimize the stress transfer efficiency at the interface. One important issue to highlight is that the inter-fiber separation in FRC is relatively small even at low volume fractions of fibers. For example, it is easy to show [5] that this separation is less than one fiber diameter at a

volume fraction as low as about 0.3. This means that for most FRC there is very little space between the fibers and so the matrix may be constrained by the presence of fibers. As carbon fibers, for example are typically less than 10 μm diameter, the space matrix occupies between the fibers has dimensions of microns, so that any matrix modifiers will need to be of sub-micron dimensions, such as in the case of GRM. During composites processing methods such as resin infusion, the matrix resin needs to flow through the narrow gaps between the fibres. One of the main issues that then arises upon adding GRM to the matrix of a nanocomposite before resin impregnation is that the GRM may be filtered out by the fiber assembly during impregnation and therefore not be correctly positioned between the fibers in the final nanocomposite [43]. A number ways for overcoming this "filtering" effect have been developed, as detailed below. Filtering can be avoided by using graphene-based particles with submicrometric size, as demonstrated by the Antolin group in collaboration with Airbus and Aernnova [33]. They used highly graphitic helical ribbon carbon nanofibres (CNFs, Fig. 2.3) as additives in CF-epoxy composites for aeronautic applications, and observed no increase of viscosity during RTM and no filtering effect, ensuring that the production process could be implemented without major changes in the manufacturing process. A similar technology based on such CNF is likely also implemented in commercial sport tools [44].

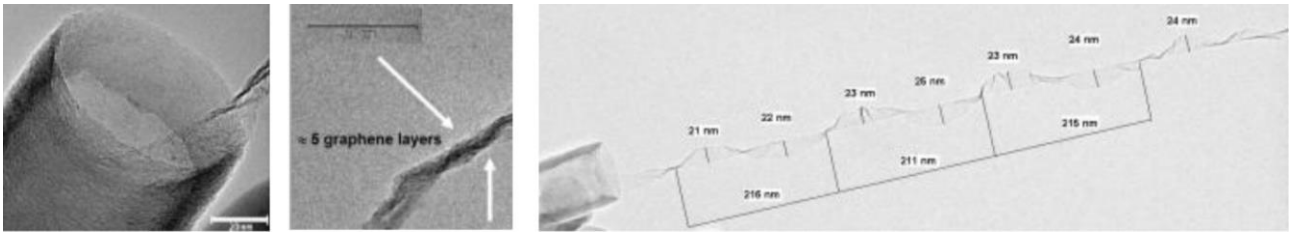

Figure 2.3: Helical ribbon carbon NanoFibre used as graphitic precursor for obtaining graphene related materials with small size, able to infiltrate into CF fabric. From Ref. [33].

Li and coworkers [34] exfoliated and dispersed natural graphite in an epoxy resin using a three-roll mill which then enabled the direct vacuum-assisted infusion of the doped resin into carbon fiber fabrics in a steel mould, without problems with particle filtering. They also pointed out that this method is industrially scalable and environmentally friendly and does not require the use of solvents. Dip-coating is a widely used method whereby a suspension of GRMs is dispersed in the resin matrix using techniques such as sonication or mechanical stirring, usually with the aid of a solvent [42,45,46]. The fiber tows can then be dipped into the GNP-modified resin as shown in

Fig. 2.4. This ensures that a good dispersion of GRMs is obtained in the matrix between the fibers when the tows are finally pressed together to produce the nanocomposite.

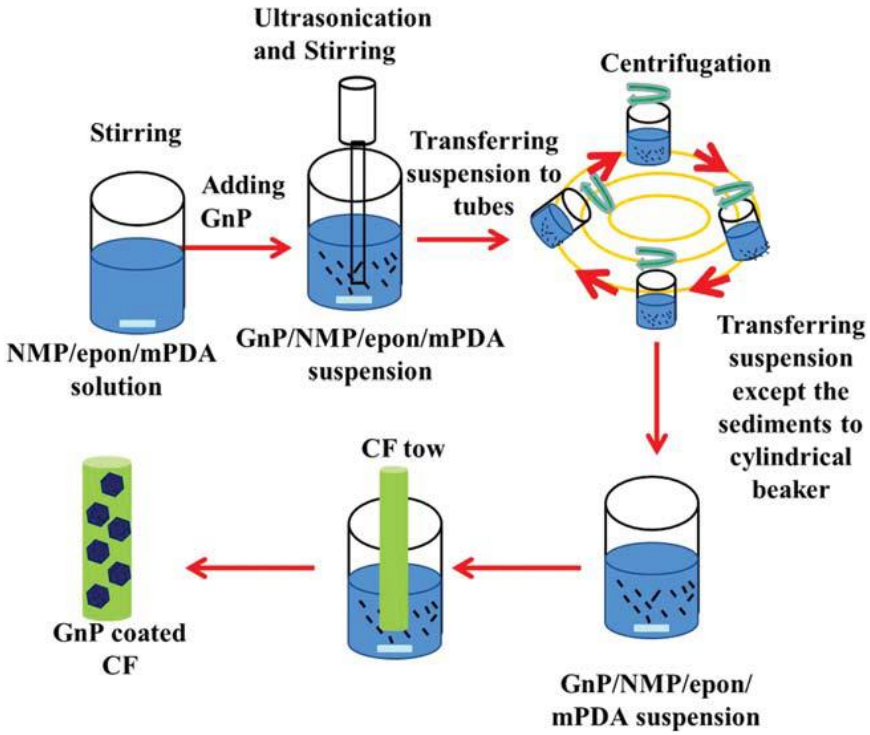

Figure 2.4: Schematic of a dip-coating method of dispersing GRM in a matrix resin and then coating a fiber tow (from Ref. [42]).

Using another technique, Du and co-workers [35] prepared partially-cured GRM/epoxy nanocomposites and used them as interleaves between sheets of carbon fiber fabric that were then cured in a hot press inside a vacuum bag as shown in Fig. 2.5. This method ensures that the GRMs are dispersed correctly in the nanocomposites although it should be pointed out that a solvent needs to be employed in the manufacture of the interleaves. Besides dispersing GRM in the whole matrix, placing them selectively on the surface of the fibers is also an interesting approach, because it would allow to use minimal amounts of GRM and reinforce selectively the most critical part of FRC, i.e. the fiber-polymer interface. The surface modification of carbon fibers using GRM has recently been reviewed by Hung and coworkers [37] who gave a detailed account of the methods that can be employed to coat the fibers with GRM for the manufacture of GRM-modified FRC. Hence only a brief summary will be given here. There are essentially two main methods used, electrophoretic deposition and chemical grafting.

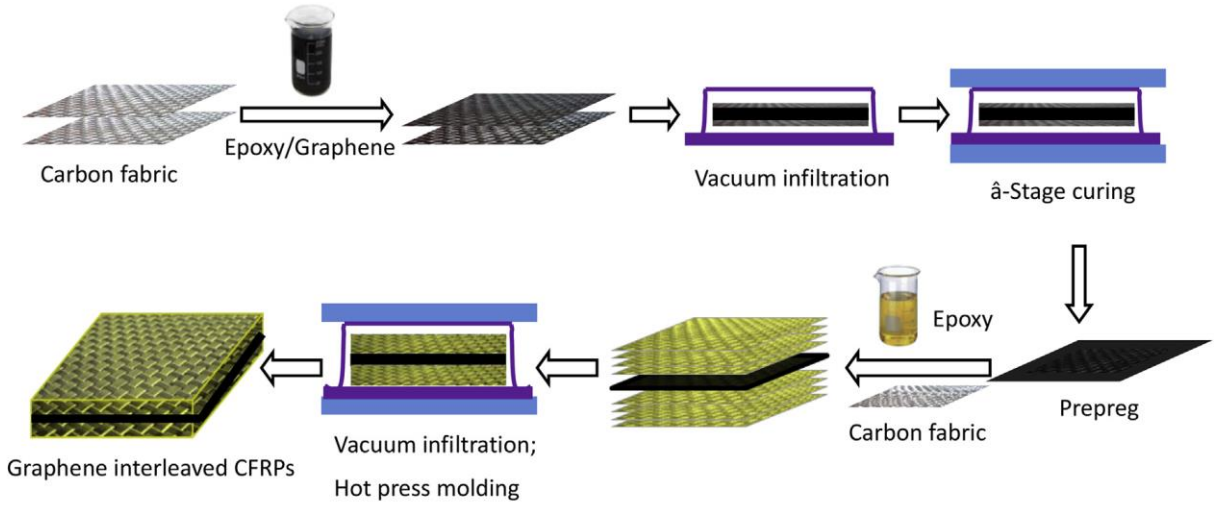

Figure 2.5: Schematic diagram of the fabrication of GRM interleaved FRCs (After [35]).

Strong interaction between nanofillers and fiber surfaces can be achieved when the two are bonded together chemically. The surfaces of carbon fibers generally contain few functional groups and so normally need to be oxidised to produce reactive functional groups on their surfaces [37]. Because it contains functional groups, GO is favoured for chemical grafting with surface-modified carbon fibers [38–40]. Oxidising carbon fibers can potentially lead to a deterioration in their mechanical properties through the creation of defects on their surfaces but chemical modification through carboxyl functionalization has recently been shown to maintain fiber strength by avoiding the creation of surface defects [47]. An effective chemical functionalization to attack GO nanosheets on mesoscopic objects is by formation of amide bonds. The fibers' surface is first functionalized to create NH2 groups, for example using (3-Aminopropyl)triethoxysilane (APTES). This results in uniform coating (Fig. 2.6), and improves inter-laminar shear strength (ILSS) [41]. The opposite approach is also possible, functionalizing first the GO with NH2 groups, and then attaching them to CF functionalized with acyl chloride groups (-COCl) [38].

More complex coatings, stacked multilayers of GO and polymers, can be fabricated on the fibers using layer-by-layer deposition [48–50]. This is a powerful technique based on successive dipping the fibers in a solution of positively charged polymer and negatively charged GO. Each step deposits a well-defined bilayer, with nanometric thickness, self-limited due to electrostatic interactions; the number of layers deposited can be tuned by the number of dipping steps, and works even on complex geometrical shapes, allowing to obtain composite GRM multilayers for

packaging [49] or energy storage applications [50]. Deposition of up to 15 GO-PEI bilayers on carbon fibers led to improvements in interfacial shear strength (IFSS), tensile strength storage modulus and elongation at break in PP/CF–GO hierarchical composites.

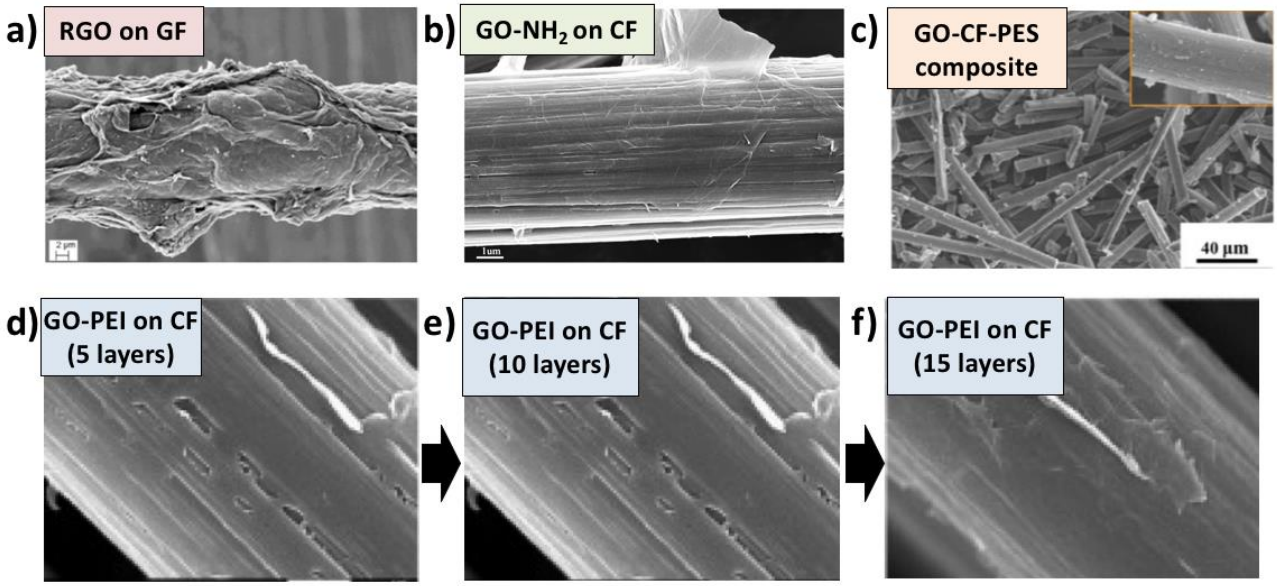

Figure 2.6: Examples of fibers coated with GO, from literature. See text for more details. a) GF electrophoretically coated with GO deposited at 10 V/cm and subsequently reduced to rGO [51]. b) GO-NH2 directly grafted onto CF [38]. c) 0.5 wt% GO-coated SCF/PES composite, image taken after removing PES matrix by thermal ablation in N2 atmosphere [52]. d-f) CF coated with an increasing number of GO-polymer layers using LbL technique. Scale bar in d-f is 1 µm [48].

Electrophoretic deposition can be used to produce a homogenous high surface area coating of electrically-conductive nanofiller on fibers [37]. This has been demonstrated for both carbon [53,54] and glass [51] fibers. This process is, however, only really applicable to GO which is negatively charged in solution and has hydrophilic functional groups. The negatively-charged GO migrates to a positively-charged fiber and gives it a uniform coating. Pristine graphene, on the other hand, is not suitable for this process since it is hydrophobic and so will not disperse uniformly in aqueous solvents. In this case other methods have to be employed such as by spray coating GNP on to fiber fabrics before resin infusion [55]. An original approach to produce innovative FRC-GRM is based on continuous CNT fiber fabric preform in a polymer matrix with chemically-modified CNT or GRM as matrix modifiers such as that shown in Fig. 2.7 [30]. In this case, the same nano-additives would be present both in the fibers part and in the matrix region of the FRC, thus enhancing the interaction and the strength of the FRC.

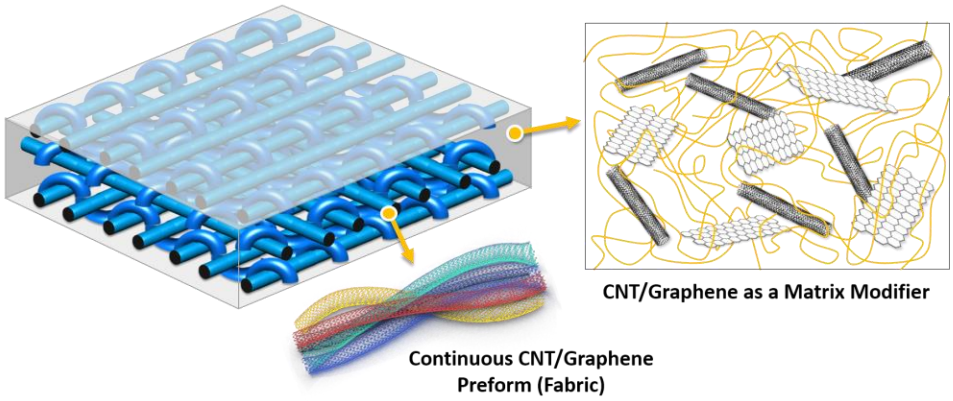

Figure 2.7: A schematic illustration of a futuristic CNT/graphene polymer composite that consists of continuous CNT fiber preform (fabric) in a polymer matrix and chemically-modified CNT/graphene as matrix modifiers [30].

2.2.2 Nanoscale interfacial interactions of GRM with the polymer matrix of FRC

GRM, thanks to their nanometric size, high flexibility and ultimate strength can be an ideal additive to both toughen the matrix and improve adhesion between mesoscopic fibers and polymers in a composite. The study and the control of such interaction is, however, challenging in a material having a complex hierarchical structure going from the nano-to the macro-scale. Here we summarize recent results obtained to better understand and enhance the benefits of GRM in FRC, in particular for structural reinforcement, while benefits on the electrical or thermal properties have been discussed in previous publications [56, 57]. The mechanical integrity of FRC depends primarily on the strength of the interface between the polymer, the GRM and the fibers. A detailed study of the micromechanics of the deformation of individual graphene monolayer flakes has shown that continuum mechanics is still applicable at the nano-level [58], enabling a full understanding of the deformation of graphene in bulk nanocomposites to be obtained [23]. A number of different micromechanical test methods have been devised to determine the strength of the interface [59] involving single-fiber model composites. One method that has been employed is the micro-bond test whereby the force needed to pull a single fibre out of a resin droplet is measured from which the strength of the interface (IFSS) can be determined. This has been done both for specimens where the GRM is introduced into the sizing of carbon fibres [60] and others for which the GRM has been added to the resin used for the droplet [61]. In both cases a significant increase is found in the interfacial shear strength with the presence of the GRM. The behaviour is shown clearly in Table 2.2 where it can be seen that the IFSS increases with the addition of pristine

graphene to the epoxy resin in the droplet [61], in particular when the graphene is chemically functionalized.

Table 2.2: Measured values of IFSS for a series of carbon fiber microbond specimens with epoxy resin droplets containing different loading of graphene, both pristine and functionalized [61].

Graphene Content (wt%)	Interfacial shear strength (MPa)		
	Pristine graphene	COOH graphene	COOH + NH_2 graphene
0	62.4 ± 5.7	62.4 ± 5.7	62.4 ± 5.7
0.1	72.7 ± 7.3	73.9 ± 4.0	73.9 ± 4.8
0.3	76.3 ± 5.4	75.8 ± 4.4	77.2 ± 4.8
0.5	79.0 ± 6.1	80.2 ± 5.6	82.4 ± 6.1

Lee and coworkers [61] examined the surfaces of their fibers after a droplet of polymer matrix was detached and concluded that the interfacial failure mechanism was not affected by the presence of the graphene in the epoxy resin matrix. They explained the increase in IFSS with the presence of the GRM in the resin as being due to the graphene leading to a more complicated path through resin adjacent to the carbon fiber as shown in Fig. 2.8.

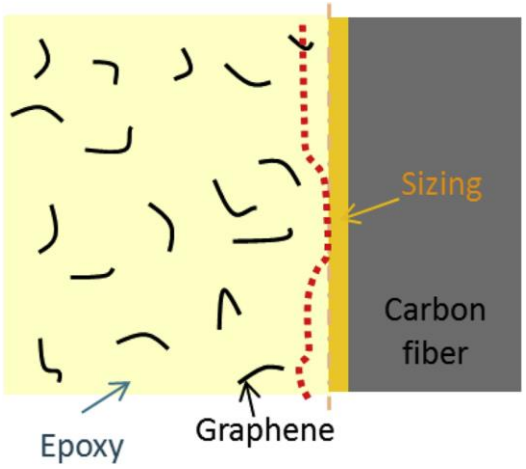

Figure 2.8: Schematic diagram of the path of crack propagation through a GRM-modified epoxy matrix near the surface of an embedded carbon fiber (After [61]).

It is also possible to evaluate the strength of the interface between fiber laminates (ILSS) for a GRM-modified FRC, rather than for single-fiber model composites, using techniques such as the short-beam shear test upon unidirectional composites. Zhang and co-workers [60] introduced GO into the sizing of carbon fibres and correlated its effect upon both the single-fiber IFSS

measurements and ILSS values for unidirectional composites. They found an increase in both parameters upon the addition of the GRM to the sizing. Research upon the effect of the modification of FRC with GRM upon the values of IFSS and ILSS has recently been reviewed by Hung and coworkers [37]. Overall it is found that both parameters increase with the addition of the GRM, with the IFSS values typically increasing by 30–90% whereas the increase in ILSS is smaller, generally by no more than 40%. We have undertaken extensive studies of stress transfer at composites interfaces at the nanoscale using Raman spectroscopy [32,58,62-65]. A strong interaction allows to have a shorter "critical length" of the flakes actively reinforcing the composite [32,66]. We recently demonstrated that such interaction can be enhanced by the generation of atomic defects [67] and investigated it by means of AFM nano-mechanical mapping and Raman microscopy [68]. In addition, we demonstrated that the graphene/polymer interface can exhibit a mechanical recovery after cycling loading conditions under the influence of moderate thermal stimulus [69]. Controlling the interfacial adhesion between the graphene and the polymer substrate can be achieved by modulating the surface conditions such as its roughness. In this way the fracture mechanism of graphene can be altered [70]. GRM can thus act as structural linkers between the matrix and the fibers in hierarchical composites. To this aim, the simplest system that has been studied is a single CF filament-epoxy matrix model composite. Single fibers were subjected to quasi-static tension and simultaneous Raman spectra acquisition, to measure the shear stress on the fibre outer surface [71]. GRM gave a 50% enhancement of the fibre-matrix interface (using the shear stress value as the criterion) compared to the non-doped epoxy matrix materials, confirming the finding of the earlier studies using the micro-bond test described above [61]. Overall, GRM can work as hierarchical fillers (with high surface area and capillary wetting by the surrounding polymer) to improve the interfacial interactions of the FRC; the mechanisms of such improvement are still under investigation, being probably due to increased mechanical locking (friction), the local enhancement of the shear modulus of the matrix caused by the GRM sheets and a more tortuous path of crack propagation [71].

2.2.3 Mesoscopic mechanisms of structural reinforcement of GRM in FRC

The addition of GRM to FRC can lead to a significant improvement in mechanical properties of the FRC also at the meso/macro-scale. Recent research in this field has recently been reviewed by Hung and coworkers [37]. In general it is found that the increases are obtained in Young's modulus

[52,72–74] and tensile strength [52,53,72–74] upon the addition of the GRM to an FRC. Fig. 2.9 shows a typical improvement observed for GO-coated short carbon fibers in a polyethersulphone (PES) matrix [52]. It can be seen that the optimal loading is around 0.5 wt% of GO. Above this loading level the modulus still increases slightly but the strength starts to decrease.

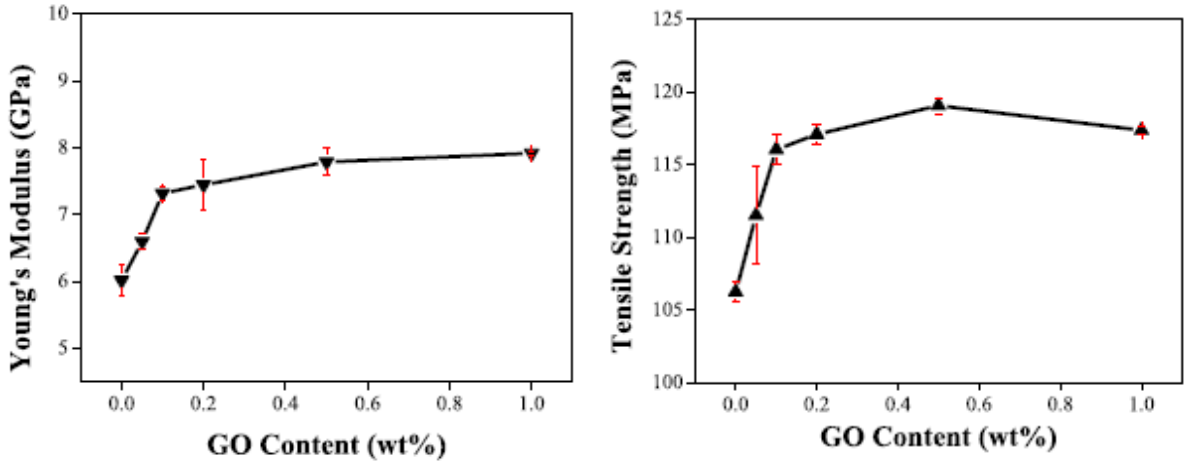

Figure 2.9: Effect of GO content upon (a) Young's modulus and (b) Tensile strength for short CF/PES composites. (After [52]).

We have recently undertaken a detailed study of the effect of the addition of graphene to the matrix of a unidirectionally-reinforced carbon fiber epoxy composite. It was found that the addition of around 2% by weight of graphene can lead to a significant enhancement in mechanical properties [75]. In particular, it was found that the axial stiffness of the composites could be increased by the order of 10 GPa accompanied by an increase in axial strength of 200 MPa. X-ray computed tomographic imaging and polarized Raman spectroscopy demonstrated that the graphene was highly aligned parallel to the axes of the carbon fibers. Moreover stress-induced Raman band shifts showed that the self-aligned graphene is subjected to high levels of stress during axial deformation of the composite [75]. The graphene was found to have an effective Young's modulus in the composite of around 880 GPa, approaching its theoretical value of 1.05 TPa. This behaviour was modelled using the rule of mixtures and shear-lag analysis and it was demonstrated that highly-aligned graphene in a constrained environment between high-modulus fibers can give significantly better mechanical reinforcement than graphene in conventional polymer-based nanocomposites [75]. Fig. 2.10a–c shows different characterization of a typical FRC-GRM composite made with a specific graphene nanoplatelets (GNP) with average lateral dimensions of ~5–10 μm (Fig. 2.10a). The position of the symmetric 2D band at 2660 cm^{-1} in the Raman spectrum from the GNP (Fig.

2.10b) shows that it is few-layer graphene (~5 layers) [76]. The Raman spectra of the neat epoxy and T700 carbon fiber are also shown in Fig. 2.10b. The spectrum of the carbon fiber has very broad D and G bands, in accordance to the turbostratic structure in PAN-based carbon fibers [2]. The presence of the GNP in the enhanced carbon-fiber composite was confirmed by examination of the polished transverse section shown in Fig. 2.10c. Also for such systems, a positive improvement of ILSS (þ45%) is observed by addition of GRM up to 0.5%, with degradation of the properties for higher loadings (Fig. 2.10d) [77].

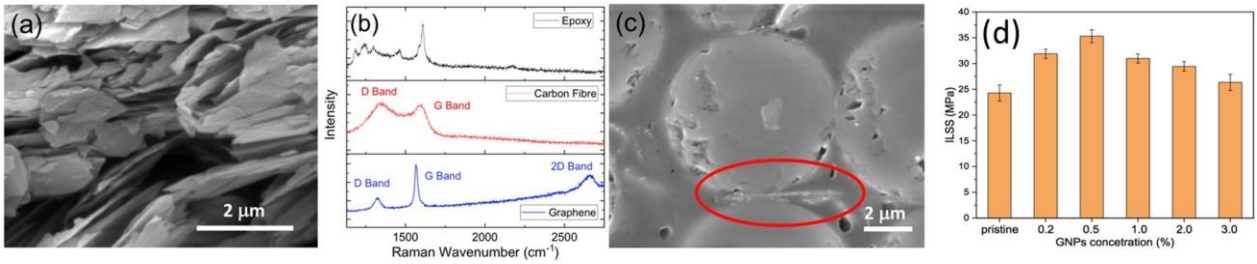

Figure 2.10: Characterization of the different materials of a FRC-GRM composite. (a) SEM micrograph of the graphene flakes. (b) Raman spectra of the epoxy resin, T700 carbon fiber and graphene flakes. (c) SEM micrograph of a polished section of the graphene-enhanced composite showing a graphene flake (highlighted) confined between the carbon fibers. (After [75]). D) Interlaminar Shear Stress values of GRM-doped CFRP for graphene loading of 0.5 wt%, (After [77]).

The dispersion of the graphene can be quantified by determining the ratio of the intensity of the graphene Raman 2D band (*I*2D) to the resin intensity at the wavenumber of 1900 cm^{-1} (*I*1900) (Fig. 2.11a) [75]. The dispersion of graphene was also analysed by using X-ray CT scans that revealed the spatial arrangement of both the graphene and fibers (Fig. 2.11d). The majority of the graphene flakes are within ±20 parallel to the fibers with their normals at right angles to the direction of the fiber axis. This suggests that the graphene flakes are aligned and flattened when the graphene/epoxy mixture passed through the gaps between the fibers (Fig. 2.11c).

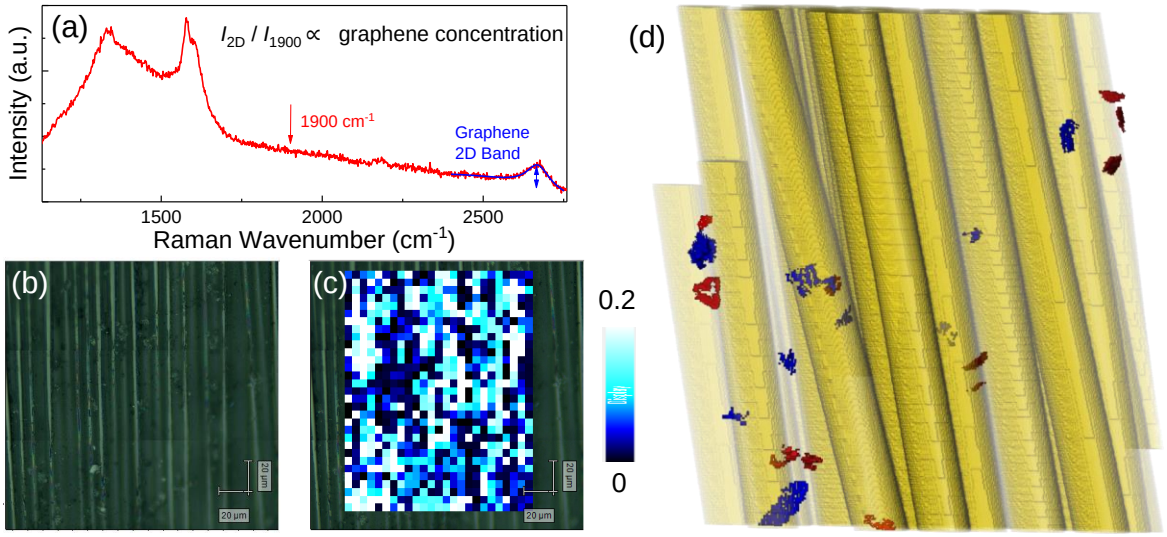

Figure 2.11: Graphene-enhanced carbon-fiber composite. (a) Raman spectrum showing the method of determining the Raman band intensities for the graphene and epoxy resin. (b) Optical micrograph. (c) Raman map of the variation of I2D/I1900 in (b) showing the distribution of graphene. (d) CT scan showing the spatial arrangement of the carbon fibers and graphene (After [75]).

Delamination in FRC is a major issue [6] and poor delamination resistance limits the use of FRC in a number of applications. Srivastava and coworkers [78] compared the effect of the addition of GNP, CNT or carbon black to the matrix of a woven carbon fabric reinforced polymer composite upon the mode I and mode II fracture toughness. They showed that both the GRM and CNT led to an increase in toughness whereas the addition of carbon black actually reduced toughness. Overall the CNT gave better properties than the GRM.

.

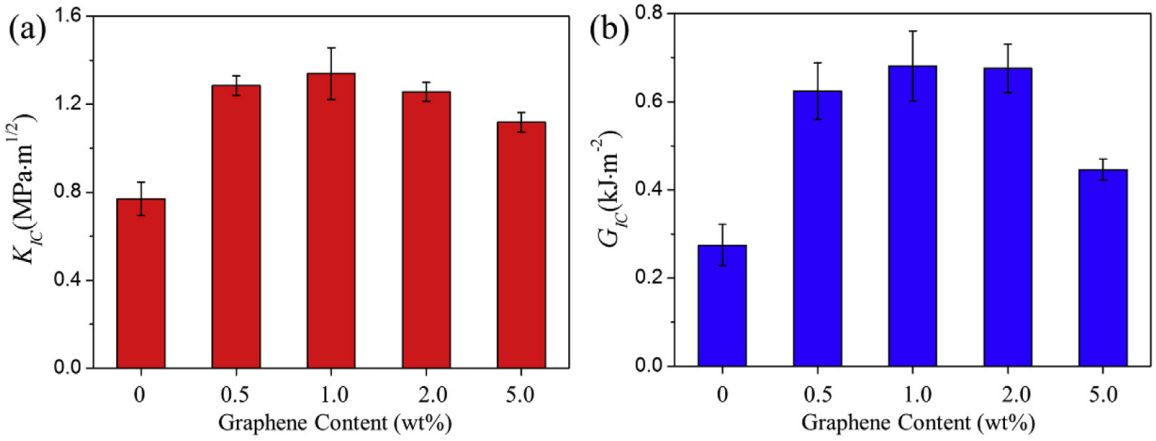

Figure 2.12: Values of (a) fracture toughness, KIC and (b) fracture energy GIC of carbon fiber/epoxy composite laminates containing GRM/epoxy nanocomposites interleaves with the indicated graphene contents (After [35]).

GRM/epoxy interleaves in carbon fiber/epoxy composite laminates can show significantly improved delamination toughening fiber-matrix adhesion, interlaminar properties (interlaminar shear strength), off-axis properties (90° flexural strength and modulus), and even the 0° flexural and compressive strengths of CF-epoxy unidirectional composites [35,45]. Fig. 2.12 shows that the highest level of toughening is found for a graphene loading of 1.0 wt%. even in this case, the properties deteriorate above this loading as a result of agglomeration of the GRM in the resin. SEM images of fracture surfaces (Fig. 2.13) are also often used to confirm an improvement in interfacial adhesion, with a switch from a purely interfacial failure mode with non-coated fibers to a cohesive failure mode between fibers with GRM.

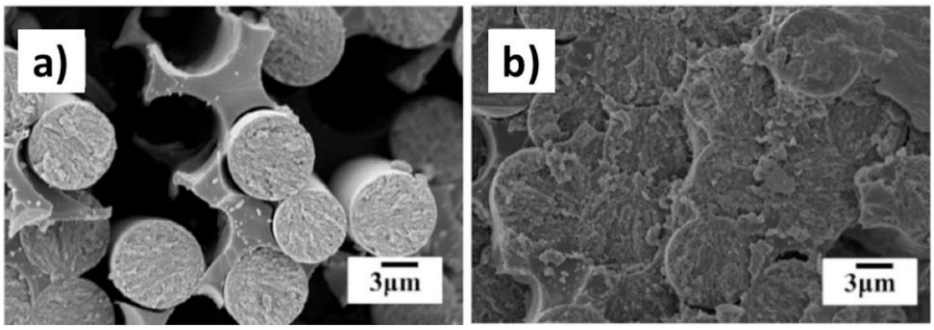

Figure 2.13: SEM micrographs of CF composites fracture samples after flexural 0° test: (a) non-coated CFs, (b) GRM coated CF. From Ref. [45].

2.2.4 Modelling of hierarchical composites

Understanding the macroscopic reinforcement effect of GRM in hierarchical structures is challenging, due to the very different length scales involved. That is why modelling and computational approaches are even more important here than in the study of uniform, conventional composites. Various multiscale numerical models capable of simulating fracture propagation in heterogeneous/hierarchical/multiscale materials have been developed, to capture the mechanisms involved in the optimization of the global material mechanical properties and aid in preparing experimental solutions [79], In a typical multiscale approach, interaction of graphene layers and an epoxy matrix could be first modelled with atomic resolution using Molecular Dynamics (MD), see Fig. 2.14a. The properties calculated in the MD unit cell are then used as input for mesoscopic analysis in a system that contains additional sub-cells of pure epoxy to arrive at the desired GNP volume fraction, using the generalized method of cells (GMC) micromechanics theory, Fig. 2.14b.

Finally, the data obtained for the GNP epoxy matrix are implemented into a GNP/Carbon fiber/Epoxy composite, Fig. 2.14c [80].

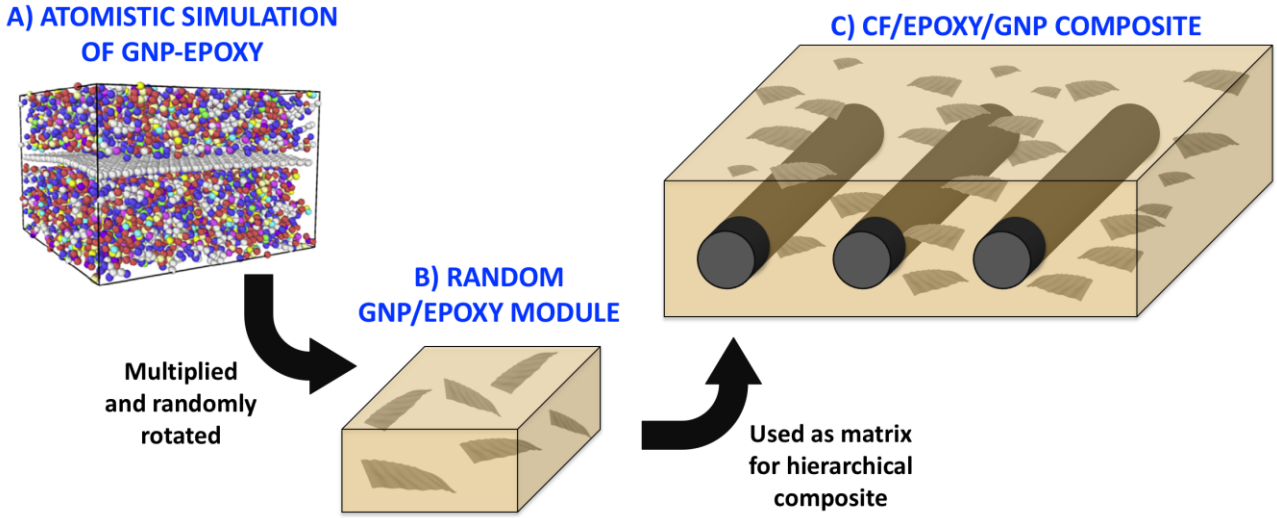

Figure 2.14: Multiscale modeling technique. Adapted from Ref. [80]

The so-called Fiber Bundle Model [81] is also particularly appropriate for the simulation of fibrous materials common in FRC. Hierarchical implementations [82,83] have shown that specific combinations of hierarchy and material heterogeneity can lead to increased strength and toughness thus representing the ideal tool for the optimal design of hierarchical composites. [84]. The Hierarchical Fiber Bundle Model has already been used to estimate the strength and stiffness of hierarchical carbon nanotube fibers, also including the effect of defects at the nanoscale [83]. Further examples of modelling approaches are the Lattice Spring [85] or Random Fuse models [86], which both provide a continuum description of the media through a network of discrete elements (springs or "resistors"), and which have been used to simulate plasticity, damage propagation and avalanche statistics in heterogeneous materials and extended for treating hierarchy. Other computational approaches that could also be used in a multilevel scheme are 3D meshless models (based on the element-free Galerkin method) to simulate complex 3-D heterogeneous media with non-local effects [87] or more standard Finite Element Modelling (FEM strategies) [88].

Fracture nucleation and propagation is challenging to model by FEM, especially in the dynamic regime. Generally, this limit is overcome with the use of erosion algorithms that on the other hand show a strong dependence on the mesh size, and are not feasible with complex geometries at the

mesoscale. An exception to this is a periodic structure, e. g. a honeycomb structure, whereby the whole structure can be characterized by simply modelling the basic cell [89]. Mesh-adaptive refinement on the go can represent a solution, even if it is computationally expensive. When fracture is expected in preferential regions, such as at materials interfaces (e.g., see Ref. [90]), the Cohesive Zone Model (CZM)-based elements can be used to describe the cohesive forces that occur under tensile fracture [91]. Extended FEM (XFEM) approaches need to be used instead for damage propagation within the continuum, implementing enriched shape functions that allow the treatment of discontinuous field functions with singularities without need of mesh refinement. Both are more expensive computationally than standard FEM, so that their use within a model should be carefully assessed. Silling proposed a non-local and integral reformulation of the standard continuum theory of solid mechanics, called *peridynamics* [92]. Unlike partial differential equations, peridynamics equations are applicable even when cracks and other singularities appear in the deformation field. Thus, continuous and discontinuous media can be modelled with a single set of equations. This theory naturally yields a meshless method the non-local response of which represents an ideal bridge between atomistic (MD) and continuum methods (FEM). Improvements in specific extreme properties, e.g. impact toughness, may also be obtained with the aid of numerical design, by the adoption of GRM-based nanocomposites [93,94]. Modelling has been shown to provide new insights into controlling failure initiation in interphase regions between fiber/graphene/matrix, a process complex to understand due to the nonlinear response and intrinsic multiscale feature of the damage in this region [95].

2.3 Possible benefits of graphene in industrial applications of FRC

2.3.1 Challenges for the use of FRC in the aerospace industry

There has been increasing use of FRC materials by the aerospace industry over recent years as can be seen from Fig. 2.15a. A remarkable example is the Airbus A350 XWB, which has its entire fuselage, wing covers and tails made of CFRC – more than half of the structural weight; its production now requires >9000 tons of FRC per year. This can be contrasted with the A300 Airbus produced in the 1970s that contained less than 5% by weight of FRC. The reason for this is that FRC are lighter, stronger and more corrosion resistant than traditional metallic components and provide a higher strength-to-weight ratio. They also require 50% fewer structural maintenance

tasks, and the threshold for airframe checks is at 12 years compared to 8 years for the A380.

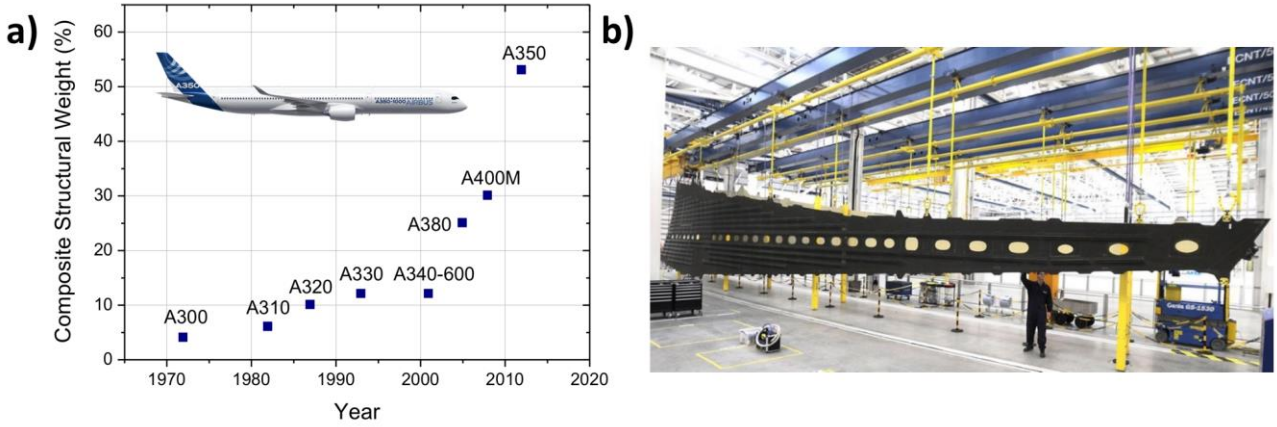

Figure 2.15: a) The percentage by weight of FRC materials in airplanes manufactured by Airbus over the past 50 years. b) The lower CFRC wing cover for a A350 XWB aircraft [96].

Airbus and Boeing in the development of CFRC manufacturing to meet the demanding requirements in modern aviation. Fig. 2.15b shows the 32 m by 6 m lower wing cover for an A350 XWB Airbus. This is the largest single composite part currently being produced in commercial aviation. In spite of this impressive change in materials selection, some of the main challenges that still need to be solved to increase the use of FRC in aerospace further are reported below:

- **Electrical conductivity.** While CFRC can replace metals for structural applications, their electrical conductivity is very low, in particular in the direction perpendicular to the CFRC panel plane. Thus, FRC-based airplanes need to be coated with metallic nets, to act as a Faraday cage against lightning strike. The integration of the electrical functionality within the aircraft composite structure through the application of graphene could yield a significant weight saving. CFRC with electrical conductivities in the order of 105 S/m would be required to remove the metallic nets

. - **Fracture toughness** is critical for CFRC, that can crack after impact with birds or with flying debris. Typical CFRC used for this task have a compression after impact strength (CAI) of 275 MPa. A 20% improvement on such values would be significant.

- **Thermal conductivity** is often an issue in CFRC. The inhomogeneous structure of the composites gives poor and uneven heat transport across the CF and the polymer matrix. Increasing thermal conductivity could benefit key aeronautical applications such as the development of anti- and de-icing of structures, and enabling composite curing and welding through resistive heating [57].

- **Gas barrier properties.** Moisture adsorption due to the airplane changes of altitude and pressure is a critical process in CFRC, because water degrades the mechanical properties of the polymer resins currently used and weakens the resin/fiber interface. Barriers able to slow down or block these processes are highly desirable. Here, key targets would be to reduce diffusion coefficient of water in the material by ≥50%, reduce maximum absorbed water (at equilibrium) also by ≥ 20%, to achieve a maximum water uptake by CF epoxy composite ≤1.5% wt.
- **Multi-functionality.** One of the key areas where more effort is being made is the addition of non-inherent functionalities to aeronautic materials such as *piezo-resistivity***,** to allow deformation and damage sensing in case of impacts, strain and dynamic loads. Also, adding an *energy storage* functionality to structural CFRC is high desirable, due to the ever increasing need of distributed electrical power in all parts of modern airplanes [97]. Another key challenge would be to improve the flame resistance and flame retardant performance of all materials used in aerospace.

2.3.2 Benefits of using GRM in the aerospace industry

GRM are perceived as potential enablers to overcome many of the above-mentioned drawbacks of using composites in aerospace sector. Within the wide scenario of potential applications of GRM to improve aerospace composites, Airbus has defined priorities to focus on, based on added value versus development and industrialization efforts. On the basis of the earlier work [35], as discussed in section 2, GRM can improve the mechanical properties of the composite by hindering or deflecting crack propagation, thus reducing the weight penalty linked to low fracture toughness and/or poor damage tolerance behavior of aeronautical composites. GRM can be a suitable additive to the carbon fiber/epoxy resin prepreg widely used in commercial aircraft such as the A350, where it represents more than 95% of composite structural weight (>100 tons per Aircraft, 13 Aircraft per month), although this material share will likely change for future Long Range and/or Single Aisle aircraft models. GRM can also improve the properties of A350 parts made by RTM (Resin transfer Molding), i.e. the HTP leading edge, the design of which is driven by developing resistance to bird impact [33]. GRM have also been used to decrease the moisture absorption of epoxy resin which leads to significant decrease of properties after Hot/ Wet ageing, by applying the graphene in bulk and/or on the material surface. Significant improvement in water diffusion coefficient and water uptake was observed in aeronautical composites in this way [36]. Multifunctionality properties enabled by GRM have also been demonstrated with the use of flexible graphene papers

and serpentines as electro-thermal systems for de-/anti-icing, which can be integrated industrially in composite parts affected by ice accretion during operation [98]. These innovative approaches will be able to guarantee lightweight, high integration in CFRC and homogeneous thermal behavior in a selected area. This approach can also be used to develop multifunctional applications, for example different thermoelectric systems to be applied always in CFRC as connectors with high electrical conductivity [99] or in moulds for out-of-autoclave curing, which is always a time consuming step in the production of FRC [57]. Another possible application that has been studied is the use of GRM to improve composite lighting strike protection. There have been a number of recent publications on this topic [98,100–102]. Wang and co-workers [100] fabricated a carbon fiber epoxy composite in which rGO had been added to the matrix resin and found that the surface conductivity of the FRC increased from 16 S/cm without the GRM to 440 S/cm on including the GRM. They showed that this led to an improvement in the lightning damage resistance compared with the unmodified CFRP. They pointed out, however, that further improvements in properties would be needed to match the performance of metal protection. The numbers mentioned above are still very far from the one of copper, which has a conductivity of around 6×10^5 S/cm, but also the disadvantage of undergoing corrosion and increasing the airplane weight. It is clear that the results obtained up to now indicate that use of GRM for such lightning strike protection in FRC are challenging, due to the high level of electrical conductivity required, but offer great potential if this issue can be resolved. Table 2.3 summarizes the possible impact of GRM in the different industrial sectors discussed. An estimate of quantitative improvement required is also reported, for reference.

Table 2.3: Summary of possible impact of GRM in different sectors using FRC[1].

					
	Aerospace	**Automotive**	**Wind turbines**	**Pipes**	**Indicative Target[2]**
Structural reinforcement (tensile strength, Young modulus)	**	**	**	*	Depending on application
Fracture toughness (CAI strength)	****	**	***	*	CAI >330 MPa
Electrical conductivity (lightning strike)	****	*	****	*	$\sigma > 10^5$ S/m
Electrical conductivity (antistatic-dissipative)	*	*	*	***	$R_s < 10^9$ Ω/□
Thermal conductivity	***	***	*	*	Depending on application
Gas barrier	***	*	*	*	Water uptake ≤ 1.5% wt.
Multi-functionality	*	****	*	*	Electrical conductivity, Energy storage, damage sensing etc.
Flame resistance	***	***	**	*	HVFAA[3] test passed Burn length<152 mm Flame time <15 s Drip flame time ≤3 s
Better/faster production (e.g. curing time)	****	***	**	**	Ideally, no autoclave required.

[4] Fire Test to Aircraft Material - Airbus Standard.

[a] Potential impact goes from * ¼ incremental benefit up to **** ¼ potential breakthrough.

[b] Requirements depend strongly on the target final applications. Most requirements refer to the most demanding application (aerospace).

[c] FAR: Federal Aviation Regulations; Certification Specifications and Acceptable Means of Compliance for Large Aeroplanes by the European Aviation Safety Agency: CS.

[d] Federal Motor Vehicle Safety Standard No. 302.

[e] Standard for Tests for Flammability of Plastic Materials for Parts in Devices and Appliances.

2.3.3 Challenges for the use of FRC in the automotive industry

A remarkable growth of the presence of FRC in cars is expected in future years, driven principally by the need for a reduction of CO_2 emissions through reduction of weight. A timeline for the amounts of glass and carbon fibers used in the automotive sector over the past 70 years is reported in Fig. 2.16, including some of the milestones of composites in automotive applications. It can be seen that the use of FRC in automotive dates back to the 1950s with the glass fiber reinforced composites(GFRC) being employed in the bodies of kit cars whereas CFRC have only started to be used in recent years, mainly in high-performance vehicles.

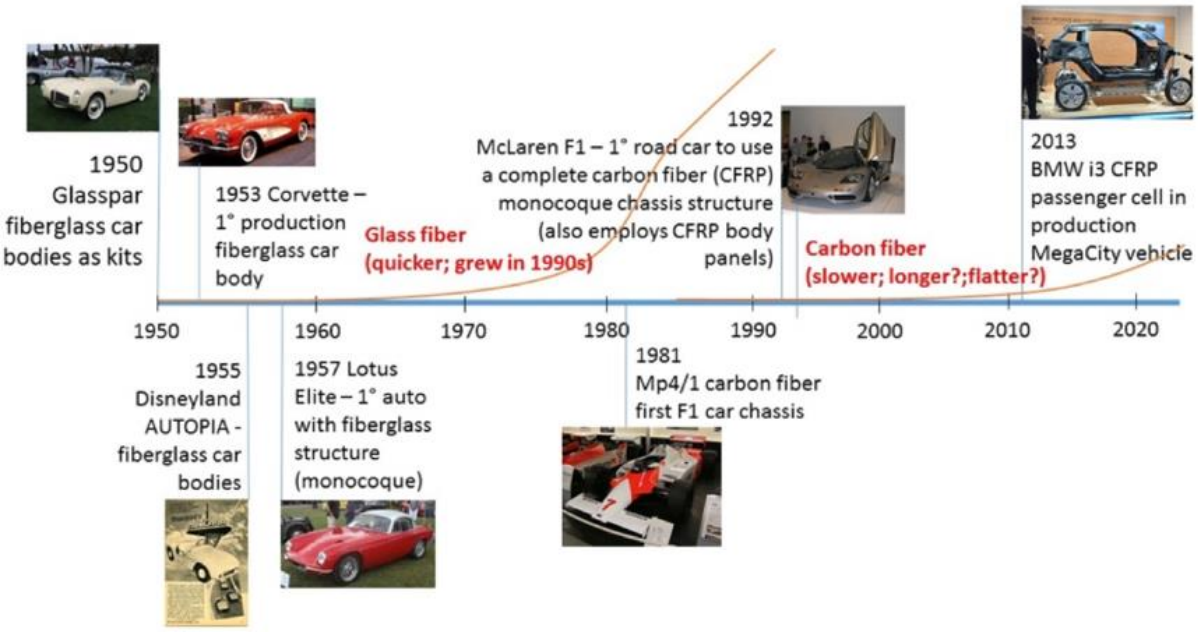

Figure 2.16: Evolution of glass fiber and carbon fiber use in the automotive sector and the main automotive applications [103].

In the near future, the European regulation on the CO_2 emissions will become more demanding, forcing car manufacturers to reduce the amount of materials used by reducing the thickness and modifying the shape of structural parts, whilst maintaining the same mechanical properties. The main efforts in this direction have been to replace metal structural parts with FRC materials. For example, the vehicle bumper beam and the anti-intrusion bar are two structural parts that could be replaced with FRC. Simulations have shown that such elements could be replaced without affecting impact energy absorption [104]. What hinders the use of FRC in the automotive sector being as widespread as in the aerospace sector is cost. The benefits of introducing FRC in the automotive

sector are normally not sufficiently profitable and competitive with respect to the conventional materials. While it is challenging to reduce further the cost of CFRC, more properties and functionalities need to be added to existing FRC to increase their added value in the automotive sector. In particular, future vehicles will be equipped with an increasing number of sensors and devices that will be an integral part of complex features designed to satisfy demanding customer (especially in the Premium brands markets). *Piezo-resistivity* could be a key property that might represent the breakthrough point for CFRC. Moreover, piezo-resistivity will be a fundamental feature for allowing the structural health monitoring of FRC which will increase the reliability of FRC components. Piezoresistivity could also be used to develop a new generation of Human interface devices (e.g. door handles, dashboard controls etc.).

2.3.4 Benefits of using GRM in the automotive industry

The key properties of GRM currently more interesting for the Automotive sector are related to the electrical conductivity of hierarchic composites filled with graphene and related materials. The GRM are planned to be used with the objective of developing new smart automotive components based on polymeric materials with electrically conductive graphenes in order to integrate wirings and switches making them lighter and more environmental friendly (reduction of copper cabling and electronics). The introduction of smart devices (integrated wirings, sensors, switches) in the automotive sectors is expected to enhance the fuel saving and consequently the CO_2 emission at different levels; the number of electronic devices installed in car is continuously growing (more than 60 actuators and 80 sensors are today installed in some cars) and the energy request in the next years on board will increase exponentially (today the average request for power is 3 kW with 4–5 km of wires and 60 kg of weight) with related needs for integrated systems helping the weight reduction and environmental friendly systems. The main focus is on vehicle interiors applications. Polymer and composite applications in the cars increased in the last decade to up to 13% the total weight of the car. Recently, a major car producer has announced large-scale application of GRM (non hierarchic) composites in car interiors to reduce noise inside its vehicles and increase performance under the hood [106]. Besides classical composites, panels and trims functionality can be improved by substituting metal electrical wirings, handles, knobs and touch pads with electrically conductive paths of GRM integrated directly into the polymer bulk materials. GRM have already been used to make innovative pressure sensors [107,108] and highly conductive and

flexible conductors, which can be embedded in polymers or textiles for electronics or internet-of-things applications [99]. The possible advantages of using GRM the industrial process are: 1) Add new functionalities, as example piezoresistive properties in GFRC for sensing. 2) Improve recyclability of dashboard and internal components, through the elimination of electrical wires with CFRP, i.e. rear dashboard connections and switches [109]. 3) Decrease costs of electronics by realizing conductive tracks, without adding any extra material to the component [110], hence decrease component weight by producing all-plastic components. 4) Tune mechanical properties of GFRC and CFRP, which can be settled according to the structural application, i.e. front-end complete system (which is made on GFRC). 5) Ensure compatibility with mass production lines. 6) Replacing metal wires as heating elements in the steering wheel heating system. GRM can give advantages in structures for multifunctional and semi-structural components for: i) system weight reduction (up to 20%), ii) integration capabilities with reduced assembling costs (up to 15%), iii) expected decrease of cost staying within 2–3 €/kg saved and iv) compatibility with existing production processes lines. Advanced racing vehicle technology (as example in Formula 1) is expected to be the spearhead for the GRM-doped FRCs to penetrate the automotive industry at the commercial product level, by introducing mass production multifunctional polymer-based parts with better thermal, impact, weight and flame resistance properties.

2.3.5 Use of FRC in other sectors: wind turbines, pipes and tanks

Wind turbines are one of the largest markets for FRC with a market penetration of 20%, used in blades and in nacelles [111]. FRC (either with glass or carbon fibers) are used to improve the mechanical properties in the most demanding region of the blade spar cap and edges of panels to achieve the fatigue, deflection and buckling specifications. To achieve this goal, an improvement in mechanical performance - particularly the fracture energy GIc, ultimate strength and fatigue response - is needed. Fire represents the second major cause of accidents in wind turbines following lightning strike or blade failure. The combustion of wind turbines can trigger forest fires in many areas, leading to several tens of millions of euros of losses [112,113]. Thus, flame retardancy is a key issue in this field (Table 2.3). Market penetration of composites in pipes and tanks is smaller than in wind turbines, and represents only 3% of the global materials market for this sector. Pipes and tanks manufactured using the centrifugal casting and filament winding processes are primarily used in the oil/gas and chemical industries. There is also here a significant advantage in using FRC

especially in buried pipes for water and waste water projects due to their better chemical resistance compared with metals. Improving FRC electrical conductivity (e.g. for antistatics) and flame resistance would, however, be needed to expand their potential applications and increase market penetration [114,115]. Also in these applications GRM can give significant benefits. For example, we recently demonstrated how amine-functionalized graphene oxide (GO) using aminopropylsilane with low lateral size (D50 ¼ 5 μm) is able to improve the mechanical performance of unsaturated polyester resin (UPR) E-glass fiber composites for wind turbines at low loadings (0.5 wt%) [116]. It has also been demonstrated that GRM can also improve the fire resistance of FRC [117]. Doping a CFRC with 0.5 wt% of graphene materials is able to reduce the peak of the Heat Release Rate (PHHR) by 30%. A 1 wt% loading is able to give rise to reduction of 45% in PHHR in a cone calorimeter test [118,119].

2.4 Examples of FRC-GRM in commercial products

Composite materials represent one of the most mature applications for GRM, with several products already commercially available. Nowadays it is possible to find numerous products for the sports and leisure market that contain GRM, for example: tennis rackets, skis, fishing rods, watches, shoes, hockey sticks, etc. (Fig. 2.17). Here we give some representative, non-exhaustive examples of commercial products with FRC and GRM.

Figure 2.17: Some examples of commercial products using GRM in hierarchic composites.

Innovative materials are often introduced on the market as sporting goods before reaching strategic sectors such as aeronautical and automotive. The first commercial widespread application of GRM was in 2013, when HEAD launched a new tennis racquet series with GRM, which allow the weight redistribution in the racquet (up to 20% lighter) providing better manoeuvrability and increased swing weight. Thanks to the success obtained, in the following years Head commercialized new series of racquets, skis and snowboards reinforced with GRM [120, 121], Padel rackets are also currently commercialized, with GRM claimed to provide more rigidity to the racket, better control over the ball, and resistance [44,122].

Vittoria Industries has developed a new class of cycling tyres and CFRC wheels with GRM. They claimed that GRM-enhanced composites show around 10–30% improvement in material properties. The addition of GRM into the cycle wheels has a great positive impact, reinforcing the brake track for increased safety and durability [123]. Also Dassi released the first cycle with a frame reinforced with GRM giving both a strength and weight benefit [124]. G-Rods International introduced the first GRM-based fishing rods on the market. Their patented graphene technology gives an enhancement of the fishing rods by generating 25% more strength, while reducing weight by 25% [125]. Ashland composites reported in 2016 the first industrial tanks of glass FRC with graphene, developed in collaboration with Avanzare [126,127].

2.5 Conclusions

The use of nano-additives such as GRM in FRC is more challenging than in conventional, non-hierarchic composites such as in extruded plastics. This is due to the FRC complex hierarchic structure, different composition on different length scales, strongly anisotropic properties and presence of several different geometrical interfaces. CF, GRM and polymer matrices can be combined to achieve complex hierarchical structures featuring order on different scales: polymer chains (1–10 nm), GRM nanosheets (10–1000 nm) and mesoscopic glass or carbon fibers (1–1000 μm). The GRM nanosheets can be positioned in the polymer matrix, on the fiber surface, in the pre-peg or in between different FRC layers. Notwithstanding this additional complexity in manufacturing, the first end-user product containing GRM ever mass-produced was a tennis racket made of FRC. Many other similar FRC-GRM products have been commercialized since then. Besides applications already commercialized in sport tools, GRM could give massive breakthroughs in key industrial sectors such as aerospace and automotive, potentially allowing to

overcome some of the major bottlenecks limiting FRC use. Some of the promising applications discussed are to improve impact strength and lightning strike, add flame retardancy or improve thermal conductivity. A challenging but potentially disruptive breakthrough would be to use the complexity of the hierarchical architectures to enable new functionalities, as example to exploit the hierarchic structure of FRC components to store energy, as batteries, or to sense deformation, pressure, etc. This would foster the diffusion of the internet-of-things (IOT) applications also find important uses in the aerospace or automotive sectors.

2.6 References

[1] High Performance Carbon Fibers - National Historic Chemical Landmark, 2003. https://www.acs.org.

[2] [H. Okuda, R.J. Young, F. Tanaka, J. Watanabe, T. Okabe, Tensile failure phenomena in carbon fibres, Carbon 107 (2016) 474–481.

[3] F. Tanaka, T. Okabe, H. Okuda, M. Ise, I.A. Kinloch, T. Mori, R.J. Young, The effect of nanostructure upon the deformation micromechanics of carbon fibres, Carbon 52 (2013) 372–378.

[4] F. Tanaka, T. Okabe, H. Okuda, I.A. Kinloch, R.J. Young, Factors controlling the strength of carbon fibres in tension, Compos. Appl. Sci. Manuf. 57 (2014) 88–94.

[5] R.J. Young, P.A. Lovell, Introduction to Polymers, third ed., CRC Press, Boca Raton, 2011.

[6] D. Hull, T.W. Clyne, An Introduction to Composite Materials, second ed., Cambridge University Press, Cambridge ; New York, 1996.

[7] A. Kovtun, E. Treossi, N. Mirotta, A. Scidà, A. Liscio, M. Christian, F. Valorosi, A. Boschi, R.J. Young, C. Galiotis, I.A. Kinloch, V. Morandi, V. Palermo, Benchmarking of graphene-based materials: real commercial products versus ideal graphene, 2D Mater. 6 (2) (2019) 025006.

[8] H.W. Kroto, J.R. Heath, S.C. Obrien, R.F. Curl, R.E. Smalley, C-60 - Buckminsterfullerene, Nature 318 (6042) (1985) 162–163.

[9] S. Iijima, Helical microtubules of graphitic carbon, Nature 354 (6348) (1991) 56–58.

[10] S. Iijima, T. Ichihashi, Single-Shell carbon nanotubes of 1-nm diameter (vol 363, pg 603, 1993), Nature 364 (6439) (1993), 737-737.

[11] M.M.J. Treacy, T.W. Ebbesen, J.M. Gibson, EXceptionally high Young's modulus observed for individual carbon nanotubes, Nature 381 (6584) (1996) 678–680.

[12] E.W. Wong, P.E. Sheehan, C.M. Lieber, Nanobeam mechanics: elasticity, strength, and toughness of nanorods and nanotubes, Science 277 (5334) (1997) 1971–1975.

[13] C.A. Cooper, R.J. Young, Investigation of structure/property relationships in particulate composites through the use of Raman spectroscopy, J. Raman Spectrosc. 30 (10) (1999) 929–938.

[14] F.M. Blighe, K. Young, J.J. Vilatela, A.H. Windle, I.A. Kinloch, L.B. Deng, R. J. Young, J.N. Coleman, The effect of nanotube content and orientation on the mechanical properties of polymer-nanotube composite

fibers: separating intrinsic reinforcement from orientational effects, Adv. Funct. Mater. 21 (2) (2011) 364–371.

[15] K. Young, F.M. Blighe, J.J. Vilatela, A.H. Windle, I.A. Kinloch, L.B. Deng, R. J. Young, J.N. Coleman, Strong dependence of mechanical properties on fiber diameter for polymer-nanotube composite fibers: differentiating defect from orientation effects, ACS Nano 4 (11) (2010) 6989–6997.

[16] Z. Spitalsky, D. Tasis, K. Papagelis, C. Galiotis, Carbon nanotube-polymer composites: chemistry, processing, mechanical and electrical properties, Prog. Polym. Sci. 35 (3) (2010) 357–401.

[17] L.B. Deng, S.J. Eichhorn, C.C. Kao, R.J. Young, The effective young's modulus of carbon nanotubes in composites, ACS Appl. Mater. Interfaces 3 (2) (2011) 433–440.

[18] J.N. Coleman, U. Khan, W.J. Blau, Y.K. Gun'ko, Small but strong: a review of the mechanical properties of carbon nanotube–polymer composites, Carbon 44 (9) (2006) 1624–1652.

[19] G. Trakakis, D. Tasis, C. Aggelopoulos, J. Parthenios, C. Galiotis, K. Papagelis, Open structured in comparison with dense multi-walled carbon nanotube buckypapers and their composites, Compos. Sci. Technol. 77 (2013) 52–59.

[20] G. Trakakis, G. Anagnostopoulos, L. Sygellou, A. Bakolas, J. Parthenios, D. Tasis, C. Galiotis, K. Papagelis, EpoXidized multi-walled carbon nanotube buckypapers: a scaffold for polymer nanocomposites with enhanced mechanical properties, Chem. Eng. J. 281 (2015) 793–803.

[21] K.S. Novoselov, A.K. Geim, S. Morozov, D. Jiang, Y. Zhang, S. Dubonos, I. Grigorieva, A. Firsov, Electric field effect in atomically thin carbon films, Science 306 (5696) (2004) 666–669.

[22] A.K. Geim, K.S. Novoselov, The rise of graphene, Nat. Mater. 6 (3) (2007) 183–191.

[23] D.G. Papageorgiou, I.A. Kinloch, R.J. Young, Mechanical properties of graphene and graphene-based nanocomposites, Prog. Mater. Sci. 90 (2017) 75–127.

[24] A. Bianco, H.M. Cheng, T. Enoki, Y. Gogotsi, R.H. Hurt, N. Koratkar, T. Kyotani, M. MonthiouX, C.R. Park, J.M.D. Tascon, J. Zhang, All in the graphene family - a recommended nomenclature for two-dimensional carbon materials, Carbon 65 (2013) 1–6.

[25] P. Wick, A.E. Louw-Gaume, M. Kucki, H.F. Krug, K. Kostarelos, B. Fadeel, K. A. Dawson, A. Salvati, E. Vazquez, L. Ballerini, M. Tretiach, F. Benfenati, E. Flahaut, L. Gauthier, M. Prato, A. Bianco, Classification framework for graphene-based materials, Angew. Chem. Int. Ed. 53 (30) (2014) 7714–7718.

[26] C. Lee, X. Wei, J.W. Kysar, J. Hone, Measurement of the elastic properties and intrinsic strength of monolayer graphene, Science 321 (5887) (2008) 385–388.

[27] J.N. Coleman, M. Lotya, A. O'Neill, S.D. Bergin, P.J. King, U. Khan, K. Young, A. Gaucher, S. De, R.J. Smith, I.V. Shvets, S.K. Arora, G. Stanton, H.Y. Kim, K. Lee, G.T. Kim, G.S. Duesberg, T. Hallam, J.J. Boland, J.J. Wang, J.F. Donegan, J. C. Grunlan, G. Moriarty, A. Shmeliov, R.J. Nicholls, J.M. Perkins, E.M. Grieveson, K. Theuwissen, D.W. McComb, P.D. Nellist, V. Nicolosi, Two-dimensional nanosheets produced by liquid exfoliation of layered materials, Science 331 (6017) (2011) 568–571.

[28] K.R. Paton, E. Varrla, C. Backes, R.J. Smith, U. Khan, A. O'Neill, C. Boland, M. Lotya, O.M. Istrate, P. King, T. Higgins, S. Barwich, P. May, P. Puczkarski,I. Ahmed, M. Moebius, H. Pettersson, E. Long, J. Coelho, S.E. O'Brien, E. K. McGuire, B.M. Sanchez, G.S. Duesberg, N. McEvoy, T.J. Pennycook, C.

Downing, A. Crossley, V. Nicolosi, J.N. Coleman, Scalable production of large quantities of defect-free few-layer graphene by shear exfoliation in liquids, Nat. Mater. 13 (6) (2014) 624–630.

[29] A.E. Del Rio Castillo, V. Pellegrini, A. Ansaldo, F. Ricciardella, H. Sun, L. Marasco, J. Buha, Z. Dang, L. Gagliani, E. Lago, N. Curreli, S. Gentiluomo, F. Palazon, M. Prato, R. Oropesa-Nun~ez, P.S. Toth, E. Mantero, M. Crugliano, A. Gamucci, A. Tomadin, M. Polini, F. Bonaccorso, High-yield production of 2D crystals by wet-jet milling, Materials Horizons 5 (5) (2018) 890–904.

[30] I.A. Kinloch, J. Suhr, J. Lou, R.J. Young, P.M. Ajayan, Composites with carbon nanotubes and graphene: an outlook, Science 362 (6414) (2018) 547–553.

[31] T. Ramanathan, A.A. Abdala, S. Stankovich, D.A. Dikin, M. Herrera-Alonso, R. D. Piner, D.H. Adamson, H.C. Schniepp, X. Chen, R.S. Ruoff, S.T. Nguyen, I. A. Aksay, R.K. Prud'homme, L.C. Brinson, Functionalized graphene sheets for polymer nanocomposites, Nat. Nanotechnol. 3 (6) (2008) 327–331.

[32] R.J. Young, I.A. Kinloch, L. Gong, K.S. Novoselov, The mechanics of graphene nanocomposites: a review, Compos. Sci. Technol. 72 (12) (2012) 1459–1476.

[33] Graphene flagship, Deliverable D15.5, https://graphene-flagship.eu/search/P ages/deliverablesresults.aspX.

[34] Y. Li, H. Zhang, Z.H. Huang, E. Bilotti, T. Peijs, Graphite nanoplatelet modified epoXy resin for carbon fibre reinforced plastics with enhanced properties, J. Nanomater. (2017) #9.

[35] X.S. Du, H.L.Z. Zhou, W.F. Sun, H.Y. Liu, G.N. Zhou, H.M. Zhou, Y.W. Mai, Graphene/epoXy interleaves for delamination toughening and monitoring of crack damage in carbon fibre/epoXy composite laminates, Compos. Sci. Technol. 140 (2017) 123–133.

[36] T. Blanco, J. Sanchez Gomez, S. Lazcano, V. Palermo, E. Treossi, N. Mirotta, A. Scidà, MultifunctionaL Diffusion Barrier, WIPO patent WO2018167255, 2018.

[37] P.Y. Hung, K.T. Lau, B. FoX, N. Hameed, J.H. Lee, D. Hui, Surface modification of carbon fibre using graphene-related materials for multifunctional composites, Compos. B Eng. 133 (2018) 240–257.

[38] R.L. Zhang, B. Gao, Q.H. Ma, J. Zhang, H.Z. Cui, L. Liu, Directly grafting graphene oXide onto carbon fiber and the effect on the mechanical properties of carbon fiber composites, Mater. Des. 93 (2016) 364–369.

[39] Y.B. Li, Q.Y. Peng, X.D. He, P.A. Hu, C. Wang, Y.Y. Shang, R.G. Wang, W.C. Jiao, H.Z. Lv, Synthesis and characterization of a new hierarchical reinforcement by chemically grafting graphene oXide onto carbon fibers, J. Mater. Chem. 22 (36) (2012) 18748–18752.

[40] R.L. Zhang, B. Gao, W.T. Du, J. Zhang, H.Z. Cui, L. Liu, C.G. Wang, F.H. Li, Enhanced mechanical properties of multiscale carbon fiber/epoXy composites by fiber surface treatment with graphene oXide/polyhedral oligomeric silsesquioXane, Compos. A Appl. Sci. Manuf. 84 (2016) 455–463.

[41] J. Chen, D. Zhao, X. Jin, C.C. Wang, D.Z. Wang, H.Y. Ge, Modifying glass fibers with graphene oXide: towards high-performance polymer composites, Compos. Sci. Technol. 97 (2014) 41–45.

[42] W.Z. Qin, F. Vautard, L.T. Drzal, J.R. Yu, Modifying the carbon fiber-epoXy matriX interphase with graphite nanoplatelets, Polym. Compos. 37 (5) (2016) 1549–1556.

[43] H. Zhang, Y. Liu, S.S. Huo, J. Briscoe, W. Tu, O.T. Picot, A. Rezai, E. Bilotti, T. Peijs, Filtration effects of graphene nanoplatelets in resin infusion processes: problems and possible solutions, Compos. Sci. Technol. 139 (2017) 138–145.

[44] Antolin-group. www.granph-acm.com.

[45] W.Z. Qin, F. Vautard, L.T. Drzal, J.R. Yu, Mechanical and electrical properties of carbon fiber composites with incorporation of graphene nanoplateletsat the fiber- matriX interphase, Compos. B Eng. 69 (2015) 335–341.

[46] S. Menbari, A. Ashori, H. Rahmani, R. Bahrami, Viscoelastic response and interlaminar delamination resistance of epoXy/glass fiber/functionalized graphene oXide multi-scale composites, Polym. Test. 54 (2016) 186–195.

[47] G.J. Ehlert, Y.R. Lin, H.A. Sodano, CarboXyl functionalization of carbon fibers through a grafting reaction that preserves fiber tensile strength, Carbon 49 (13) (2011) 4246–4255.

[48] W. Luo, B. Zhang, H.W. Zou, M. Liang, Y. Chen, Enhanced interfacial adhesion between polypropylene and carbon fiber by graphene oXide/polyethyleneimine coating, J. Ind. Eng. Chem. 51 (2017) 129–139.

[49] D. Pierleoni, M. Minelli, S. Ligi, M. Christian, S. Funke, N. Reineking, V. Morandi, F. Doghieri, V. Palermo, Selective gas permeation in graphene oXide–polymer self-assembled multilayers, ACS Appl. Mater. Interfaces 10 (13) (2018) 11242–11250.

[50] Z.Y. Xia, M. Christian, C. Arbizzani, V. Morandi, M. Gazzano, V. Quintano, Kovtun, V. Palermo, A robust, modular approach to produce graphene–MOX multilayer foams as electrodes for Li-ion batteries, Nanoscale 11 (12) (2019) 5265–5273.

[51] H. Mahmood, A. Pegoretti, D. Pedrazzoli, K. Kalaitzidou, Improving fiber/matriX interfacial strength through graphene and graphene-oXide nano platelets, Mater. Sci. Eng. 139 (2016), 012004.

[52] F. Li, Y. Liu, C.B. Qu, H.M. Xiao, Y. Hua, G.X. Sui, S.Y. Fu, Enhanced mechanical properties of short carbon fiber reinforced polyethersulfone composites by graphene oXide coating, Polymer 59 (2015) 155–165.

[53] C.F. Wang, J. Li, S.F. Sun, X.Y. Li, F. Zhao, B. Jiang, Y.D. Huang, Electrophoretic deposition of graphene oXide on continuous carbon fibers for reinforcement of both tensile and interfacial strength, Compos. Sci. Technol. 135 (2016) 46–53.

[54] J.M. Wu, J. Chen, Y.Y. Zhao, W.X. Liu, W.B. Zhang, Effect of electrophoretic condition on the electromagnetic interference shielding performance of reduced graphene oXide-carbon fiber/epoXy resin composites, Compos. B Eng. 105 (2016) 167–175.

[55] Y. Li, H. Zhang, Y. Liu, H.S. Wang, Z.H. Huang, T. Peijs, E. Bilotti, Synergistic effects of spray-coated hybrid carbon nanoparticles for enhanced electrical and thermal surface conductivity of CFRP laminates, Compos. Appl. Sci. Manuf. 105 (2018) 9–18.

[56] A.J. Marsden, D.G. Papageorgiou, C. Valles, A. Liscio, V. Palermo, M.A. Bissett, R. J. Young, I.A. Kinloch, Electrical percolation in graphene-polymer composites, 2D Mater. 5 (3) (2018), 032003.

[57] L. Mazzocchetti, T. Benelli, E. D'Angelo, S. Ligi, G. Minak, E. Poodts, F. Tarterini, V. Palermo, L. Giorgini, Managing heat phenomena in epoXy composites production via graphenic derivatives: synthesis, properties and industrial production simulation of graphene and graphene oXide containing composites, 2D Mater. 4 (1) (2017) #015020.

[58] L. Gong, I.A. Kinloch, R.J. Young, I. Riaz, R. Jalil, K.S. Novoselov, Interfacial stress transfer in a graphene monolayer nanocomposite, Adv. Mater. 22 (24) (2010) 2694.

[59] E. Pisanova, S. Zhandarov, E. Mader, I. Ahmad, R.J. Young, Three techniques of interfacial bond strength estimation from direct observation of crack initiation and propagation in polymer-fibre systems, Compos. Appl. Sci. Manuf. 32 (3–4) (2001) 435–443.

[60] X.Q. Zhang, X.Y. Fan, C. Yan, H.Z. Li, Y.D. Zhu, X.T. Li, L.P. Yu, Interfacial microstructure and properties of carbon fiber composites modified with graphene oXide, ACS Appl. Mater. Interfaces 4 (3) (2012) 1543–1552.

[61] M.W. Lee, T.Y. Wang, J.L. Tsai, Characterizing the interfacial shear strength of graphite/epoXy composites containing functionalized graphene, Compos. B Eng. 98 (2016) 308–313.

[62] G. Tsoukleri, J. Parthenios, K. Papagelis, R. Jalil, A.C. Ferrari, A.K. Geim, K. S. Novoselov, C. Galiotis, Subjecting a graphene monolayer to tension and compression, Small 5 (21) (2009) 2397–2402.

[63] G. Anagnostopoulos, C. Androulidakis, E.N. Koukaras, G. Tsoukleri, I. Polyzos, J. Parthenios, K. Papagelis, C. Galiotis, Stress transfer mechanisms at the submicron level for graphene/polymer systems, ACS Appl. Mater. Interfaces 7 (7) (2015) 4216–4223.

[64] C. Androulidakis, E.N. Koukaras, J. Rahova, K. Sampathkumar, J. Parthenios, K. Papagelis, O. Frank, C. Galiotis, Wrinkled few-layer graphene as highly efficient load bearer, ACS Appl. Mater. Interfaces 9 (31) (2017) 26593–26601.

[65] A. Manikas, M. Pastore Carbone, C. Woods, Y. Wang, I. Souli, G. Anagnostopoulos, M. Hadjinicolaou, K. Novoselov, C. Galiotis, Stress transfer at the nanoscale on graphene ribbons of regular geometry, Nanoscale 11 (2019), 14354.

[66] V. Palermo, I.A. Kinloch, S. Ligi, N.M. Pugno, Nanoscale mechanics of graphene and graphene oXide in composites: a scientific and technological perspective, Adv. Mater. 28 (29) (2016) 6232–6238.

[67] N. Koutroumakis, Interface investigation of CFRP and CFR hybrid polymer composites, ECCM 2018, in: Proceeding of the 18th European Conference on Composite Materials, 2018.

[68] G. Anagnostopoulos, G. Paterakis, I. Polyzos, P.N. Pappas, K. Kouroupis-Agalou, N. Mirotta, A. Scida, V. Palermo, J. Parthenios, K. Papagelis, C. Galiotis, Strain engineering in highly wrinkled CVD graphene/epoXy systems, ACS Appl. Mater. Interfaces 10 (49) (2018) 43192–43202.

[69] G. Wang, E. Gao, Z. Dai, L. Liu, Z. Xu, Z. Zhang, Degradation and recovery of graphene/polymer interfaces under cyclic mechanical loading, Compos. Sci. Technol. 149 (Supplement C) (2017) 220–227.

[70] J.-H. Lee, D.-W. Jang, S.-G. Hong, B.C. Park, J.-H. Kim, H.-J. Jung, S.-B. Lee, Fracture mechanism and electromechanical behavior of chemical vapor deposited graphene on flexible substrate under tension, Carbon 118 (2017) 475–484.

[71] A.C. Koutroumanis, P.N. Pappas, C. Galiotis, Interface Investigation of CFRP and CFR Hybrid Polymer Composites ECCM 2018 - Proceeding of the 18th European Conference on Composite Materials, Athens, Greece, 2018, 2018.

[72] B.K. Deka, A. Hazarika, K. Kong, D. Kim, Y.B. Park, H.W. Park, Interfacial resistive heating and mechanical properties of graphene oXide assisted CuO nanoparticles in woven carbon fiber/polyester composite, Compos. Appl. Sci. Manuf. 80 (2016) 159–170.

[73] A. Ashori, H. Rahmani, R. Bahrami, Preparation and characterization of functionalized graphene oXide/carbon fiber/epoXy nanocomposites, Polym. Test. 48 (2015) 82–88.

[74] S.A. Jiang, Q.F. Li, J.W. Wang, Z.L. He, Y.H. Zhao, M.Q. Kang, Multiscale graphene oXide-carbon fiber reinforcements for advanced polyurethane composites, Compos. A Appl. Sci. Manuf. 87 (2016) 1–9.

[75] J.W. Chu, R.J. Young, T.J.A. Slater, T.L. Burnett, B. Coburn, L. Chichignoud, Vuilleumier, Z.L. Li, Realizing the theoretical stiffness of graphene in composites through confinement between carbon fibers, Compos. A Appl. Sci. Manuf. 113 (2018) 311–317.

[76] L.M. Malard, M.A. Pimenta, G. Dresselhaus, M.S. Dresselhaus, Raman spectroscopy in graphene, Physics Reports-Review Section of Physics Letters 473 (5–6) (2009) 51–87.

[77] A.C. Koutroumanis, Interface investigation of hybrid polymer composites with graphene modified matriX, in: Proceedings of the 12th Hellenic Conference of Chemical Engineering, 2019.

[78] V.K. Srivastava, T. Gries, D. Veit, T. Quadflieg, B. Mohr, M. Kolloch, Effect of nanomaterial on mode I and mode II interlaminar fracture toughness of woven carbon fabric reinforced polymer composites, Eng. Fract. Mech. 180 (2017) 73–86.

[79] G.B. Olson, Computational design of hierarchically structured materials, Science 277 (5330) (1997) 1237–1242.

[80] O. Aluko, S. Gowtham, G.M. Odegard, Multiscale modeling and analysis of graphene nanoplatelet/carbon fiber/epoXy hybrid composite, Compos. B Eng. 131 (2017) 82–90.

[81] S. Pradhan, A. Hansen, B.K. Chakrabarti, Failure processes in elastic fiber bundles, Rev. Mod. Phys. 82 (1) (2010) 499–555.

[82] L. Mishnaevsky, Hierarchical composites: analysis of damage evolution based on fiber bundle model, Compos. Sci. Technol. 71 (4) (2011) 450–460.

[83] N.M. Pugno, F. Bosia, A. Carpinteri, Multiscale stochastic simulations for tensile testing of nanotube-based macroscopic cables, Small 4 (8) (2008) 1044–1052.

[84] F. Bosia, T. Abdalrahman, N. Pugno, Investigating the role of hierarchy on the strength of composite materials: evidence of a crucial synergy between hierarchy and material miXing, Nanoscale 4 (Modelling for the nanoscale) (2012) 1200–1207.

[85] G.A. BuXton, C.M. Care, D.J. Cleaver, A lattice spring model of heterogeneous materials with plasticity, Model. Simul. Mater. Sci. Eng. 9 (6) (2001) 485–497.

[86] S. Zapperi, A. Vespignani, H.E. Stanley, Plasticity and avalanche behaviour in microfracturing phenomena, Nature 388 (1997) 658.

[87] S.W. Yang, P.R. Budarapu, D.R. Mahapatra, S.P.A. Bordas, G. Zi, T. Rabczuk, A meshless adaptive multiscale method for fracture, Comput. Mater. Sci. 96 (2015) 382–395.

[88] B. Bar-On, F.G. Barth, P. Fratzl, Y. Politi, Multiscale structural gradients enhance the biomechanical functionality of the spider fang, Nat. Commun. 5 (2014).

[89] Q. Chen, Q. Shi, S. Signetti, F.F. Sun, Z.Y. Li, F.P. Zhu, S.Y. He, N.M. Pugno, Plastic collapse of cylindrical shell-plate periodic honeycombs under uniaxial compression: experimental and numerical analyses, Int. J. Mech. Sci. 111 (2016) 125–133.

[90] C.E. Killian, R.A. Metzler, Y.T. Gong, T.H. Churchill, I.C. Olson, V. Trubetskoy, M.B. Christensen, J.H. Fournelle, F. De Carlo, S. Cohen, J. Mahamid, A. Scholl, Young, A. Doran, F.H. Wilt, S.N. Coppersmith, P. Gilbert, Self-sharpening mechanism of the sea urchin tooth, Adv. Funct. Mater. 21 (4) (2011) 682–690.

[91] M. Elices, G.V. Guinea, J. Gomez, J. Planas, The cohesive zone model: advantages, limitations and challenges, Eng. Fract. Mech. 69 (2) (2002) 137–163.

[92] S.A. Silling, Reformulation of elasticity theory for discontinuities and long-range forces, J. Mech. Phys. Solids 48 (1) (2000) 175–209.

[93] J.-H. Lee, P.E. Loya, J. Lou, E.L. Thomas, Dynamic mechanical behavior of multilayer graphene via supersonic projectile penetration, Science 346 (6213) (2014) 1092–1096.

[94] K. Yoon, A. Ostadhossein, A.C.T. van Duin, Atomistic-scale simulations of the chemomechanical behavior of graphene under nanoprojectile impact, Carbon 99 (2016) 58–64.

[95] J.P. Johnston, B. Koo, N. Subramanian, A. Chattopadhyay, Modeling the molecular structure of the carbon fiber/polymer interphase for multiscale analysis of composites, Compos. B Eng. 111 (2017) 27–36.

[96] Airbus, www.airbus.com.

[97] G. Fredi, S. Jeschke, A. Boulaoued, J. Wallenstein, M. Rashidi, F. Liu, R. Harnden, D. Zenkert, J. Hagberg, G. Lindbergh, P. Johansson, L. Stievano, L.E. Asp, Graphitic microstructure and performance of carbon fibre Li-ion structural battery electrodes, Multifunctional Materials 1 (1) (2018) 015003.

[98] P. Nordin, Graphene De-icing/Anti-icing and Lightning Strike Protection, 2015. www.innovativesurfaces.ch/vio/images/NordinPart4.pdf.

[99] A. Scida, S. Haque, E. Treossi, A. Robinson, S. Smerzi, S. Ravesi, S. Borini, V. Palermo, Application of graphene-based flexible antennas in consumer electronic devices, Mater. Today 21 (3) (2018) 223–230.

[100] B. Wang, Y.G. Duan, Z.B. Xin, X.L. Yao, D. Abliz, G. Ziegmann, Fabrication of an enriched graphene surface protection of carbon fiber/epoXy composites for lightning strike via a percolating-assisted resin film infusion method, Compos. Sci. Technol. 158 (2018) 51–60.

[101] M. Raimondo, L. Guadagno, V. Speranza, L. Bonnaud, P. Dubois, K. Lafdi, Multifunctional graphene/POSS epoXy resin tailored for aircraft lightning strike protection, Compos. B Eng. 140 (2018) 44–56.

[102] S.A.S. Kumar, M.N. Udin, N.N. Raman, R. Asmatulu, Introducing graphene thin films into carbon fiber composite structures for lightning strike protection, Polym. Compos. (2019) E517–E523.

[103] Fiat-Chrysler-Automobiles, www.fcagroup.com.

[104] G. Belingardi, Lightweight solutions for vehicle frontal bumper: crash design and manufacturing issues, in: Elsevier (Ed.), Dynamic Response and Failure of Composite Materials and Structures, Amsterdam, 2017.

[105] G. Colucci, O. Ostrovskaya, A. Frache, B. Martorana, C. Badini, The effect of mechanical recycling on the microstructure and properties of PA66 composites reinforced with carbon fibers, J. Appl. Polym. Sci. 132 (29) (2015).

[106] Ford, Cell phones, sporting goods, and soon, cars: Ford innovates with “miracle”material, powerful graphene for vehicle parts, https://media.ford.com.

[107] C.-B. Huang, S. Witomska, A. Aliprandi, M.-A. Stoeckel, M. Bonini, A. Ciesielski, P. Samorì, Molecule–graphene hybrid materials with tunable mechanoresponse: highly sensitive pressure sensors for health monitoring, Adv. Mater. 31 (1) (2019) 1804600.

[108] C.S. Boland, U. Khan, C. Backes, A. O’Neill, J. McCauley, S. Duane, R. Shanker, Y. Liu, I. Jurewicz, A.B. Dalton, J.N. Coleman, Sensitive, high-strain, high-rate bodily motion sensors based on graphene-rubber composites, ACS Nano 8 (9) (2014) 8819–8830.

[109] A. Veca, Motor-vehicle Passenger-Compartment Component, and a Method for Manufacturing This Component, US10005390B2, 2018.

[110] A. Zecchina, D. Demarchi, A. Veca, Process for Producing Conductive And/or Piezoresistive Traces on a Polymeric substrate., WO/2012/055934, 2012.

[111] L. Mishnaevsky, K. Branner, N.H. Petersen, J. Beauson, M. McGugan, F. B. Sørensen, Materials for wind turbine blades: an overview, Materials 10 (11) (2017).

[112] CFPA, Wind Turbines Fire Protection Guideline, 2012.

[113] S. Uadiale, Overview of problems and solutions in fire protection engineering of wind turbines, Fire Saf. Sci. 11 (2014) 983.

[114] P. Tran, Q.T. Nguyen, K.T. Lau, Fire performance of polymer-based composites for maritime infrastructure, Compos. B Eng. 155 (2018) 31–48.

[115] M. Biron, Future prospects for thermoplastics and thermoplastic composites, in: W.A. Publishing (Ed.), Thermoplastics and Thermoplastic Composites, third ed., 2018.

[116] J. Gomez, Relevance of an Adequate Selection of the Graphene Materials and Processing Conditions in the Preparation of GRM Composites, GRAPHIN, Bilbao, 2018, 2018.

[117] A.F. Avila, M.I. Yoshida, M.G.R. Carvalho, E.C. Dias, J. de Avila, An investigation on post-fire behavior of hybrid nanocomposites under bending loads, Compos. B Eng. 41 (5) (2010) 380–387.

[118] E. Garrido, Preparation of New Multifunctional EpoXy MatriX Nanocomposites Using Graphene Materials, Ph.D. Thesis - Universidad de La Rioja, 2017.

[119] F. Bertocchi, G. Giannini, M. Maione, Graphene-based sheets, method for preparing said sheets, composite material and uses of said graphene-based sheets, Eur. Patent EP3081604A1 (2016).

[120] Head, http://www.head.com/g/us/graphene/.

[121] R.J. Young, M.F. Liu, The microstructure of a graphene-reinforced tennis racquet, J. Mater. Sci. 51 (8) (2016) 3861–3867.

[122] siuX-diablo-granph, Padel, www.padelnuestro.com.

[123] Vittoria, http://www.vittoria.com/wheel/race/.

[124] Dassi, https://dassi.com/.

[125] G-rods, https://g-rods.com/.

[126] Ashland, Graphene boosts resin performance, www.insidecomposites.com.

[127] Ashland, Product reference 873044.

3. Benchmarking of commercial GRM-based master batches

Polymers have long been studied in order to improve their characteristics by adding fillers such as silica, clay, reinforced fibers, and other anisotropic reinforcements to create composite and hybrid materials. The incorporation of nanofillers such as GRM into polymers to produce polymer nanocomposites is a recent development. Polymer nanocomposites have demonstrated superior mechanical, thermal, optical, and electrical capabilities than neat polymer materials [1-2-3-4-5]. In this chapter we characterized commercial GRM-based master-batches from different industrial suppliers all over the world evaluating the morphological, thermal and electrical properties compared to the bare polymers. These analyses are not exhaustive of all the benefits that GRM could bring in the commercial products but they give an idea of which kind of GRM has been employed and the enhancements from electrical and thermal point of view. In section 3.1 the advantages that GRM could bring in polymer will be briefly described especially those ones indicated by the manufacturers, followed by a quick overview on the materials that we studied. Section 3.2 will be focused on the techniques used for the morphological, thermal and electrical characterization while in section 3.3 the overall results will be given in order to show the main trends associated to GRM.

3.1 Introduction

New materials have always prompted the development of new technologies. In recent years, there has been considerable progress in the field of composites. They have been widely employed in a variety of applications such as aerospace, automotive, biotechnology, electrochemical sensors, energy storage, and so on, as previously discussed. Because composite materials are made up of many phases, the continuous phase is known as the “matrix” phase, and the other phases scattered in the matrix are known as “reinforcement” (fibers, particles, and layered materials) [1].

At the macro scale, the distribution of reinforcement in the matrix and its size identify the properties of composite materials. Graphene, a one-atom thick planar sheet of carbon atoms with a honeycomb crystal lattice structure, has intrigued researchers due to its interesting features among the nanofillers applied to polymer materials. Four major elements influence GRM's function in improving the mechanical characteristics of polymers and they are:

1. Excellent mechanical characteristics of graphene;

2. High aspect ratio and great surface area of graphene nanoplatelets (GNP) addition in the polymer;
3. GRM distribution uniformity in the polymer matrix;
4. GRM-polymer matrix binding strength.

Polymer nanocomposites containing graphene nanofillers have demonstrated superior mechanical, thermal, and electrical characteristics than pure polymer materials. The strength and conductivity of polymer composites can be enhanced by overcoming weak van der Waals forces and splitting bulk graphite into few carbon layer platelets. Many studies have encountered aggregation of graphene particles in the composite during the manufacture of nanocomposites. As a result, dispersion of the filler in the polymer is a significant difficulty and still challenging for both researchers and industry [5].

3.1.1 Commercial GRM-based master batches

We purchased several commercial GRM-based master batched from industrial companies. In table 3.1 we reported the list of the companies and the respective products that we characterized.

United Nanotech Innovations was a subsidiary of United Motors & Heavy Equipment which produces both industrial and research grade of graphene. The company worked in three major segments production of graphene oxide & carbon nanotubes, application development of carbon nano-materials and R&D in the field of nanotechnology. Products offered by the company includes graphene oxide, reduced graphene oxide, single & multi-walled CNT, and graphene phosphate. Currently, it seems as if the company is no longer in business [6].

NanoXplore produces graphene and related composites used to improve material performance across a wide range of industries. Graphene-polymer composites are particularly interesting as the addition of very small amounts of graphene can dramatically improve the properties of the base polymer. Excellent improvements in thermal conductivity, anti-corrosion protection and mechanical strength have been achieved [7].

Thomas Swan's Advanced Materials division is a global leader and innovator in the R&D and manufacturing of graphene and other 2D-nanomaterials. They claim to have the ability to manufacture 20-40 tonnes of high-quality, bulk graphene products, and to integrate nanomaterials into their customers' wide ranging applications from nanocomposites to concrete, lubricants and batteries [8].

CANOE is a R&D center specialized in formulation and manufacturing techniques for the development of finished and semi-finished products in the field of composites and advanced materials. They assist companies in the development of innovative products and processes to meet industrial needs [9].

Suppliers	GRM-based master batch
United Nanotech Innovations	Neat PC
	PC+ 5% wt GRM
	Neat PP
	PP + 5% wt GRM
NanoXplore	PA66 + 15 % wt GRM
	PP + 15 % wt GRM
Thomas Swan	Neat LDPE
	LDPE + 10% wt GRM
CANOE	Neat PP
	PP + 20% wt GRM
	Neat PA12
	PA12 + 20% wt GRM
	Neat PEEK
	PEEK + 20% wt GRM

Table 3.1: List of the companies and their GRM-based master batches.

As indicated in the technical data sheet, all these GRM based master batches are generally designed to exhibit:

- Superior mechanical properties, e.g. strength, modulus and dimensional stability;
- Thermal stability;
- Flame retardancy and reduced smoke emissions;
- Chemical resistance;
- Electrical and thermal conductivity.

Many traditional components can benefit from these improvements, for example, aircraft interior and engine components, dashboards and instrumental panel. Moreover, microelectronic enclosures, passive heat sinks with complex shapes, and novel electrical motor casings, all with superior heat dissipation performance, can be created. Polymers are used in a wide range of challenging engineering applications, from composite wind turbine blades in the renewable energy sector to highly complex structural parts of airplanes [7].

3.2 Methods

We assessed the characteristics of the GRM-based master batches using morphological, thermal and electrical analyses such as SEM-EDS, XRD, TGA, DSC and 4-point probe.

3.2.1 Scanning Electron Microscopy / Energy Dispersive Spectroscopy (SEM-EDS)

The most well-known and commonly used surface analysis technique is scanning electron microscopy with energy dispersive spectroscopy (SEM/EDS). A highly focused, scanning (primary) electron beam is utilized to generate high resolution pictures of surface topography with an exceptional depth of field. Primary electrons with energies ranging from 0.5 to 30 kV enter a surface and create a large number of low energy secondary electrons. The strength of these secondary electrons is substantially determined by the sample's surface topography. By monitoring secondary electron intensity as a function of the position of the scanning primary electron beam, a picture of the sample surface may be produced.

Because the main electron beam may be focused to a very small point (10 nm), high spatial resolution is feasible. When a primary electron beam with an energy of 1 kV is used, a high sensitivity to topographic features on the outermost surface (< 5 nm) is attained. Primary electron bombardment produces backscattered electrons and X-rays in addition to low energy secondary electrons. The atomic number of the element inside the sample volume may be used to calculate the intensity of backscattered electrons. As a result, some qualitative elemental data can be collected. The study of distinctive X-rays generated by the material (EDX or EDS analysis) provides more quantitative elemental information. This type of X-ray analysis may be performed in analytical volumes as tiny as 1 cubic micron. SEM, in conjunction with X-ray examination, is regarded as a reasonably quick, low-cost, and essentially non-destructive method of surface investigation [10].

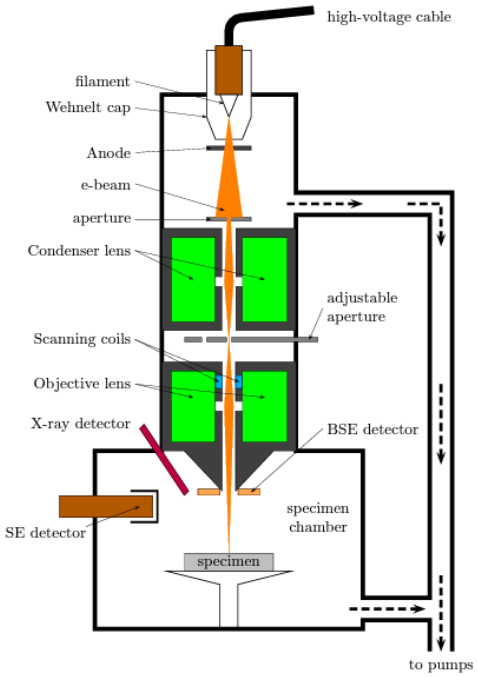

Figure 3.1: Schematic representation of the scanning electron microscope [11].

Two SEMs were utilized in this thesis, both installed at CNR-IMM laboratories in Bologna. A Gemini 1530 with a field-emission gun and an EVO LS 10 with a LaB6 thermionic source, both manufactured by Zeiss. The EVO LS10 can be operated at variable column pressure for analysis of poorly-conducting surfaces.

3.2.2 X-Ray Diffraction (XRD)

Soft x-ray radiation with energy in the few keV range has a wavelength in the sub-nm range and may thus be used as a probe for resolving atomic structures. Indeed, x-ray diffraction (XRD) measurements have been utilized for decades to characterize the non-destructive structural properties of materials ranging from molecules to huge polycrystalline alloys. The coherent elastic scattering of light from ordered lattice planes in a crystal, which obeys Bragg's law, is the fundamental principle of x-ray diffraction [12]:

$$2d\sin(\theta_B) = n\lambda$$

where θ_B and λ are respectively the incident angle and the wavelength of the incoming electromagnetic wave, while d is the interplanar spacing between lattice planes with the same crystallographic orientation.

We performed a specular θ-2θ scan, in which the scattering vector was preserved parallel to the surface normal of the sample. As a result, the angle of incident radiation and the angle of (collected) scattered radiation, θ and 2θ, are related. Both angles are measured in relation to the sample's surface. When the lattice planes in the sample are parallel to the scattering vector, diffraction occurs and a peak emerges in the spectrum.

Furthermore, the FWHM of the diffracted peak ($\Delta 2\theta_B$) is correlated with the coherence length L along the z- direction by the Warren-Scherrer formula [13]:

$$L = \frac{K \cdot \lambda}{\Delta 2\theta_B \cdot \cos(\theta_B)}$$

where K is a constant, generally equal to 0.9 for carbon structures, and θ_B is the angle at which Bragg reflection occurs. L can be viewed as the mean thickness (z-size) of crystalline domains in the sample. Indeed, a crystalline domain is composed of ordered lattice planes that do not disrupt the coherence of the x-ray beam. Dividing L for spacing distance of graphite (0.3359 nm) it is possible to have a rough estimation of the number of layers which is composed the samples. This analysis is useful to determine the degree of exfoliation of the GRM used in the polymeric matrix and to understand if it is more similar to bulk graphite or graphene.

A PANalytical Xpert Pro x-ray diffractometer, in the Department of Chemistry "Giacomo Ciamician" in Bologna, was utilized for these ex-situ structural characterizations. We kindly thank Dott. M. Gazzano for performing the measurements and for the assistance in the interpretation of XRD data.

3.2.3 Thermogravimetric Analysis (TGA)

TGA is a powerful technique for the measurement of thermal stability of materials including polymers. In this method, changes in the weight of a specimen are measured while its temperature is being increased. Moisture and volatile contents of a sample can be measured by TGA. The apparatus basically consists of a highly sensitive scale to measure weight changes and a programmable furnace to control the heat up rate of the sample. The balance is located above the furnace and is thermally isolated from the heat. A high precision hang-down wire is suspended from the balance down into the furnace. At the end of the hang-down wire is the sample pan, the position of which must be reproducible. The balance must be isolated from the thermal effects (e.g.,

by use of a thermostatted chamber) to maximize the sensitivity, accuracy, and precision of weighing [14].

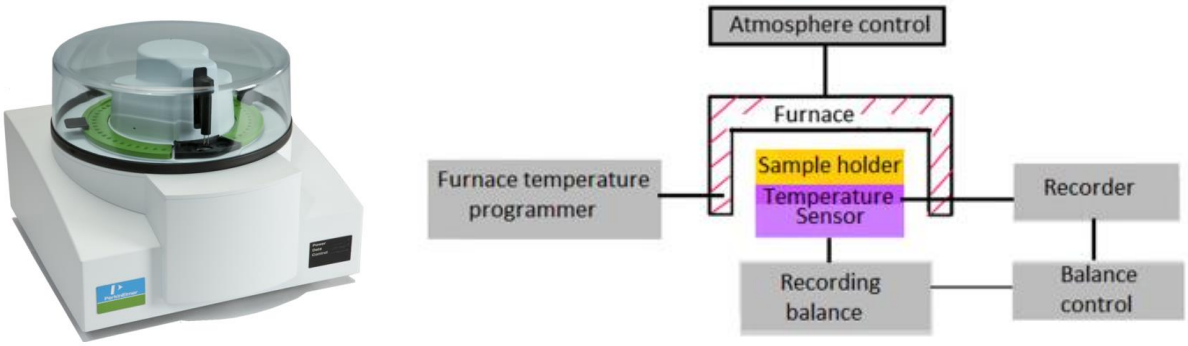

Figure 3.2: A) TGA instrument used for the analysis and B) its working scheme [15].

3.2.4 Differential Scanning Calorimetry (DSC)

Differential Scanning Calorimetry (DSC) is a thermal analysis technique that measures heat flow into or out of a sample as a function of temperature or time while the sample is subjected to a temperature control program. It is a very effective approach for assessing material attributes such as glass transition temperature, melting, crystallization, specific heat capacity, cure process, purity, oxidation behavior, and thermal stability. DSC also monitors the rate of heat flow and examines discrepancies between the test sample's and known reference materials' heat flow rates. Variations in material composition, crystallinity, and oxidation are determined by the difference [16].

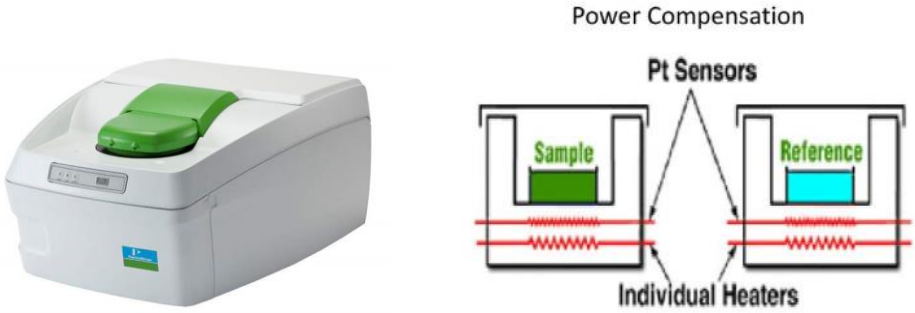

Figure 3.3: DSC instrument used for the analysis and its working scheme.

3.2.5 Electrical characterization of GRM-based master batches

Bulk electrical properties were characterized using the ASTM D4496 standard procedure "DC Resistance of Conductance of Moderately Conductive Materials". 4-probe was used for measuring the resistance and resistivity of polymeric master batch while the electrical contact was made by painting with common silver paint (silver nanoparticles in acetone) parallel 2 mm c.a. strips at fixed distances (L=20 mm), with fixed channel width (W=12 mm). After application, the contacts were dried for several hours. A typical 4-point probe setup was used to minimize artifacts due to high contact resistance on the final measurements. A fixed current was injected into the 2 outer contacts, reading the current on the 2 inner contacts.

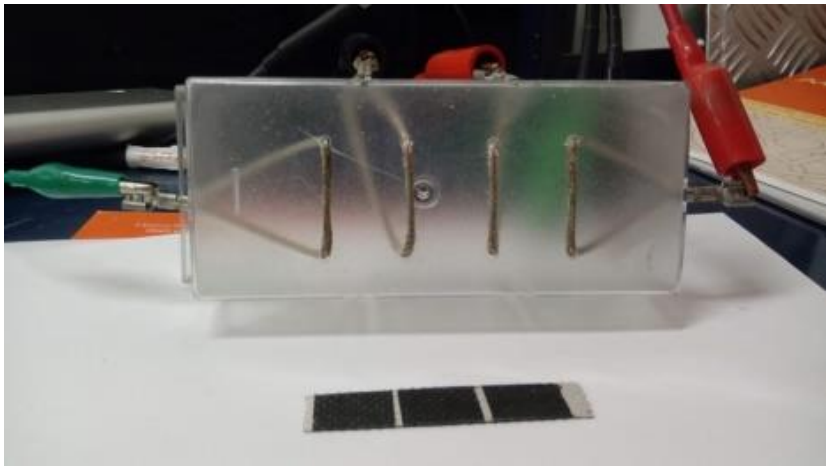

Figure 3.4: Setup for electrical characterization of GRM-based master batches.

Current scan (0.1 nA-100 uA) was performed in order to check the ohmic behavior of the thermoplastics, which was confirmed in all the conductive samples. The 4-probe electrical characterization allows one to estimate the resistance of the sample without the contact resistance, which is not a negligible factor in this kind of conductive composites: in some cases, the contact resistance could be up to 3-4 times the bulk resistance. Contact resistance usually follows a non-ohmic behavior, as confirmed by 2-probe measurements. The conductivity is measured as:

$$\sigma = \frac{L}{R \cdot t \cdot W}\left[\frac{S}{m}\right]$$

Where R = measured resistance (slope of V/I curve); t= thickness of sample, W=24 mm, L=22 mm.

3.3 Results and discussion

Morphological, thermal and electrical results are discussed for all the materials analyzed and summarized in tables in order to have a general view to understand the main trend. The GRM-products which exhibited significant improvements compared to the reference will be discussed in details.

3.3.1 Morphological analysis (SEM and XRD)

SEM images were taken of the fracture surface of each GRM-based master batch: the pellet was cooled in liquid nitrogen and immediately broken transversally into two halves at high speed by impacting it with a hammer. Some of SEM micrographs of GRM-based commercial master batches are reported in figure 3.5: the edges of the GRM can be seen on the fracture surface and it appears that they are well distributed with no preferred orientation and have maintained their lateral dimensions in the nanocomposite.

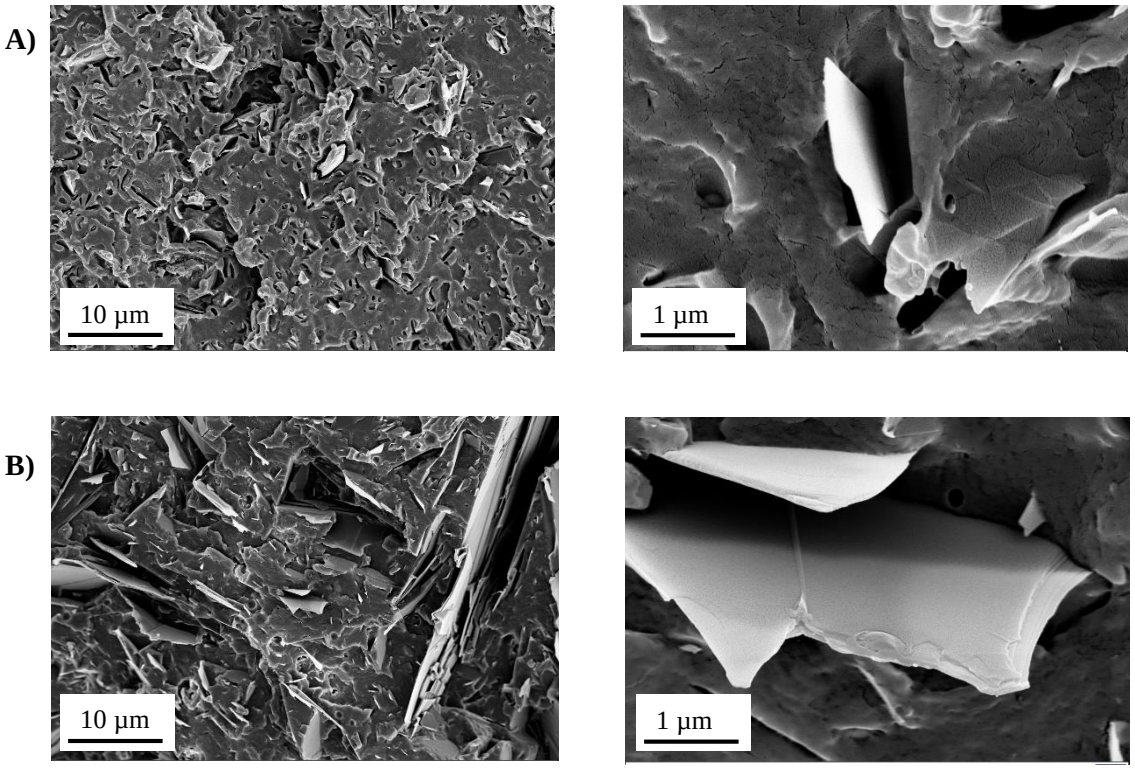

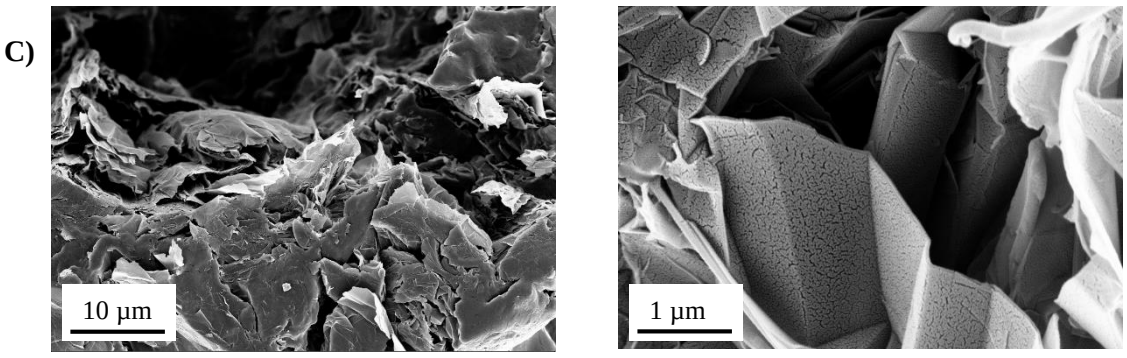

Figure 3.5: SEM images of A) PC+ 5%wt GRM, B) PA66+15%wt GRM and C) PP+20%wt GRM.

As example, the X-ray diffraction (XRD) patterns of the neat PP and PA12 supplied by CANOE and their corresponding nanocomposite with the same content (20% wt) of GRM are shown in figure 3.6. The XRD patterns are characteristic of PP and PA12 with the exception of the presence of a sharp peak at 2θ ≈ 26.4° which is typical of graphite content. This peak can be indexed as (0 0 2) from the GRM and its presence means that the GRM particles retain their crystalline form in the nanocomposites, without being intercalated or exfoliated during the melt mixing process.

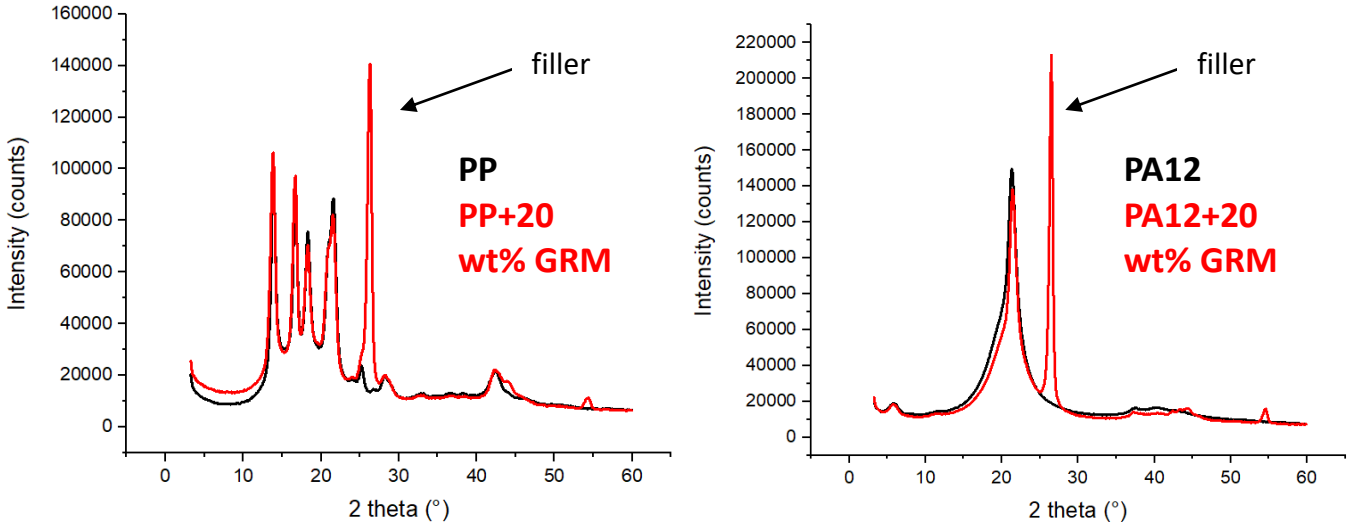

Figure 3.6: XRD diffraction patterns of PP/GRM and PA12/GRM nanocomposites at 20%wt GRM loadings.

As previously stated, we calculated the approximate number of layers by measuring the FWHM of the correspondent graphite peak (θ = 13,2°) from XRD patterns of each GRM-master batch obtaining the results shown in table 3.2.

Samples	FWHM (°)	Number of layers
PC+ 5% wt GRM	0.467 ± 0,001	66 ± 1
PP + 5% wt GRM	0.495 ± 0,001	62 ± 1
PA66+15 % wt GRM	0.355 ± 0,001	88 ± 1
PP+14,8 % wt GRM	0.329 ± 0,001	95 ± 1
LDPE + 10% wt GRM	0.488 ± 0,001	63 ± 1
PA12 + 20% wt GRM	0.515 ± 0,001	59 ± 1
PP + 20% wt GRM	0.613 ± 0,001	49 ± 1
PEEK + 20% wt GRM	0.561 ± 0,001	54 ± 1

Table 3.2: Determination of the layers of graphite of each GRM used in commercial master batch.

From XRD analysis, we can conclude that the GRM added to these commercial master batches generally exhibit a low degree of exfoliation (between 50 and 95 layers), resembling more to the bulk graphite rather than an exfoliated material like graphene.

3.3.2 Thermal analysis (TGA and DSC)

Thermogravimetric analysis (TGA) was employed to evaluate the effect of filler loading on the thermal stability of the polymers. The loss in weight of the pure master batch and its nanocomposites with different filler loadings, is evaluated as a function of temperature (between 30 and 900°C) in a nitrogen gas atmosphere. Both neat polymer and its nanocomposites follow a single-step degradation process, observed for each different master batch.

The addition of GRM brings about an improvement of thermal stability, as can be seen from the evaluation of extrapolated onset temperature (T_{onset}) that denotes the temperature at which the weight loss begins (table 3.3). We used the extrapolated onset temperature because it is a reproducible temperature calculation and it is specified to be used by ASTM [17].

The weight loss is caused by the volatile decomposition of polymer under high temperature. The presence of GRM impedes the movement of volatiles and improves the thermal stability of the composites.

As shown in table 3.3, the addition of GRM to the neat polymers does not compromise the thermal properties of the neat polymers and in some cases (PC+5%wt and PP+20%wt) there is a great

enhance of their thermal stability, as shown in figure 3.7. Especially for PC loaded at 5% of GRM, we observed an improvement of about 30°C compared to the reference.

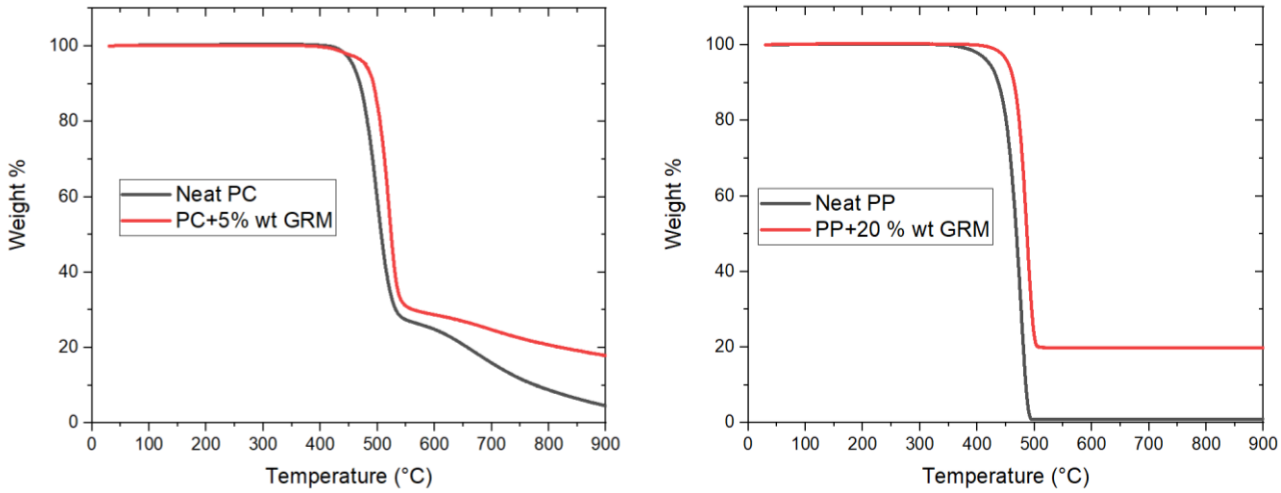

Figure 3.7: TGA curves of PC and PP and their corresponding GRM-loaded nanocomposite.

Samples	T_{onset} (°C)	Residual mass (%)	Improvement (°C)
Neat PC	462,7 ± 0,1	6,5 ± 1,6	> 30
PC+ 5% wt GRM	494,1 ± 4,6	16,7 ± 1,2	
Neat PP	411,5 ± 1,3	5,5 ± 0,2	≈ 6
PP + 5% wt GRM	418,2 ± 1,5	3,0 ± 0,6	
PA66+15 % wt GRM	409,2 ± 0,7	15,2 ± 1,4	-
PP+14,8 % wt GRM	435,8 ± 4,5	14,6 ± 1,9	
Neat LDPE	453,3 ± 1,1	0,3 ± 0,1	0
LDPE + 10% wt GRM	451,1 ± 3,7	4,6 ± 0,3	
Neat PP	405,9 ± 0,1	1,6 ± 0,9	≈ 10
PP + 20% wt GRM	416,2 ± 3,6	15,4 ± 1,0	
Neat PA12	457,9 ± 5,2	0,8 ± 0,2	≈ 3
PA12 + 20% wt GRM	460,3 ± 1,0	18,8 ± 1,4	
Neat PEEK	584,2 ± 3,3	49,5 ± 0,5	≈ 3
PEEK + 20% wt GRM	587,3 ± 0,7	58,0 ± 2,0	

Table 3.3: Results of TGA analysis, T_{onset} and residual mass at 900°C of GRM-based master batches.

Scanning of heat flow during heating and cooling using DSC was carried out to determine, melting temperature (T_m), and crystallization temperature (T_c) of the neat master batches and the

corresponding GRM-based ones. T_m and T_c were measured as the peak points DSC thermograms obtained during heating and cooling. From the area under the region of the melting point, we obtained the melting enthalpy ΔH_m and X_c is calculated by the ratio of $\Delta H_m / ((1- \phi) \Delta H_{100})$, where ΔH_{100} is the melting enthalpy of fully crystalline polymer, and ϕ is the weight fraction of the filler in the nanocomposite.

Samples	**T_m (°C)**	**X_c (%)**	**T_c (°C)**
Neat PP	165,4 ± 2,2	50,0 ± 3,6	123,2 ± 0,2
PP + 5% wt GRM	164,6 ± 0,9	42,1 ± 0,5	124,4 ± 0,4
PA66+15 % wt GRM	262,9 ± 1,8	29,6 ± 0,9	243,3 ± 0,1
PP+14,8 % wt GRM	167,2 ± 1,3	40,4 ± 0,5	124,9 ± 0,2
Neat LDPE	112,5 ± 2,5	43,5 ± 0,9	95,9 ± 0,7
LDPE + 10% wt GRM	109,8 ± 0,4	40,7 ± 0,5	96,6 ± 0,2
Neat PP	165,2 ± 0,8	50,2 ± 2,0	120,5 ± 0,9
PP + 20% wt GRM	165,9 ± 0,6	51,2 ± 0,6	130,0 ± 0,1
Neat PA12	180,1 ± 0,9	27,9 ± 2,9	149,8 ± 0,5
PA12 + 20% wt GRM	179,3 ± 0,8	30,0 ± 2,7	160,8 ± 0,4
Neat PEEK	348,1 ± 0,5	40,6 ± 5,2	309,2 ± 0,8
PEEK + 20% wt GRM	347,9 ± 0,1	44,8 ± 2,4	312,3 ± 0,4

Table 3.4: Results of DSC analysis, melting temperature (T_m), degree of crystallinity (X_c) and crystallization temperature (T_c) of GRM-based master batches.

Results showed that the addition of GRM to the neat polymers generally rises their degree of crystallinity (X_c) and crystallization temperature (T_c) which means that nucleation occurs earlier considering as starting point the melt state. In the case of LDPE+10% wt GRM and PP+5%wt GRM the crystallinity content has been reduced instead. The melting temperature (T_m) has not been affected significantly by the presence of GRM compared to the reference.

3.3.3 Electrical properties of GRM-based master batches

For the electrical characterization, we used a 50-ton hot press (Ormamacchine) that can be heated to 400°C to realize the samples through melt compression. We cut the specimens with sizes 12 x 67 x 2 mm from the printed panel with dimensions 100 x 100 mm.

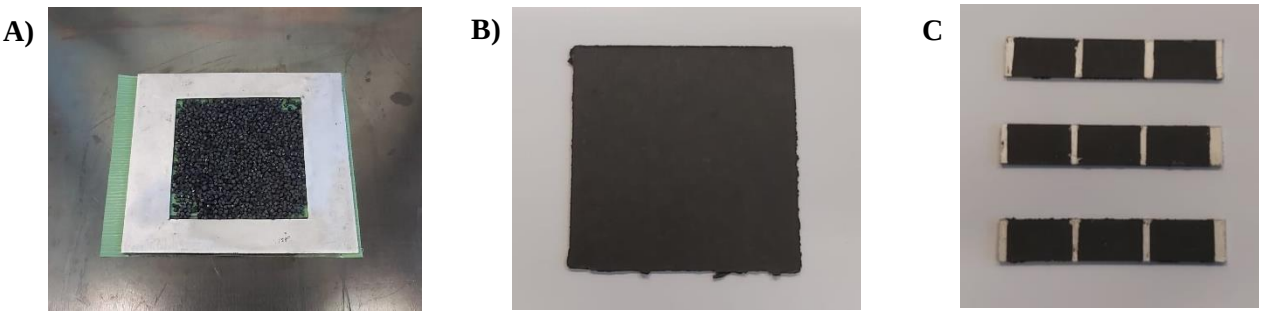

Figure 3.8: Manufacturing procedure of samples for electrical characterization A) GRM-based master batch in hot press, B) printed 100 x 100 mm panel and C) cut and silver painted samples.

The results of electrical characterization are shown in table 3.5, although PEEK+20 wt% GRM was not tested due to sample printing issues.

Samples	σ (S/m)
PC+ 5% wt GRM	INSULATOR
PP + 5% wt GRM	INSULATOR
PA66+15 % wt GRM	2-20 10^{-4}
PP+14,8 % wt GRM	INSULATOR
LDPE + 10% wt GRM	INSULATOR
PA12 + 20% wt GRM	1-2
PP + 20% wt GRM	10-15

Table 3.5: Results of electrical analysis of GRM-based master batch (INSULATOR < 10^{-11}S/m).

The electrical conductivity of the nanocomposite polymer was dramatically improved in the case of PA12 and PP at 20%wt GRM, with conductivities of 1-2 and 10-15 S/m, respectively, compared to an insulator behavior (10^{-11} S/m). The percolation/hopping process can explain the electrical resistivity change from insulating to semi-conductive materials. It is plausible to conclude that utilizing this amount of GRM, the electrical percolation threshold of these two nanocomposite was

overcome, and the dispersion was sufficient to produce an electrical conductive network inside the insulating matrix. Other commercial products do not exhibit this tendency.

3.4 Conclusions

It has been found that by dispersing a small amount of graphene in polymers, many properties of the resulting composites, such as tensile strength and elastic modulus, electrical and thermal conductivity, thermal stability, gas barrier, and flame retardance can be significantly improved. Based on these multifunctional properties, graphene/polymer composites are promising as both structural and functional composites that can be widely used in various important fields, including EMI, microwave absorption, flexible electronics, supercapacitors, biomedical devices, etc. A preliminary and limited comparison of the effectiveness of GRM as fillers in commercial polymer matrices has been made. Results showed that it is possible to increase the thermal and electrical properties as well the degree of crystallinity of neat polymers.

Graphene/polymer composites face critical challenges in i) preparing structure-controlled graphene with identical geometry as well as consistent and dependable high performance, (ii) fabricating composites with a uniformly dispersed and controlled spatial distribution of filler, and contact between graphene, and (iii) achieving strong interfacial interaction to increase load transfer from graphene to a polymer matrix. In reality, some of these problems are shared by all polymer-based composites, not just graphene/polymer composites. Two-dimensional graphene has created an alternative for the manufacturing of lightweight, low-cost, and high-performance composite materials for a variety of applications, bringing both possibilities and difficulties to fundamental research and nanotechnology in the composite area [18].

3.5 References

[1] Trivedi et al, “Graphene and its application in thermoplastic polymers as nano-filler-A review”, Polymer 240 (2022) 124486

[2] Saravanan et al, “Graphene and modified graphene-based polymer nanocomposites – A review”, Journal of Reinforced Plastics and Composites, (2014) Vol. 33(12) 1158–1170

[3] X. Ji et al. “Review of functionalization, structure and properties of graphene/ polymer composite fibers”, Composites: Part A 87 (2016) 29–45

[4] V.B. Mohan et al. “Graphene-based materials and their composites: A review on production, applications and product limitations”, Composites Part B 142 (2018) 200–220

[5] K. Kośla et al. “Preparation and properties of composite materials containing graphene structures and their applicability in personal protective equipment: A Review”, Composite materials containing graphene structures: A Review.” (2020) 59:215–242

[6] www.graphene-info.com/united-nanotech-innovations

[7] www.nanoxplore.ca/

[8] www.thomas-swan.co.uk/advanced-materials/

[9] www.plateforme-canoe.com/en/

[10] J. Zhao et al. “Electron microscopic methods (TEM, SEM and energy dispersal spectroscopy)”, Reference Module in Earth Systems and Environmental Sciences, (2022), www.doi.org/10.1016/B978-0-12-822974-3.00013-6

[11] Zoltàn Jenei, “Scanning electron microscopy (SEM) analysis of tribofilms enhanced by fullerene-like nanoparticles”, (2012) Thesis for the degree of Licentiate in Physics,Department of Physics, Stockholm University, Sweden

[12] Bragg, W.H., et al., “The reflection of X-rays by crystals” (1913) Proceedings of the Royal Society of London. Series A, Containing Papers of a Mathematical and Physical Character 88, 605, p. 428-438 www.doi.org/10.1098/rspa.1913.0040

[13] Warren, B.E. “X-ray study of the graphitization of carbon black”, (1956). in First and Second Conferences on Carbon.

[14] Sina Ebnesajjad, in Handbook of Adhesives and Surface Preparation, (2011)

[15] Loganathan et al. “Chapter 4 - Thermogravimetric Analysis for Characterization of Nanomaterials”, Micro and Nano Technologies, Thermal and Rheological Measurement Techniques for Nanomaterials Characterization, (2017), Pages 67-108, www.doi.org/10.1016/B978-0-323-46139-9.00004-9

[16] Gill et al, “Differential Scanning Calorimetry Techniques: Applications in Biology and Nanoscience”, Journal of Biomolecular Techniques (2010) 21:167–193

[17] Guide to TGA, Perkin Elmer

[18] Du, J. et al. “The Fabrication, Properties, and Uses of Graphene/Polymer Composites”, Macromolecular Chemistry and Physics, (2012), 213: 1060-1077. https://doi.org/10.1002/macp.201200029

4. GRM-coatings for water uptake reduction

Graphene is a newly discovered nanoscale material. Some of its qualities make it a viable alternative material for fulfilling some of the airframe functionality of CFRP sections. It is gaining traction in terms of evaluation and application, and is being considered for a wide range of applications: in this case, we evaluated GRM for water uptake reduction in aerospace CFRP in collaboration with Fidamc (Fundación para la Investigación, Desarrollo y Aplicación de Materiales Compuestos, Spain) and Airbus.

4.1 Introduction

Fiber reinforced epoxy resins are now employed for structural purposes in aeronautics in great amount. Because of its reduced weight and superior corrosion resistance as compared to metals, this material can significantly enhance aircraft performance. The moisture absorption resistance of these materials is a crucial aspect. Moisture, in fact, may be particularly detrimental to composites since it can damage the material's physical qualities, specifically [1-3]:

1. Adsorption of moisture can lower the glass transition temperature by plasticizing the polymer;
2. It may compromise the adhesion between the matrix and the carbon fibers that are constantly employed in airplane configuration.

Materials having a high surface-to-thickness ratio, such as graphene, should form a physical barrier against the migration of H_2O molecules in epoxy resin. Graphene also shows a highly hydrophobic surface. As a result, the inclusion of GRM might lower both the diffusion coefficient and the ultimate moisture absorption content [2, 4].

Graphene composites might be manufactured in two ways to achieve this goal [5] (figure 4.1):

- Bulk approach: graphene nanoplatelets in epoxy resin can provide a tortuous path, reducing moisture absorption inside the composite;
- Surface approach: graphene coating applied to the surface should form a physical barrier against H_2O molecule transport in epoxy resin.

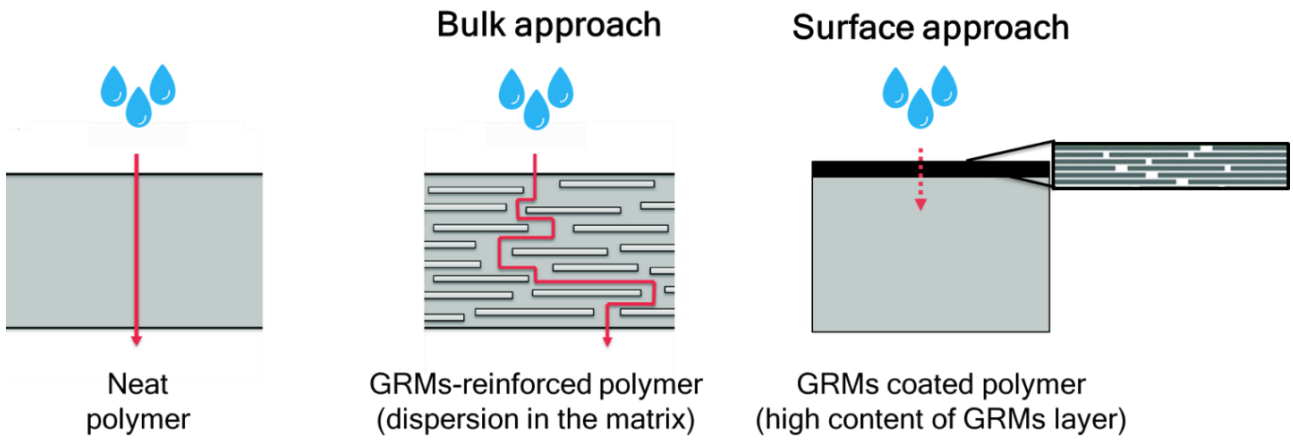

Figure 4.1: Strategies of using GRM for epoxy moisture absorption reduction.

A reduction in resin moisture absorption through the use of GRM should result in a reduction in final composite / CFRP component weight. Wet conditioning throughout in-service life must be addressed in the design and calculation of aeronautical composite constructions. Thus, in order to meet the requirements for structural component certification, controlled accelerated ageing (70°C/85 % R.H until reaching equilibrium) is usually considered in order to simulate ageing during aircraft life [6]. The major consequence of epoxy resin moisture absorption/uptake in composite materials is a loss in resin dependent mechanical characteristics. The change from unconditioned to moisture conditioned characteristics decreases the overall mechanical properties of composite material [1-4], which are considered by engineers in the design of the aeronautical constructions. Consequently, this decline then leads in heavier buildings.

In this regard, the moisture diffusion coefficient is the essential parameter that must be lowered in order to reduce the final component thickness influenced by humidity saturation, allowing the design of thinner and lighter constructions where structural requirements are the limiting factor. The strategy proposed in this work to delay the rate of water uptake is based on the surface approach using GRM-based coatings. They consist of a graphene paper (G-paper) impregnated with epoxy resin, described in detail in the next section.

Two different ways were investigated for the integration of coatings in the CFRPs:

1) coatings were bonded to a cured carbon fiber/epoxy composite panel;
2) coatings were co-cured in autoclave with the composite panels. In addition, in the co-curing strategy, a new type of G-paper with reduced graphene oxide (rGO) in its formulation was employed.

By performing an accelerated hygrothermal test in climatic chamber, we analyzed the evolution of the moisture absorption curve and determined the diffusion coefficient of bonded G-paper coated CFRP in comparison to the reference in the first part of the work.

In the second phase, we repeated the experiment on co-cured G-paper coated CFRP and also assessed their mechanical and thermal characteristics before and after ageing process, comparing the differences in CFRP properties due to the two different G-papers used.

4.2 Materials

4.2.1 Graphene paper

The advancement of graphene exfoliation processes in recent years has enabled the large-scale and low-cost manufacture of many types of GRM. These GRM, particularly graphene nano and microplatelets with high anisotropic 2-dimensional structure and good processability, can be re-assembled in thick, flexible layers to make "graphene paper" (G-paper) with features distinct from crystalline bulk graphite. Because of their superior mechanical and electrical qualities, as well as their low cost and ease of manufacture, these materials can be used as gas or liquid permeation barriers but also as conductive flexible electrodes in capacitors, or even light-emitting electrical conductors in incandescent bulbs.

This exfoliation and reassembling method has been successfully used to additional 2D materials; importantly, it may be utilized to create novel composite materials with a disorderly stacking of distinct 2D nanosheets or even a mix of 2D and 1D nanostructures [7].

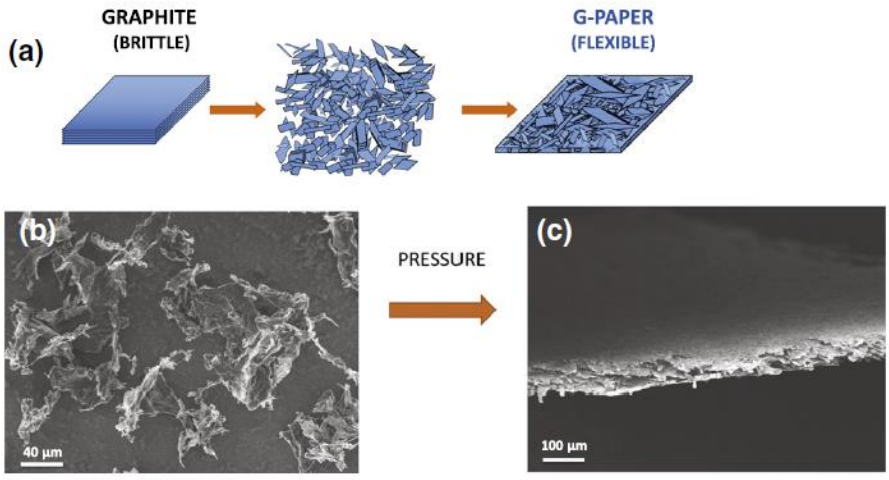

Figure 4.2: (a) Scheme describing the process used to produce graphene paper from exfoliated graphene nanoplatelets. (b and c) SEM images of (b) the graphene nanoplatelets and (c) the graphene paper realized with them [7].

In this work we used different kinds of graphene papers provided by commercial producer NANESA (Italy) in order to coat CFRP coupons supplied by Fidamc:

- G2Nan/RTM6: G-paper reinforced with epoxy resin where its composition is 70% GNP (G2Nan) and 30% of resin (RTM6);
- G2Nan/rGO/RTM6: G-paper reinforced with epoxy resin where its composition is 69% GNP (G2NAN), 1% rGO and 30% of resin (RTM6);

4.3 Methods

We assessed the characteristics of the bare G-papers using morphological, chemical, and electrical analyses such as SEM-EDS, XPS, and 2 and 4-point probe. Fidamc evaluated moisture absorption by executing an accelerated hygrothermal process in a climatic chamber on CFRP coated and reference samples, as well as their mechanical properties before and after ageing (DMA and inter laminar shear strength).

4.3.1 X-Ray Photoelectron Spectroscopy (XPS)

X-ray photoelectron spectroscopy is a surface-sensitive quantitative spectroscopic technique based on the photoelectric effect that can identify the elements that exist within a material (elemental composition) or cover its surface, as well as their chemical state, overall electronic structure, and density of electronic states in the material. XPS is a strong measuring technique since it displays not only what elements are there, but also what additional elements are bound to them. When combined with ion-beam etching, the process may be utilized for line profiling of the elemental composition throughout the surface as well as depth profiling. It is frequently used to investigate chemical reactions in materials in their as-received form or after cleavage, scraping, heat exposure, reactive gasses or solutions, ultraviolet radiation, or ion implantation.

XPS is a type of photoemission spectroscopy in which electron population spectra are acquired by irradiating a material with an X-ray beam. Chemical states are determined by measuring the kinetic energy and the number of electrons expelled. XPS needs high vacuum (residual gas pressure p 10^{6} Pa) or ultra-high vacuum (p 10^{7} Pa) conditions, while ambient-pressure XPS, in which samples are evaluated at pressures of a few tens of millibars, is a current field of investigation [8].

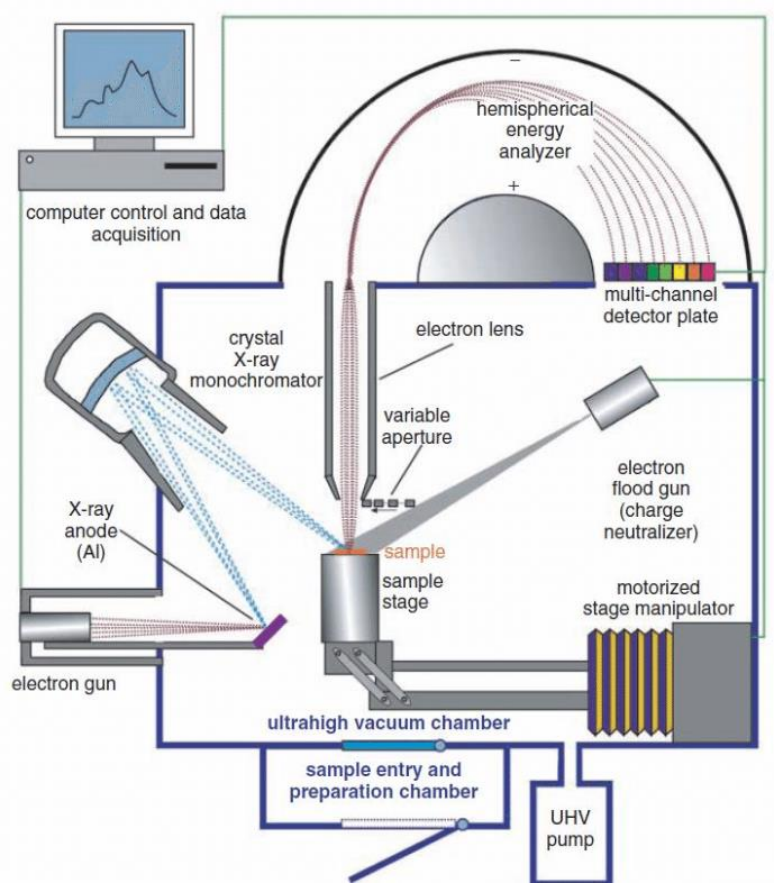

Figure 4.3: Schematic representation of the XPS [9].

XPS responses were acquired by a Phoibos 100 hemispherical energy analyzer (Specs, Germany) using Mg Kα radiation (ħω = 1253.6 eV). The X-ray power was set to 125 W. The spectra were recorded in the constant analyzer energy (CAE) mode with analyzer pass energies of 10 eV for the high-resolution spectra. The base pressure in the analysis chamber during analysis was 1 × 10−8 mbar. G-papers were analyzed after peeling the surface by a Magic Tape (3M, USA), constituting a procedure often used to obtain fresh surfaces in layered material (i.e., in highly oriented pyrolytic graphite) because the pristine G-paper surface contained significant amounts of Silicon, due to sample storage and fabrication procedure. High-resolution XPS spectra of C 1s were analyzed by CasaXPS (Casa Software, Ltd.); the curve fitting was carried out using Gaussian/Lorentzian curves shape (GL(30)) for C-O groups with a full width half-maximum of 1.4 eV and an asymmetric Voigt for the C-C sp2. Detail on fitting procedure is reported in [10].

4.3.2 Electrical analysis of G-papers and G-papers-composites

We performed different type of electrical characterizations: 2 and 4-point probe resistance measurements.

Linear 4-point probe was used in order to obtain the sheet resistance of G-papers avoiding the contribution of contact resistance [11]. The electrical model used was the infinite sheet, give a 2.8 mm probe distance, c.a. 100 µm G-paper thickness and a lateral size of several tens of centimeters, as reported in figure 4.4. We have performed a current scan in the range of ±100 mA, measuring voltages in the order tens of mV. All 4-point probe measurement was performed by using Keitheley 2450.

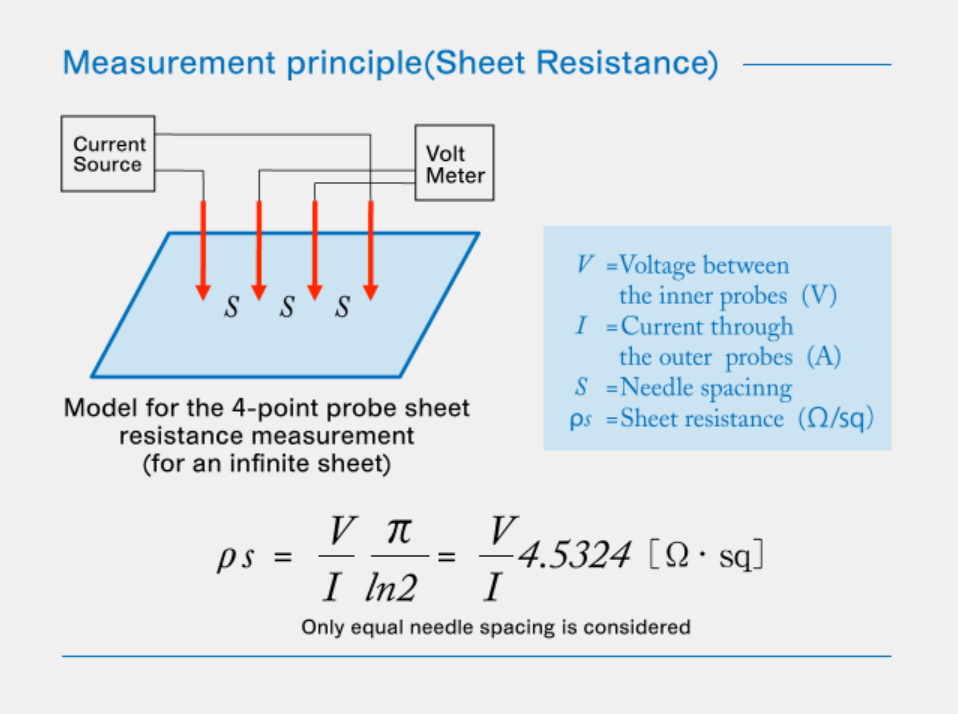

Figure 4.4: Schematic of 4-point probe to determine Sheet Resistance of G-papers.

In order to evaluate any benefit that G-papers could bring on the electrical properties of CFRP, 2-point probe was also used in bulk mode for sample used for water uptake, on LxHxW mm samples. Two different configuration was used: vertical resistance measurement (z axis) (L=2 mm S= 20x10 mm^2), where the contact was a metallic foil pressed on the G-paper coating; the horizontal

resistance measurement (x/y axis) (L= 20 mm, S= 2x10 mm^2), where the contact was set on the cut and smoothed edge.

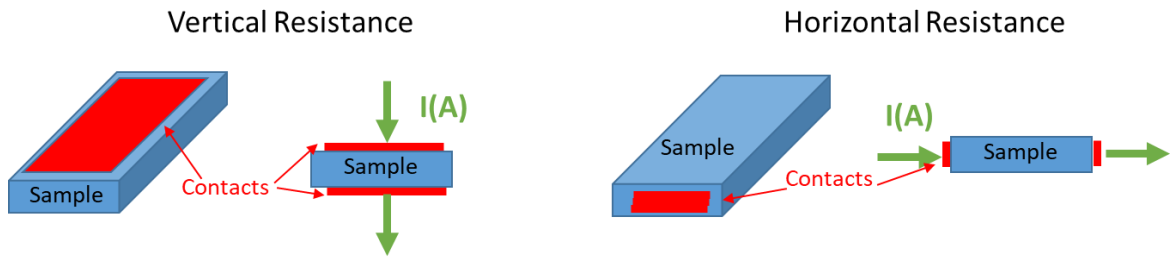

Figure 4.5: Schematic of 2-point probe to determine electrical properties in vertical (z) and horizontal (x/y) axes of G-paper coated CFRP.

4.3.3 Dynamic Mechanical Analysis (DMA)

Dynamic Mechanical Analysis, or DMA, is a technique that applies a minor deformation to a sample in a cyclic manner. This enables the study of the material's reaction to stress, temperature, frequency, and other parameters.

DMA works by applying a periodic deformation on a known geometry sample. First, a fixed amount of stress or strain is applied to the sample. Then, a variable amount of stress or strain is applied, oscillating above and below the fixed value, to simulate varying stress typical of working conditions, often leading to fatigue. The amount it deforms is proportional to its stiffness. The sinusoidal wave is generated by a force motor and sent to the sample through a drive shaft [12]. A schematic of the testing DMA setup is shown in figure 4.6.

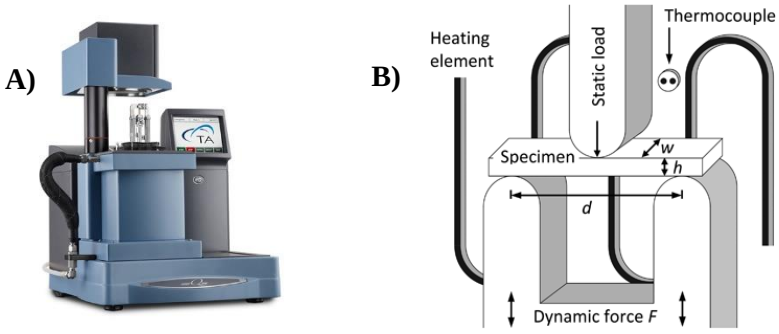

Figure 4.6: A) DMA instrument used for the analysis and B) sample tested in 3PB configuration [13].

DMA measures stiffness and damping, these are reported as storage modulus (E') and tan delta (Tanδ). Because we are applying a sinusoidal force, we can express the modulus as an in-phase component, the storage modulus, and an out of phase component, the loss modulus. The storage modulus is the measure of the sample's elastic behavior. The ratio of the loss to the storage is the tan delta and is often called damping. It is a measure of the energy dissipation of a material [12]. Fidamc performed the DMA analysis on CFRP samples prior and after ageing to evaluate any shift of T_g of composite comparing coated CFRP with reference.

4.3.4 Interlaminar Shear Strength (ILSS)

The interlaminar shear strength of laminates with a brittle matrix, for example, those made of epoxy resin, is typically determined using a short beam shear test (SBS). It makes use of the fact that shear stresses always occur in a flexure test. If the span is small in comparison to the specimen thickness, the shear stresses that occur in comparison to the normal stresses generated by the bending moment are very large. In this way, shear stress can be generated in brittle matrix materials, which enables measurement of the shear strength [14].

The shear strength of the matrix material or the quality of the fiber-matrix bonding can be characterized depending on the break type and it can be affected greatly by the presence of water [15,16].

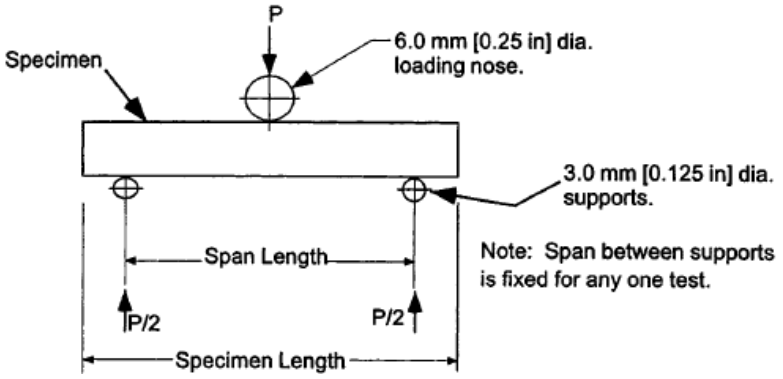

Figure 4.7: Specimen for determination of ILSS according to ASTM 2344 [17].

Fidamc performed the mechanical analysis on CFRP coated and reference samples before and after ageing in the climatic chamber.

4.4 Manufacturing of G-paper coated CFRP and ageing test

The strategy proposed in this work to delay the rate of water uptake is based on the surface approach using graphene-paper coatings. Two different ways were evaluated for the integration of coatings in the CFRPs:

1) coatings were bonded to a cured carbon fibre/epoxy composite panel;
2) coatings were co-cured in autoclave with the composite panels.

The material selected for the preparation of the CFRP samples is AS4/8552 (provided by Hexcel) a high performance tough epoxy matrix for use in primary aerospace structures. It exhibits good impact resistance and damage tolerance for a wide range of applications.

Final samples for the accelerated hygrothemal ageing in climatic chamber have sizes of 75x75x2 mm., in figure 4.8 is shown the manufacturing scheme of bonded and co-cured samples.

In the first case (bonded) CFRP were already cured and shaped with final dimensions and we used an epoxy glue (Araldite LY5052/Aradur 5052 CH) to stick the G-paper (G2Nan/RTM6) on both sides. The glue's curing was performed at room temperature for 24 hours.

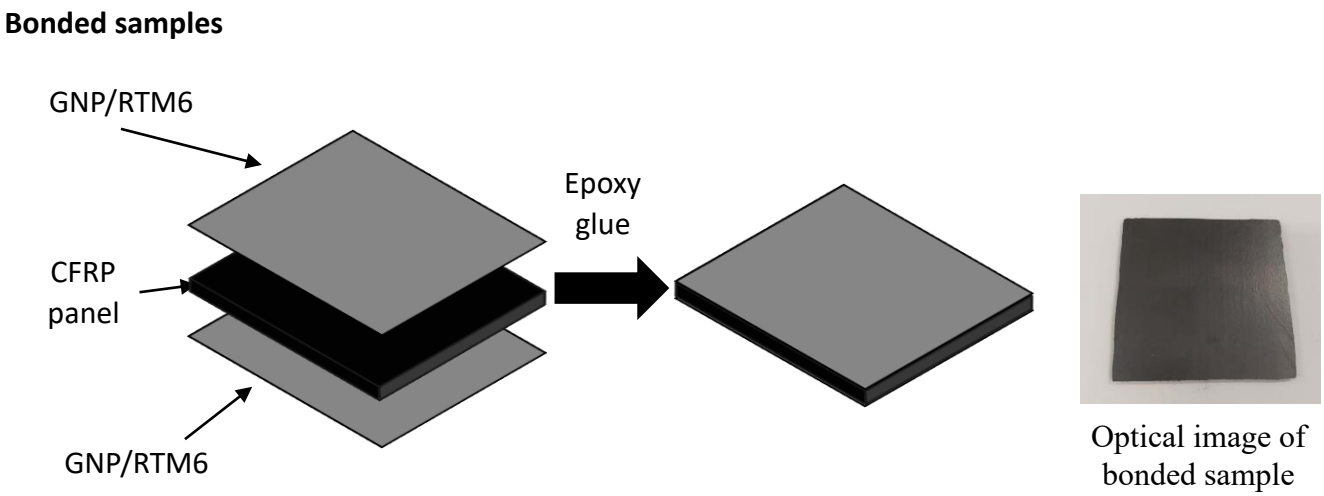

Figure 4.8: Production of bonded G-paper coated CFRP.

In the second case (co-cured) G-paper (G2Nan/RTM6 or G2Nan/rGO/RTM6) have been sticked on CFRP prepreg panel (uncured material, sizes 25 x 25 cm) and co-cured in autoclave according to aerospace production guidelines, as shown in figure 4.9. Once cured the composite, samples have been cut with the right sizes.

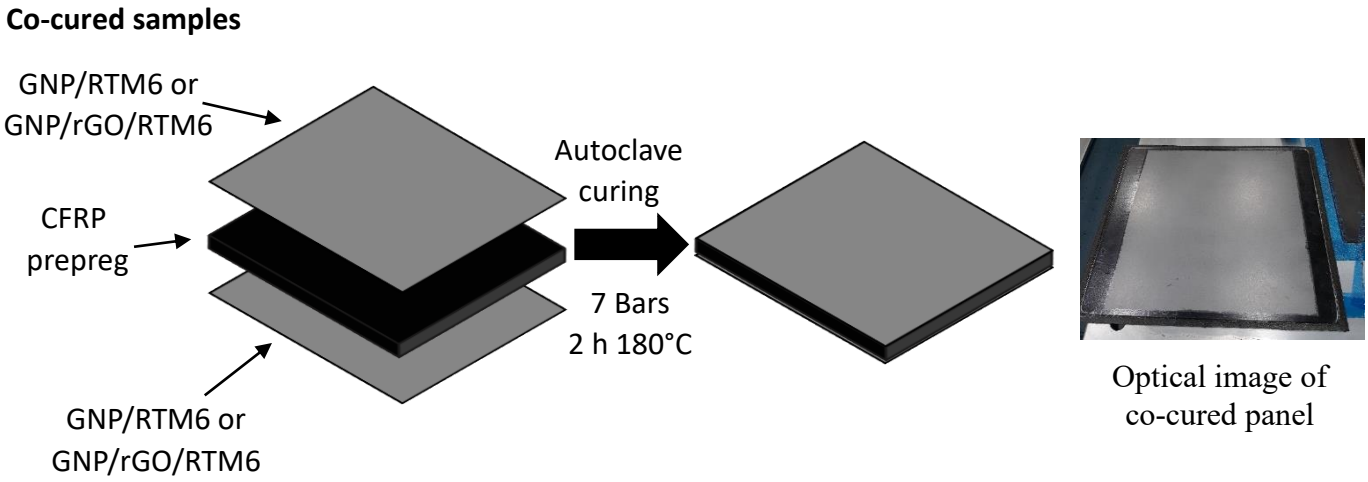

Figure 4.9: Production of co-cured G-paper coated CFRP.

Fidamc performed the moisture absorption assessment. The primary goal was to compare the moisture absorption behavior of the CFRP as a reference to that of the G-paper coated CFRP. All of the specimens had been pre-dried and conditioned. Prior to ageing/conditioning, each specimen's thickness and weight were measured. The moisture absorption test was performed in accordance with EN3615: “Fibre reinforced plastics-Determination of the conditions of exposure to humid atmosphere and of moisture absorption”. The climatic chamber used for sample conditioning must be calibrated and monitored on a regular basis to ensure appropriate operation at the specified temperature and humidity. The climatic chambers must maintain acceptable temperature and humidity levels for an extended length of time.

The test conditioning was selected as follow:

1. Pre-drying: samples introduced in an oven to be dried, 50°C/72h + 70°C/72 h + 90°C up to equilibrium;
2. Conditioning: samples introduced in an oven at 70ºC/85% R.H. up to reach equilibrium.

Weight of each specimen was recorded as showed in table 1.1 during testing in order to obtain the sample moisture pick-up curves. Percentage of moisture absorbed by each specimen and the corresponding absorption curves were reported by the testing lab, besides the temperature and any incident likely to have affected the results.

Pre-drying	Conditioning
t=0	t=0
Every week up to equilibrium	Day: 1,2,3,4,5,8,10,14 and then every week up to equilibrium
$t=t_{end}$	$t=t_{end}$

Table 1.1: Pre-drying and conditioning planning time.

4.5 Results and discussion

4.5.1 XPS, SEM-EDS and electrical analysis on G-papers

The composition of the surface was defined by X-ray photoelectron spectroscopy (XPS). Figure 4.10C reports the whole XPS spectrum acquired with the contributions ascribable to the atoms present on the surface. They show that G-papers (GNP/RTM6 and GNP/rGO/RTM6) are composed of carbon (94-95 at%), oxygen (3-4 at%), and nitrogen (1-2 at%), in strict analogy with pristine G-paper (G2Nan, pale blue line in figure 4.10C). The presence of nitrogen in the G-papers used in this work while absent in the reference is reasonably due to the contribute of epoxy resin RTM6, containing amino groups in its formulation. No metallic contaminations were observed within the XPS sensitivity range. Although the exact composition of G-paper is proprietary and undisclosed by the producer, XPS results did not show the presence of other additives or binders, indicating that the material totally consists of graphite nanoplatelets, as shown from morphological pictures in figure 4.10A and 4.10B.

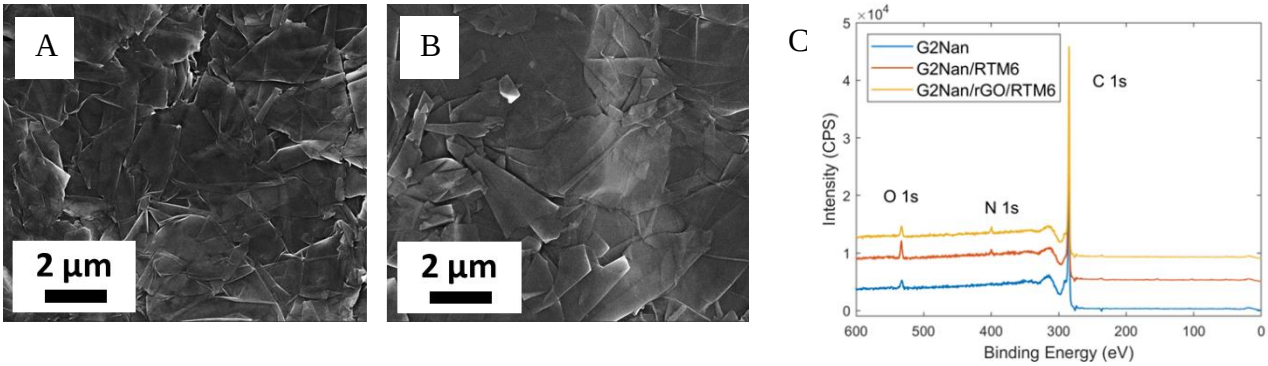

Figure 4.10: Morphological analysis of G-papers A) GNP/RTM6 and B) GNP/rGO/RTM6, C) XPS analysis of G-papers compared to reference (G2Nan).

G2Nan	RTM6	rGO	XPS			SEM-EDS	
%	%	%	C 1s 284.4eV	O 1s 532.9 eV	N 1s 400.0 eV	C %	O %
100	0	0	97.8 ±0.3	2.1 ±0.3	-	98.8 ±0.2	1.2 ±0.3
70	30	0	94.2 ±0.7	3.8 ±0.3	1.3 ±0.2	97.5 ±0.2	2.5 ±0.2
69	30	1	95.1 ±0.7	2.7 ±0.3	1.7 ±0.2	95.2 ±0.4	4.7 ±0.7

Table 4.2: Chemical composition of G-papers from XPS and SEM-EDS analysis compared to reference (G2Nan 100%).

The reason for the difference in chemical composition determined by XPS and EDS lies in the working system of the instruments: SEM-EDS effectively gives you the "bulk" concentration of elements present in a sample in an area > 1 µm while XPS on the other hand gives you the near surface region chemical composition of your sample (i.e. the elements present in the top few nm of your sample). According to SEM-EDS analysis the content of C % decreased while O % increased from pure G-paper compared to the other 2 formulations due to the presence of epoxy resin and rGO.

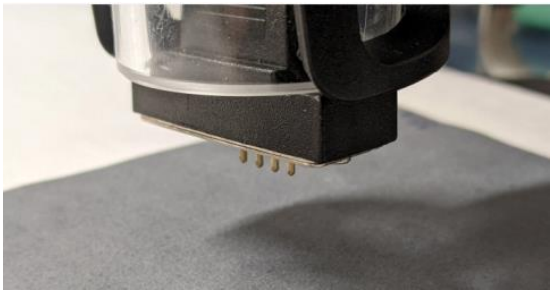

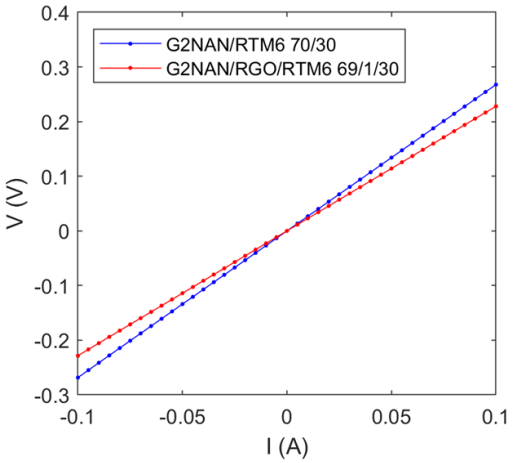

Figure 4.11:4-point probe measurement of G-paper electrical properties

Electrical characterization by 4-point probe of G-papers showed Rs values of 282 ±27 mΩ/sq and 240 ±6 mΩ/sq for G2Nan/RTM6 and G2Nan/rGO/RTM6 respectively, confirming that the addition

of 1% of rGO did not affect significantly the electrical behaviour of the material. In figure 4.11 we reported the V vs I of the bare G-papers that exhibited an ohmic behaviour being the current flowing through the material directly proportional to the voltage across it (as long as temperature is constant).

4.5.2 Water absorption study

In the first phase we analyzed the evolution of the moisture absorption curve and determined the diffusion coefficient of bonded G-paper coated CFRP in comparison to the reference. Figure 4.12 shows the moisture absorption curves and table 4.3 the diffusion coefficient of these samples.

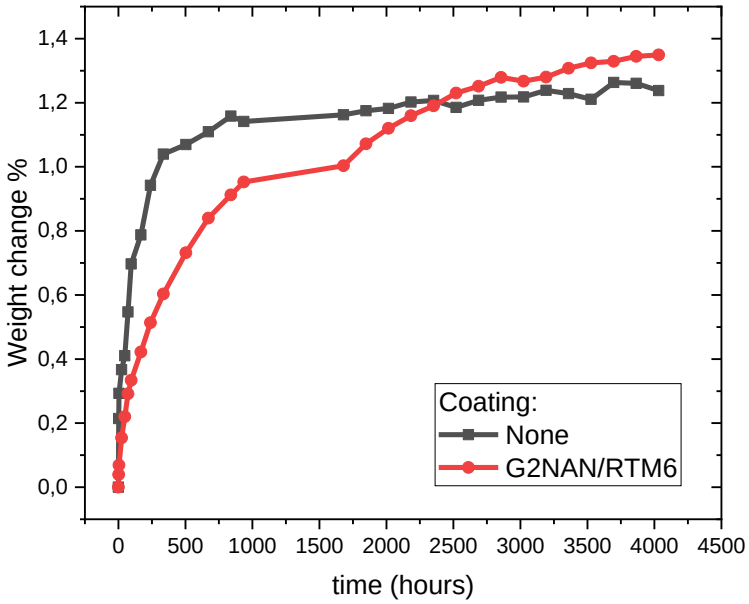

Figure 4.12: Water absorption curves of bonded G-paper (GNP/RTM6) coated CFRP compared to reference.

Coating	D (1E-9 cm^2/s)	ΔD (cm^2/s) (compared to ref.)
None (reference)	4,97 ± 0,84	-
G2Nan/RTM6	1,72 ± 0,28	-65%

Table 4.3: Calculated diffusion coefficient of bonded G-papers (GNP/RTM6) coated CFRP compared to reference.

Results showed that the maximum amount of water absorbed (Ms) is very similar (around 1,2% of weight change), however there is a clear reduction in the coefficient of diffusion (D). The value of the uncoated samples decreased by 65%, proving the beneficial effect of GRM coating.

In the second phase, we repeated the hygrothermal ageing on co-cured G-paper coated CFRP and assessed their mechanical (ILSS) and thermal characteristics (T_g) before and after ageing, comparing the differences in CFRP properties due to the two different G-papers used. The moisture absorption curves and the diffusion coefficient of these samples are shown in figure 4.13 and table 4.4.

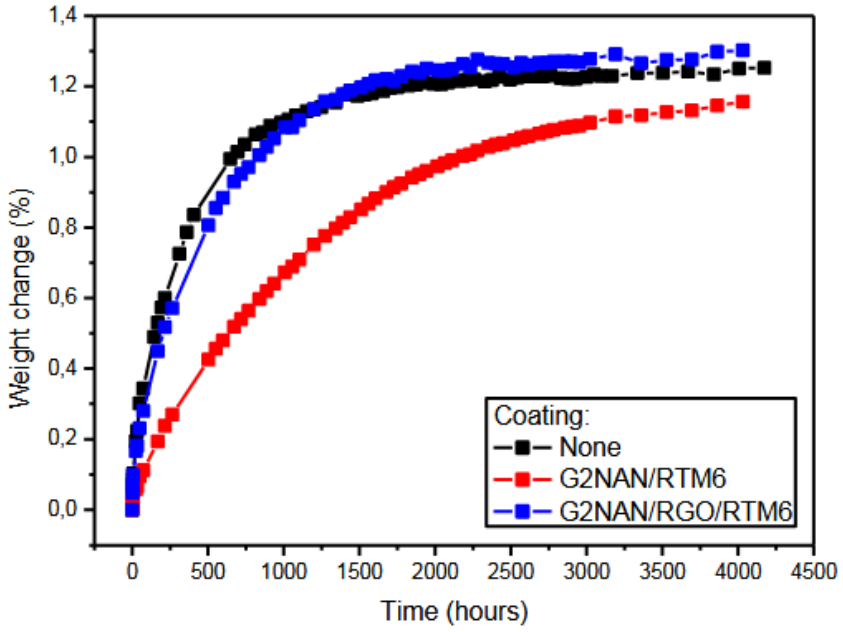

Figure 4.13: Water absorption curves of co-cured G-papers (GNP/RTM6 and GNP/rGO/RTM6) coated CFRP compared to reference.

Coating	D (1E-9 cm^2/s)	ΔD (cm^2/s) (compared to ref.)
None (reference)	2,70 ± 0,30	-
G2Nan/RTM6	1,00 ± 0,01	-62%
G2Nan/rGO/RTM6	2,20 ± 0,30	-19%

Table 4.4: Calculated diffusion coefficient of co-cured G-papers (GNP/RTM6 and GNP/rGO/RTM6) coated CFRP compared to reference.

The results showed that the G2Nan/RTM6 coating slightly decreased the amount of water uptake in saturation and the diffusion coefficient (D) is reduced by 62% compared to the uncoated reference while GNP/rGO/RTM6 coating showed no diminishing effect on the total amount of water absorbed but decreased the diffusion coefficient (D) of about 19% compared to the uncoated reference.

4.5.3 Morphological, thermal, mechanical and electrical properties of co-cured G-paper coated CFRP before and after ageing

Environmental SEM micrograph of the two co-cured G-paper coatings (GNP/RTM6 and GNP/rGO/RTM6) revealed the effects of humidity after aging test. As shown in figure 4.14B and D and figure 4.14F and H both conditioned coating presented micrometric-size black regions that could be degraded areas of coating due to the ageing. This phenomenon is especially marked for the coating with rGO that seems to be more affected by damaging (figure 4.14F and H). This could explain why the rGO coating provided less protection versus the water absorbed compared to the GNP/RTM6.

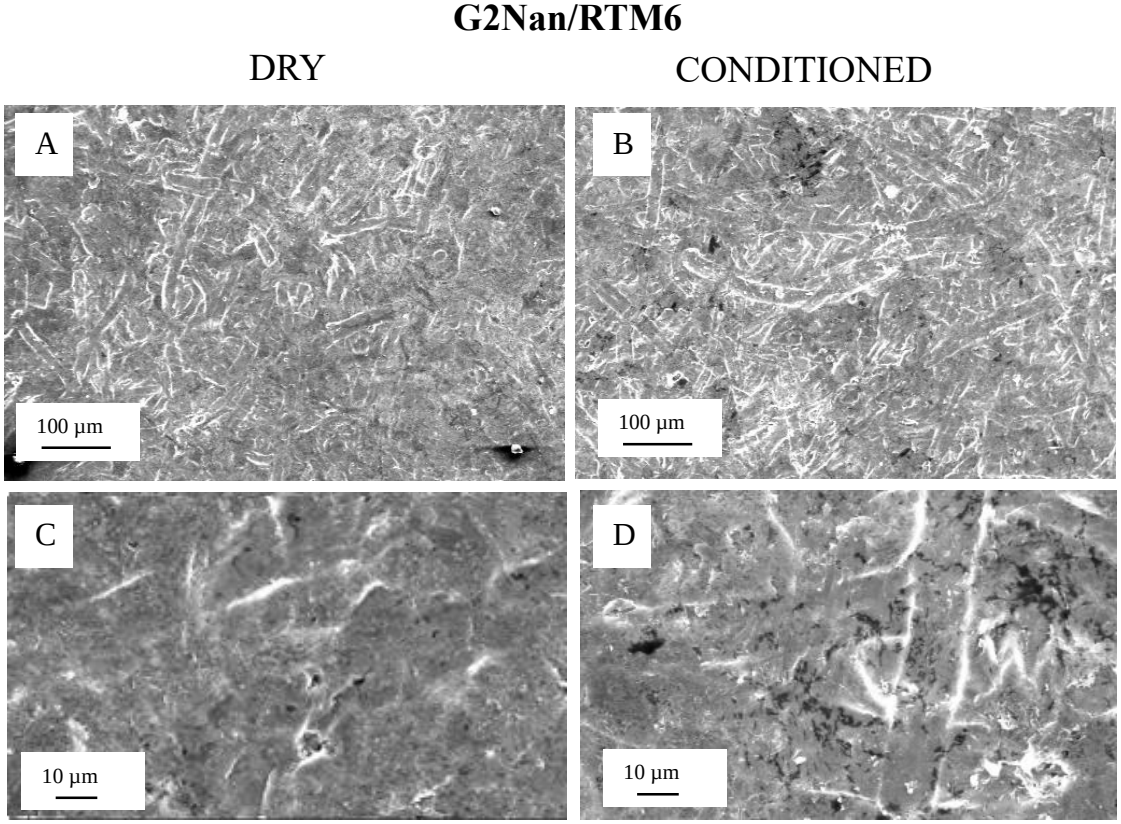

Figure 4.14: SEM images of co-cured G2Nan/RTM6 coating before and after ageing.

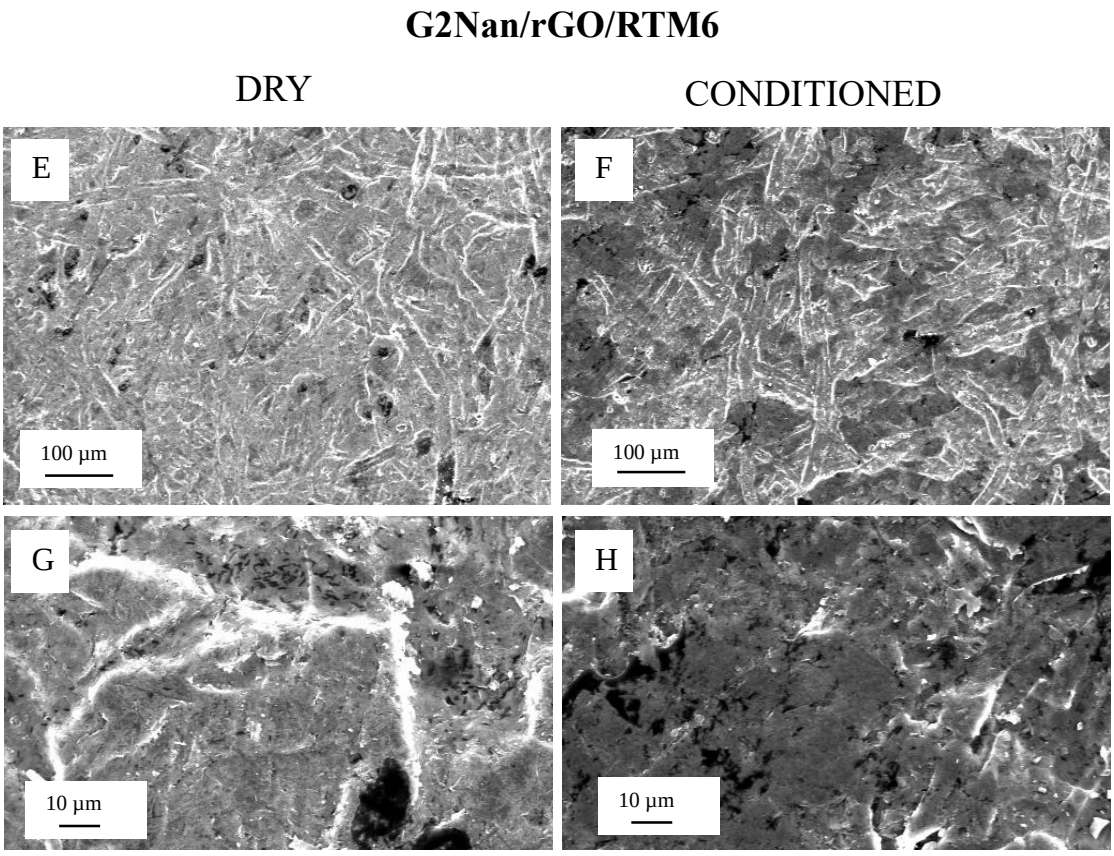

Figure 4.15: SEM images of co-cured G2Nan/rGO/RTM6 coating before and after ageing.

Results from DMA and mechanical analysis are reported in figure 4.16 and 4.17 in order to correlate the evolution of the glass transition temperature (T_g) and the interlaminar shear strength (ILSS) vs time and vs the water uptake during the ageing.

As shown in figure 4.16A, T_g value followed the same path for the two kinds of G-paper coated CFRP and it was slight higher for the uncoated CFRP, all three reaching the same value (≈170°C) at the maximum water uptake. In figure 4.16B, it can be clearly see that the coatings, especially the one with G2NAn/RTM6, provided a delay in the water uptake, and thus the loss of T_g is shifted to longer conditioning times.

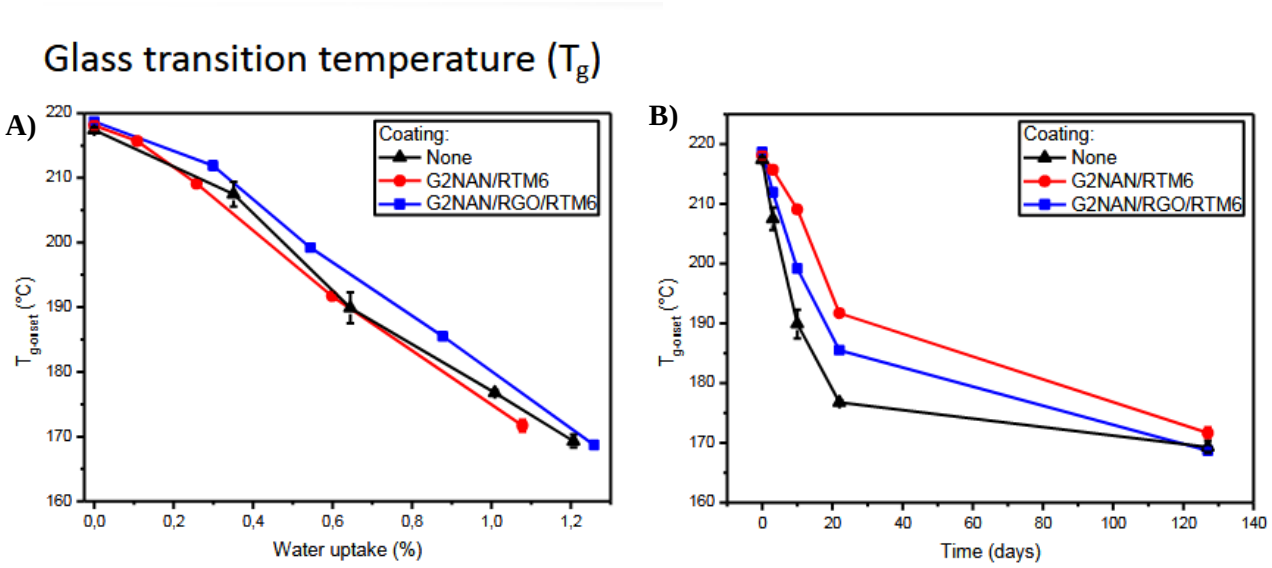

Figure 4.16: T_g values from DMA analysis a) T_g vs water uptake and b) T_g vs time.

When reaching saturation in water absorption, the ILSS values of the G-paper coated CFRP declined quicker than the uncoated samples, as seen in figure 4.17A. The similar tendency can be seen when graphing ILSS values vs time: G2NAN/RTM6 coating has the lowest ILSS value at the conclusion of the ageing procedure but its degradation is slower than the other coating with rGO. In general, we found the same decrease of ILSS for all samples examined, which ranges between 10 and 20 Mpa from the beginning point for each type.

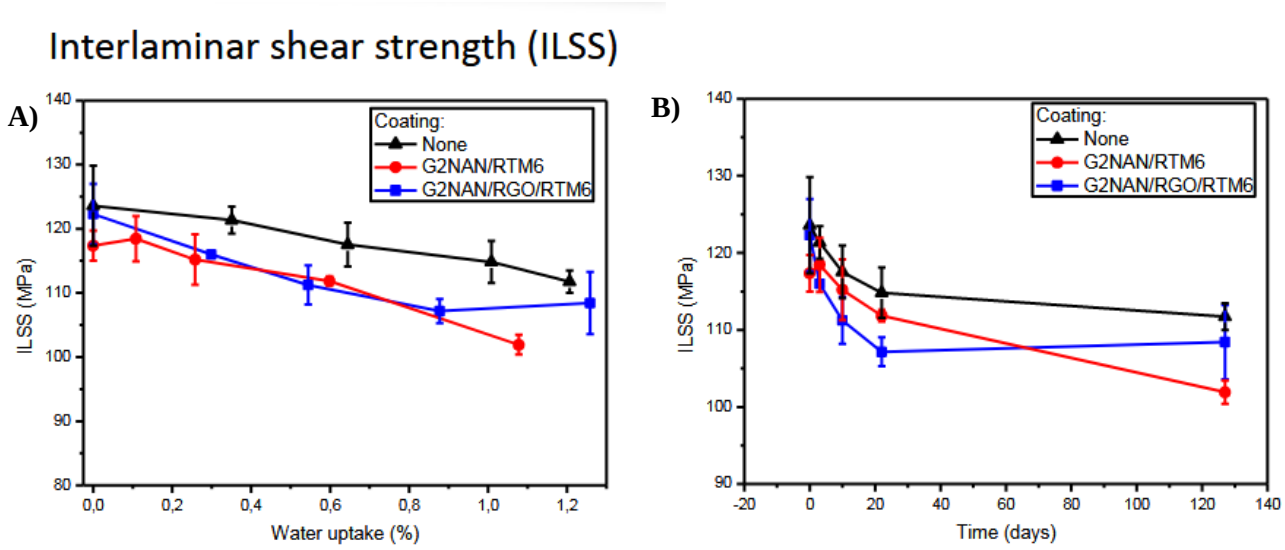

Figure 4.17: ILSS values from mechanical characterization a) ILSS vs water uptake and b) ILSS vs time.

Finally, we performed electrical measurements to see if the G-paper coating could improve electrical conductivity of the CFRP in any directions (x/y and z).

Coating	Condition	R (Ω) Vertical (z)	R (Ω) Horizontal (x/y)
None	Conditioned	250 ± 70	<2
G2NAN/RTM6	Dry	4 ± 2	<2
G2NAN/RTM6	Conditioned	5 ± 2	<2
G2NAN/rGO/RTM6	Dry	11 ± 2	<2
G2NAN/rGO/RTM6	Conditioned	7 ± 4	<2

Table 4.5: Electrical analysis (2-probe) of dry and conditioned G-paper coated CFRP compared to reference.

Results showed that both G-paper coatings were able to improve greatly the electrical conductivity of the bare CFRP in z axis while in x/y we did not observe any change. Electrical resistance was reduced from 250 Ω of the uncoated CFRP to 4-5 Ω with G2Nan/RTM6 coating and 7-11 Ω with G2Nan/rGO/RTM6, showing also no significant difference between dry and conditioned samples.

4.6 Conclusions

The solution presented in this study to delay the rate of water absorption is based on a surface approach employing GRM-based coatings. They are made of graphene paper impregnated with epoxy resin. Two approaches to coating integration in CFRPs were investigated, bonding and co-curing of g-papers coating on CFRP.

We evaluated the evolution of the moisture absorption curve and measured the diffusion coefficient of bonded G-paper coated CFRP in relation to the reference in the first part by executing an accelerated hygrothermal test in a climatic chamber. In the second phase, we repeated the

experiment on co-cured G-paper coated CFRP and also assessed their mechanical and thermal characteristics before and after ageing process, comparing the differences in CFRP properties due to the two different G-papers used.

Results show that with GRM-coating is possible to reduce greatly the diffusion coefficient providing a delay in the water uptake, and thus the loss of Tg is shifted to longer conditioning times, especially with the coating G2Nan/RTM6. In this case, the coefficient of diffusion is reduced by 62% compared to the reference samples (uncoated). From the manufacturing point of view, the co-curing strategy is preferred over the bonding, as it eliminates one step in the process and has a further beneficial effect on the water uptake. In a different approach, we also add rGO to the epoxy resin used to impregnate the G-paper. This reduces the beneficial effect of G-paper, but it is still better than the uncoated CFRP. The results obtained up to now show that graphene derivatives are a promising candidate for the reduction of moisture absorption in composites for aeronautical application.

4.7 References

[1] Roger Vodicka, "Accelerated Environmental Testing of Composite Materials", Airframes and Engines Division Aeronautical and Maritime Research Laboratory, DSTO-TR-0657

[2] S.G. Prolongo et al,"Water uptake of epoxy composites reinforced with carbon nanofillers", Composites: Part A 43 (2012) 2169–2175

[3] Broughton et al, "Accelerated Environmental Ageing of Polymeric Materials", Measurement Good Practice Guide No. 103

[4] Damari et al, "Graphene-induced enhancement of water vapor barrier in polymer nano composites", Composites Part B, 134, (2018) 218-224

[5] Patent US 2020/0102437 A1, "Multifunctional diffusion barrier"

[6] DIN EN 3615: Aerospace series - Fibre reinforced plastics - Determination of the conditions of exposure to humid atmosphere and of moisture absorption

[7] Scidà et al, Materials Today 21 (2018), 3. www.doi.org/10.1016/j.mattod.2018.01.007

[8] Boschi, "Investigation of charge transport in graphene-related materials (GRMs) thin films", (2021) PhD thesis

[9] Sowińska, "In-operando hard X-ray photoelectron spectroscopy study on the resistive switching physics of HfO2-based RRAM" (2014), Master of Science Engineer

[10] Poletti et al, Advanced Functional Materials (2022), 32, www.doi.org/10.1002/adfm.202107941

[11] Miccoli et al, Journal of Physics: Condensed Matter (2015) 27 223201

[12] Guide to DMA, Perkin Elmer

[13] Klumbach et al, Physic and Chemistry of Minerals (2017) 44:627–637

[14] www.zwickroell.com/industries/composites/interlaminar-shear-strength-ilss/

[15] Sinmazçelİk et al, Journal of Materials Science (2006) 41, 1233–1241

[16] Zhao et al, International Journal of Modern Physics (2010) 24, 15-16, 2712-2717

[17] ASTM D 2344/D 2344M "Standard Test Method for Short-Beam Strength of Polymer Matrix Composite Materials and Their Laminates"

5. GRM as thermo-electrical anti-icing /de-icing system

Commercial aircraft need protection systems against ice formation to avoid damaging effects in the airfoils and any related safety problems. Current solutions are mainly based on purges that distribute hot air from the engine to the leading edge to prevent ice accretion on the wing surface. However, these systems have some disadvantages, including incompatibility with composite parts due to the high temperatures used. A promising alternative to the current de-icing system, solving the just mentioned issues, is given by GRM based heaters in which heat is generated by the Joule effect by applying electrical voltage [1-3].

In collaboration with Airbus [4] we have been involved in developing and testing several different prototypes that led to the achievement of the TRL2 (Technology Readiness Level) in the aeronautical field (validated by Airbus) and represented the starting point for the ongoing GICE project where we are currently working to increase the level of technological maturity. In this study, I reported as example the manufacturing and characterization of one prototype, that is, the integration of GRM heating element within the carbon fiber composite, its curing cycle and subsequent processing and finally the heating and anti/de-icing functionality tests.

5.1 Introduction

Flexible heating systems, conductive coatings, or ecologically friendly technologies are becoming increasingly important in aviation applications. There is a specific necessity to prevent ice development or to readily melt ice that forms on aerodynamic surfaces. Currently, the most frequent technology used by bigger jet aircraft to keep the wing leading edge surface above the freezing temperature necessary for ice accumulation is a bleed air system. The hot air from the jet engine is "bled" into piccolo tubes that run through the wings and engine inlets.

Depending on whether the icing event happens on the wing or horizontal stabilizer, the lost lifting force might cause a pitch up or pitch down, increasing drag and, as a result, fuel consumption. Aerodynamic surfaces such as the HTP (horizontal tail plane) are now oversized due to the loss in aerodynamic performance caused by ice formation in the absence of any device to prevent it. Lighter anti/de-icing systems based on electrothermal materials will be required for the next generation of more efficient airplanes [1, 4, 5].

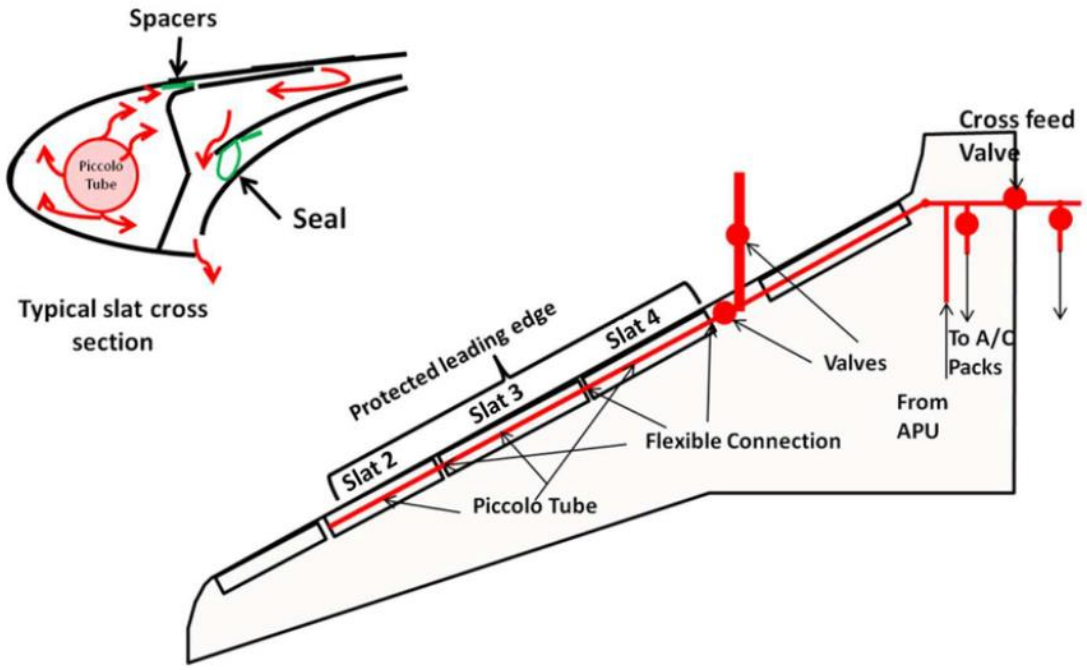

Figure 5.1: Bleed air system for anti-icing in aircrafts [6].

An electro-thermal system is another approach for ice prevention in aircrafts. They use resistive circuits built into the plane's structure that begin to heat up when a current is applied due to the Joule effect. Heat can be provided constantly to keep the aircraft from freezing (anti-ice mode), or with a pulsed current to melt the initial ice layers and allow the ice to glide (de-ice mode).

Large areas of conductive materials with low cost, low weight, ease of production, and high reliability are required for this application. For various reasons, the use of carbon material to overcome these problems appears to be quite promising.

In particular, the feasibility of using GNP preassembled in foils as the basis material for this application was investigated in this work. This material is easy to form and has a low weight, good conductivity, and chemical and thermal stability [4, 5].

Graphene-based foils (also known as graphene paper) can be simply cut, for example, using a laser cutter or a cutting plotter, or pre-formed with hollow punches, allowing them to be moulded into any pattern or circuit design without the need of any solvent or etchant. The generated flexible and conductive paths may be applied to any substrate.

5.2 Requirements for anti/de-icing system

Because the heatable graphene paper will be employed as a thermo-electrical system solution for anti-icing or de-icing of external aircraft surfaces such as the leading edge of the wing and the HTP, preliminary system and airframe integration needs must be regarded as an initial focus. Table 5.1 summarizes the qualities and criteria that represent the anti- or de-icing capabilities defined by systems. Table 5.2 summarizes the requirements from an integration standpoint [4].

System requirements for anti/de-icing of external aircraft surfaces	
Property	**Requirement**
Heat conductivity	The heat energy levels required would be around 50 kW/m^2 maximum down to a nominal 20 kW/m^2
Surface temperature	In icing conditions, the balance temperature for fully evaporative anti icing would be in the region of 40°C. For a non-evaporative system the surface temperature need only to be maintained above 0°C.
Voltage	Voltage for basic calculations should be 540 Vdc (on current aircraft: 115 Vac VF)
Lightning strike performance	Compatible with lightning strike protection system

Table 5.1: System requirements for anti/de-icing of external aircraft surfaces.

Integration requirements for anti-icing of external aircraft surfaces	
Property	**Requirement**
Compatible with design solution	As substrate material metal or composite (CFRP, GFRP) shall be considered. For CFRP: Maximum heater temperature on inner mould line is 120°C.
Durability	Resistance to operating fluids, temperature variations, rain and sand erosion resistance if applied on leading edge
Environmentally friendly	No toxic ingredients, low VOC (material requirement) low waste during application (process requirement)
Reparability	Must be repairable
Resistance to vibration	Demonstration of durability when used in conjunction with piezo-electric anti-icing systems

Table 5.2: Integration requirements for anti/de-icing solution of external aircraft surfaces.

5.3 Materials and prototype manufacturing

5.3.1 Graphene paper: GS50

We selected graphene paper GS50 produced by Nanesa as the material for the realization of the heating element showing the lowest Rs (< 0,1 Ω/□) among different types, as shown in table 5.3. GS50 was patterned by robotic cutting plotter from Silhouette Cameo in order to obtain the GRM heating element with a suitable electrical resistance (R=30 Ω) for our power supply instrumentation (TDK LAMBA GEN 40 V-38 A in direct current). Electrical connections with graphene paper were made by using copper and silver paint.

		GS-50	GS-80	GS-15 UH
Thickness (µm)		50	50-80	10-15
Max. Sheet size (mm)		400x400	400x400	120x120
Density (g/cm3)		1,5 – 1,7	1,2-1,5	1,2
Thermal conductivity (W/mK)	X, Y direction	> 1600	800-900	1000
	Z direction	50	50	50
Specific Heat @ 25°C (J/g°K)		0,8	0,8	0,8
Thermal diffusivity (cm^2/s)		14-16	8-9	10
Sheet Resistance (Ohm/sq.)		< 0,1	1-3	1-3
Bending (Cycles)		> 10000	> 30000	> 30000
Heat Resistance (°C)		500	300	200

Table 5.3: Properties of the different graphene papers produced by Nanesa [7].

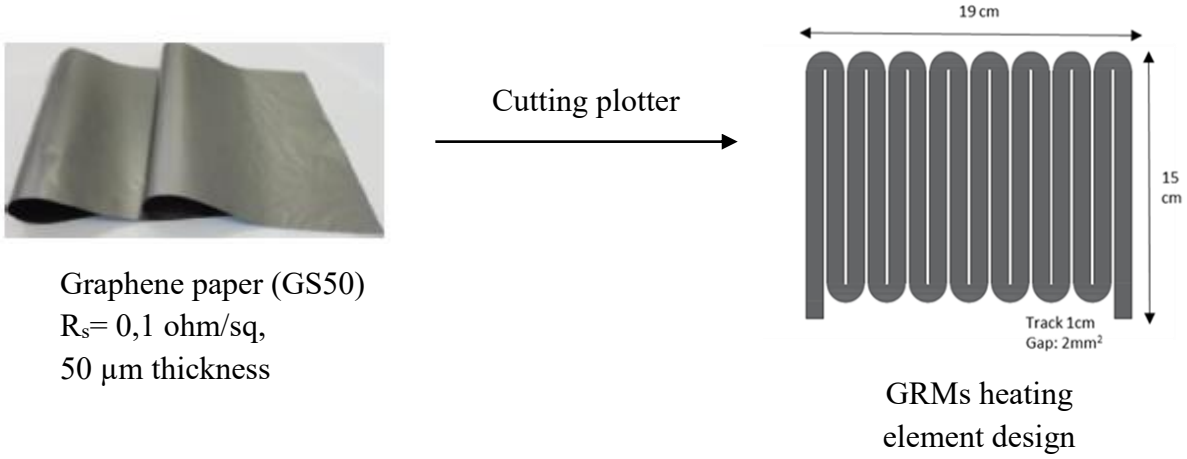

Figure 5.2: Production of the GRM heating element.

5.3.2 Manufacturing of GRM heating element

The GRM heating element was put between two insulating glass (GF) prepreg layers (VV300S-DT190-38 supplied by Deltatech) to avoid short circuits within the overall composite structure, while the lower half of the mold is made up of various layers of carbon fiber prepreg (GG200T-DT195N-42-MS supplied by Deltatech). The entire panel was then cured in a hot press at 135° for 90 minutes, as specified by the manufacturer. Figure 5.3 depicts the stratification of the layers and the final heating panel.

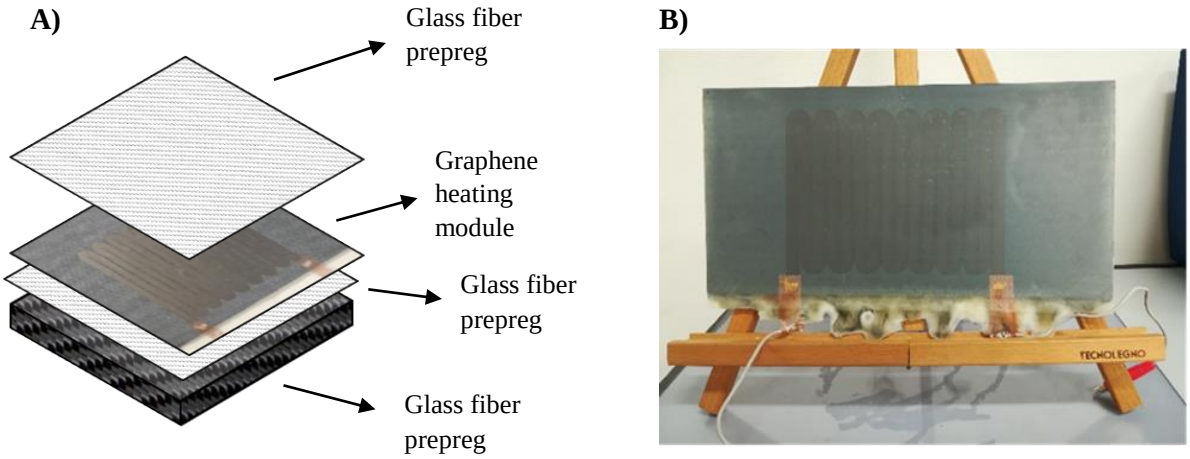

Figure 5.3: A) GRM heating module scheme production, and its B) optical image.

5.4 Characterization of Graphene paper and GRM heating module

5.4.1 SEM-EDS, XPS and 4-point analysis on G-paper GS50

X-ray photoelectron spectroscopy (XPS) was used to determine the surface's composition. Figure 5.4B depicts the whole XPS spectrum obtained with the contributions attributable to the atoms on the surface.

The results demonstrate that G-paper (GS50, 100% G2Nan) is constituted of carbon (98 at%) and oxygen (2 at%), and that no metallic contaminations, additional additives, or binders were detected within the XPS sensitivity range. Figure 5.4A shows morphological images of GS50, constituted by graphite nanoplatelets re-stacked in a paper-like matrix.

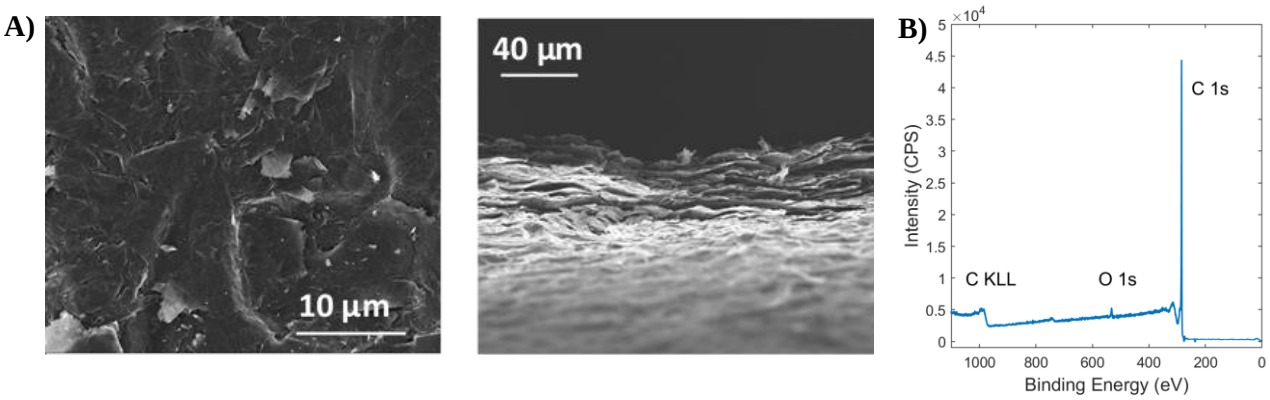

Figure 5.4: A) Morphological analysis of G-paper GS50 and its B) XPS spectra.

GS50	XPS			SEM-EDS	
	C 1s	O 1s	N 1s	C %	O %
100% G2Nan	97.8 ±0.3	2.1 ±0.3	-	98.8 ±0.2	1.2 ±0.3

Table 5.4: Chemical composition of GS50 from XPS and SEM-EDS analysis.

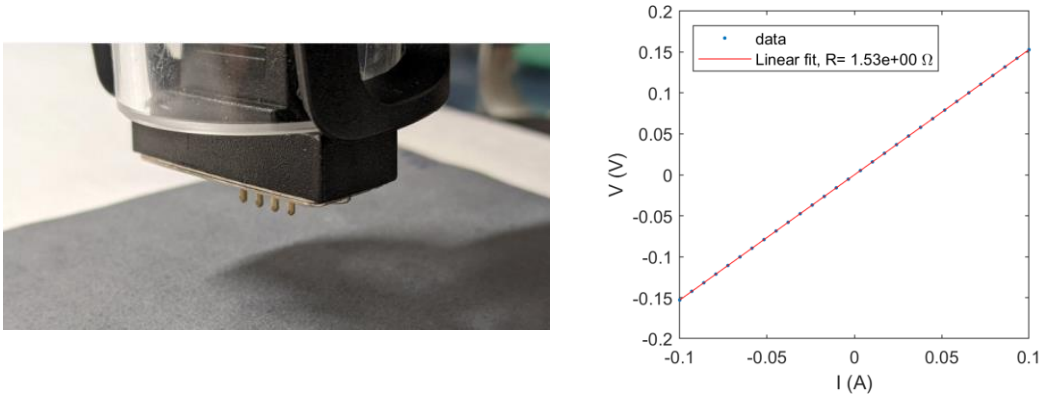

Figure 5.5: 4-point probe measurement of GS50.

Electrical characterization of G-paper GS50 using a 4-point probe revealed R_s value of 161 ±27 mΩ/sq. In figure 5.5, we reported the V vs I of bare G-paper, which displayed ohmic behavior, which means that the current flowing through the material is directly proportional to the voltage across it (as long as temperature is constant).

5.4.2 Heating tests of GRM heating module

Preliminary heating experiments were carried out at room temperature to evaluate the temperature range attained by the GRM heating module when run at various voltages. To this aim, the GRM heating mold was powered up with 15, 30, 38, and 46 V while measuring the temperature recorded by the thermocouple put in the middle of the heating module for each power.

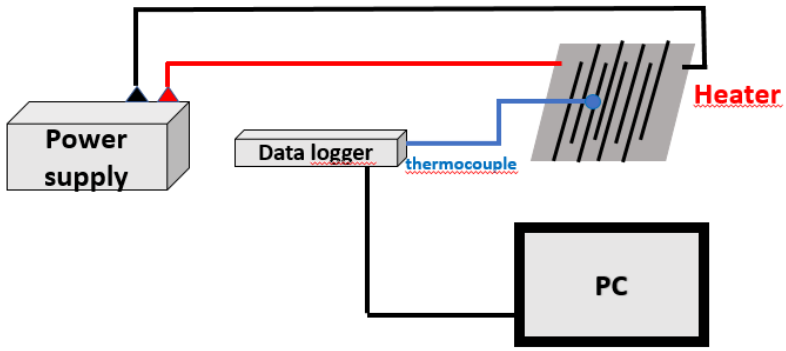

Figure 5.6: Setup for heating test at room temperature of the graphene heating system.

Results show that at the voltages utilized (15, 30, 38 and 46 V), it can be reached around 35, 65, 85 and 110°C on the surface after 600 s respectively, proving that increasing the power raises as well the temperature throughout the surface.

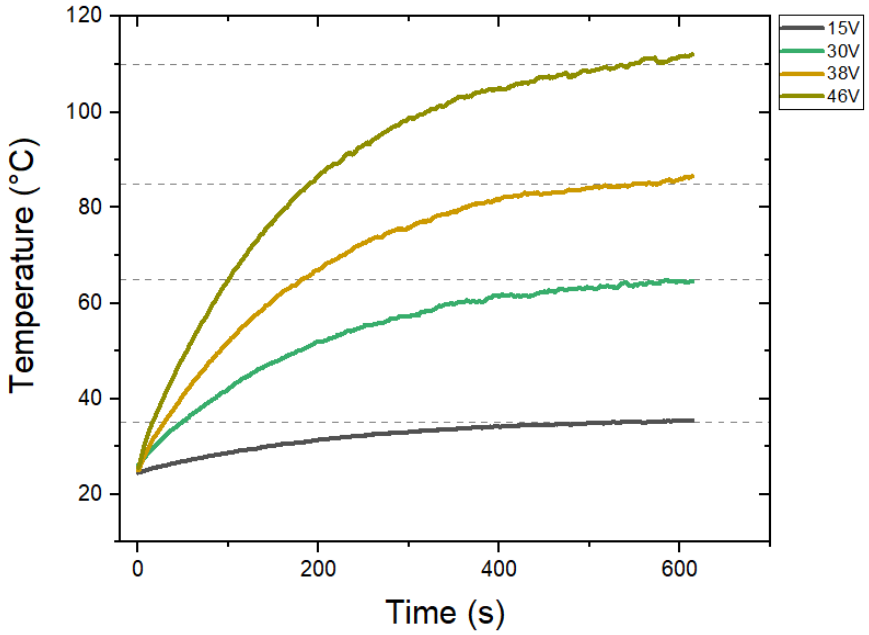

Conditions	1	2	3	4
Voltage (V)	**15**	**30**	**38**	**46**
Intensity (A)	0.5	1.0	1.3	1.6
Achieved T after 600s (°C)	35	65	85	110

Figure 5.7 and Table 5.5: Heating tests of GRM heating module. Temperature vs time plot at 15, 30, 38 and 46 V in order to evaluate the corresponding achievable temperature after 600 s.

5.4.3 Homogeneity temperature test of GRM heating module

The test performed to assess the heating homogeneity of selected GRM heating module was carried out at room temperature and without any ice accreted on panel surface, reaching the target temperature of 80°C applying 35 V and 1,2 A, selected as an average temperature among the range identified in the preliminary heating test. Temperature homogeneity was monitored through IR thermography using IR thermal camera (FLIR E60). The temperature has been recorded in 6

different spots, total area (box 1), the four corners (box 2, box 3, box 4, box 5) and the center through a thermocouple (T6).

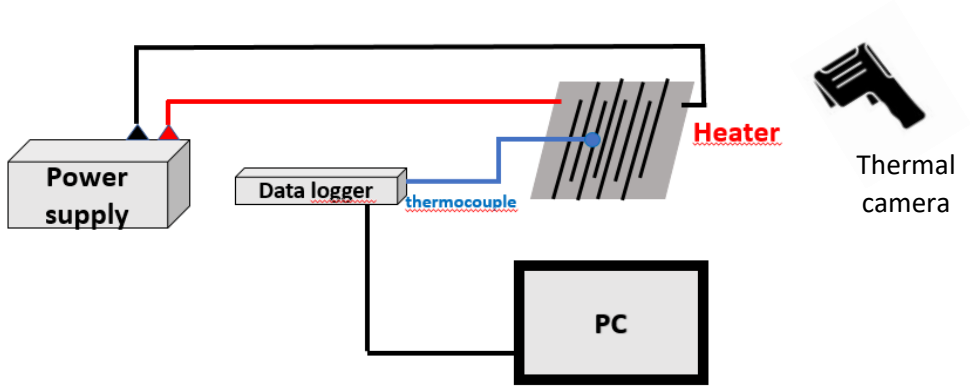

Figure 5.8: Setup for assessing the temperature homogeneity of the graphene heating system.

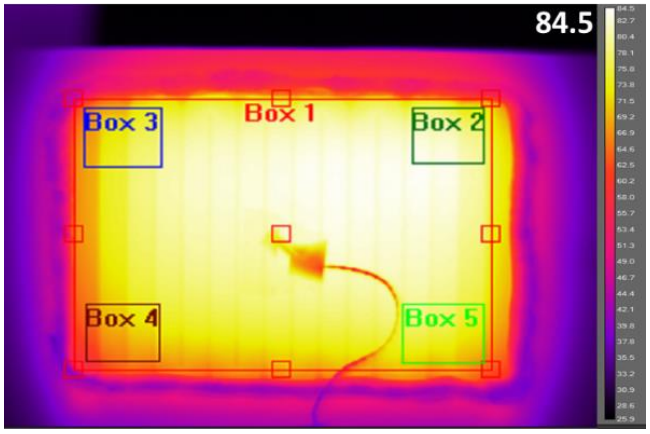

	Box1	Box2	Box3	Box4	Box5	T6
Mean T (°C)	77.2	80.2	73.4	68.1	74.5	80
St. Dev.	5.5	2.4	3.8	3.5	2.7	-

Figure 5.9 and Table 5.6: Thermal image at 84,5°C of the GRM module and the temperature variation of each box analyzed by IR thermography.

As it can be seen in figure 5.9, during this first test, the GFRP surface was quite homogeneously heated (77,2 ± 5,5 °C, Box1) in the whole area reaching the defined temperature of 80°C, although there is still room for improvement, since some colder spots/areas were identified, especially in the

corners. This can be linked to not fully optimized manufacturing process to integrate graphene serpentine in the CFRP panel, which may lead to defects, like bubbles or de-bonded areas.

5.4.4 De-icing and Anti-icing test at low temperatures of GRM heating module

Before De-icing test, we first evaluated the heating behavior putting the panel in a refrigerator at -30°C in order to evaluate the heating ramp at this condition and the time needed to reach 0°C on the surface when heated.

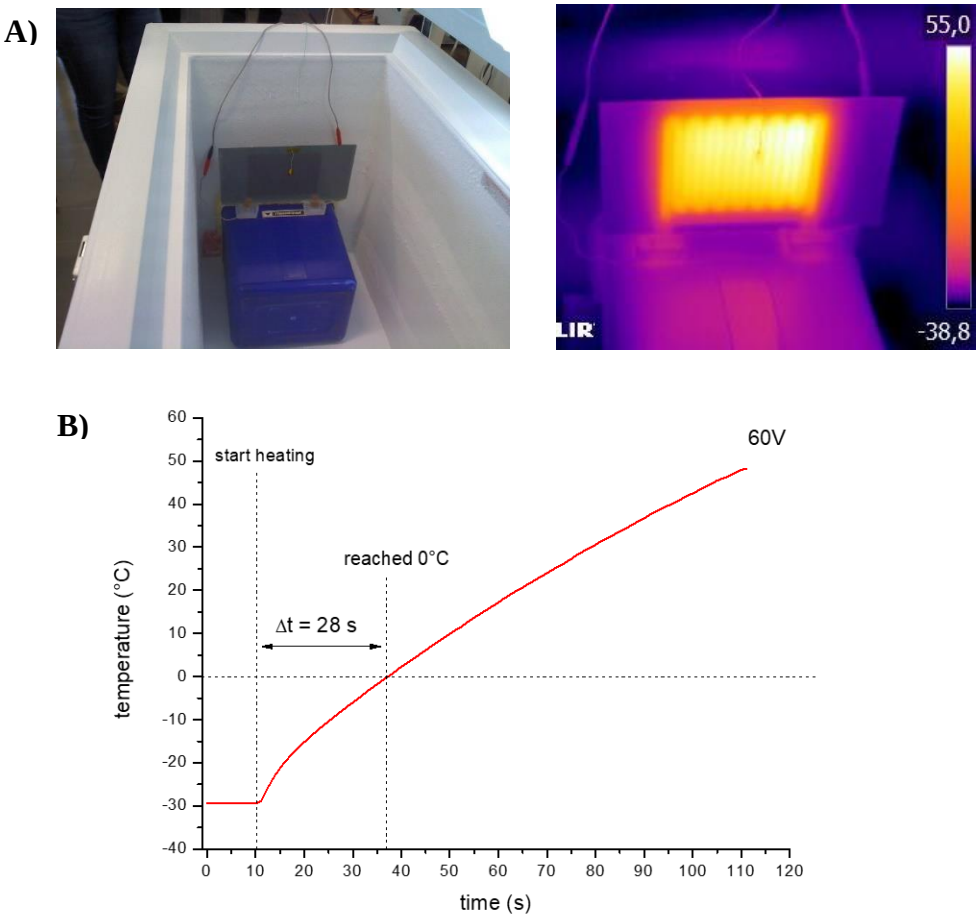

Figure 5.10: A) Optical and infrared picture of the heating panel inside the refrigerator at -30°C, B) T vs time plot when the heating panel is powered at 60V from -30°C.

Figure 5.10B shows the temperature vs time plot when the heater is powered at 60V and the time for the panel to reach 0°C from – 30°C is really fast and it is about 28 s.

The preliminary De-icing study was performed in collaboration with CNR-ISAC. Thanks to their instrumentation and expertize in ice accretion we were able to grow in a controlled way a thin ice layer on the surface of the heating panel at -30°C, as you can see in the first picture.

Figure 5.11: Ice accretion of the surface of the heating panel by a spray-gun system made by CNR-ISAC.

Then, keeping the panel at -30°C and applying 60V, the ice layer was melt, as shown in the picture below and in the heating ramp. In this case the panel reached 0°C in about 45 s.

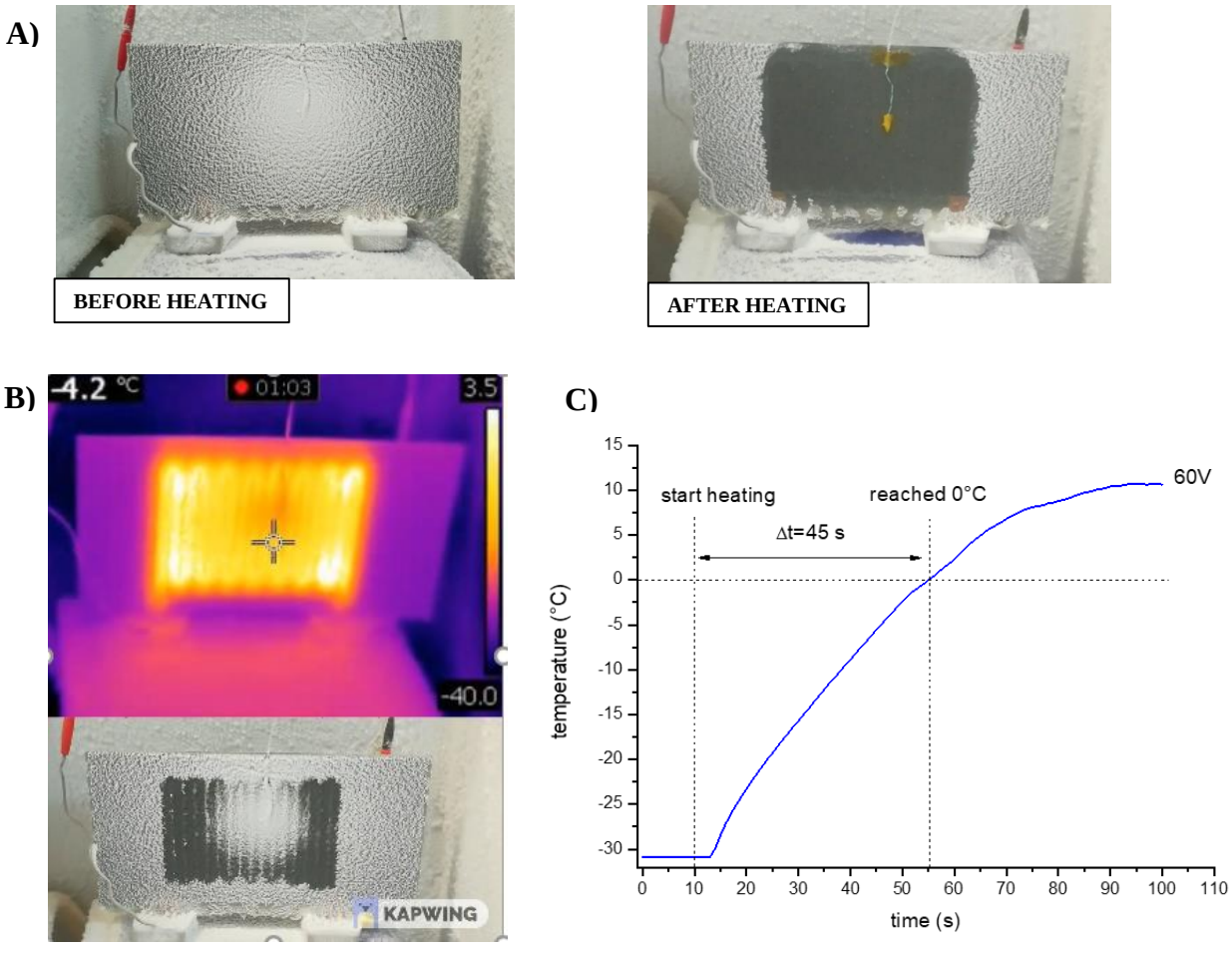

Figure 5.12: De-icing test performed at -30°C with an ice layer on the surface of the heating panel, A) optical pictures of the heating panel before and after heating, B) optical and thermal picture of the heating panel during de-icing test, C) T vs time plot during de-icing test at -30°C, applying 60V.

For the Anti-icing test, a silicone frame was created around the heater to confine water (water layer thickness 3 mm). The apparatus was put in a -20°C chamber and the water was consequently freezed. To manage the electricity, an in-house temperature controller was utilized to raise the temperature of the heater and water to 25°C and keep it constant for more than an hour (maximum power used: 50V and 1,6A).

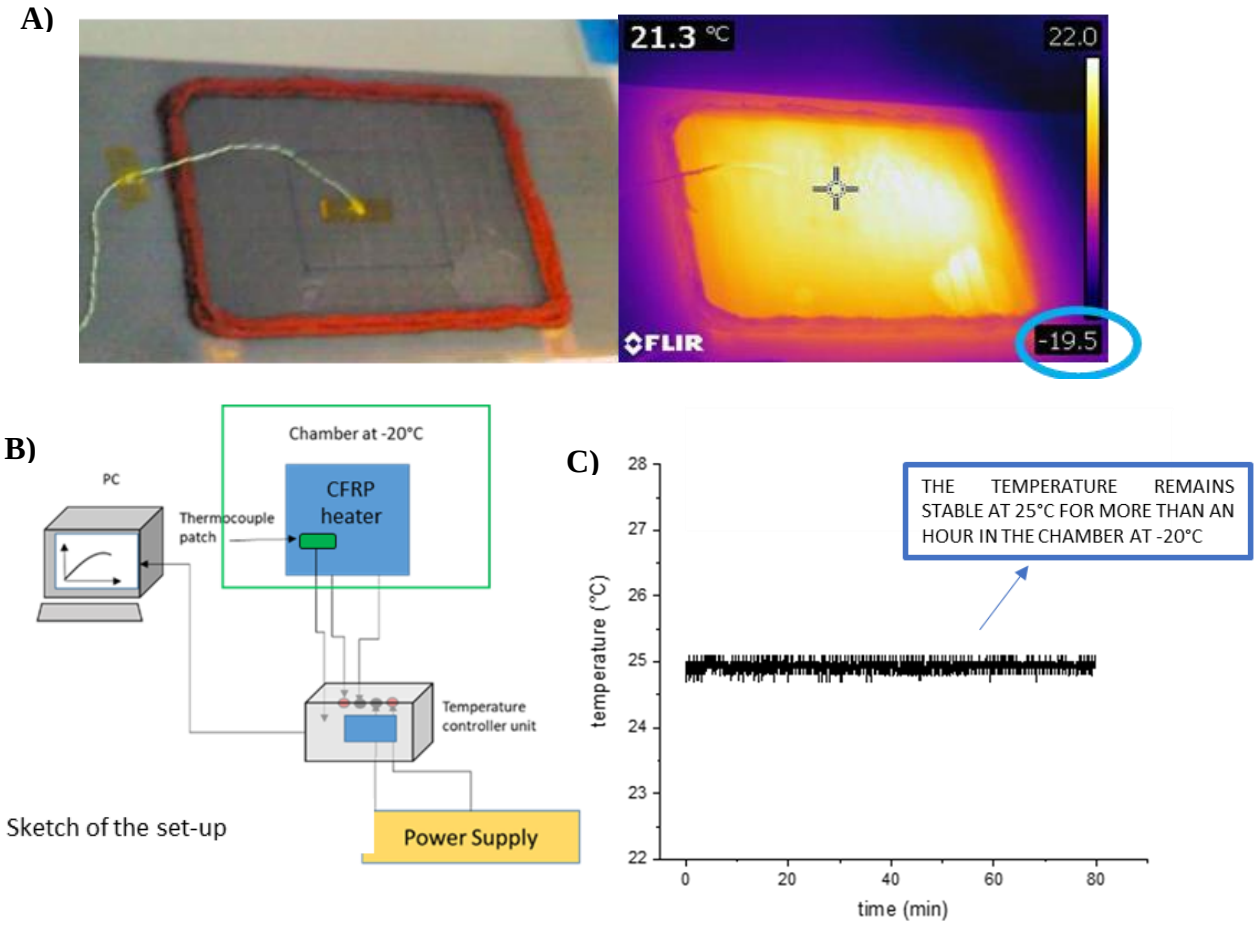

Figure 5.13: Anti-icing test performed at -20°C, A) optical and infrared picture of the heating panel during the anti-icing test, B) sketch of the setup used with the home made temperature controller, C) T vs time plot during anti-icing test at -20°C.

5.5 Comparison with other ice-protection system (IPS)

T. Blanco et al. [4] conducted a qualitative evaluation of a similar graphene-based solution for ice protection to other existing or off-the-shelf options, which is presented in table 5.7. All known options, including bleed air, electro-thermal, pneumatic, and chemical-based systems, have been considered:

- Bleed Air: state of art piccolo tube
- SprayMat®: electro-thermal system- metallic mesh heater
- FASTBoot®: pneumatic system
- Weeping wing: chemicals

Importance of feature	Market requirements \ Technology	Bleed Air	SprayMat®	FASTBoot®	Weeping wing	GRAPHENE
	Electric					
	Automation of manufacturing process → reduced RC					
	Integrability into CFRP, thermoplastics, or GFRP					
	Integrability into complex 3D structures					
	Flexibility of operation → precise control of generated heat					
	High efficiency → low power consumption					
	Reduced thermo-mechanical stresses			NA	NA	
	No oxidation & chemical inertness			NA		
	Low weight					
	Competitive price					
	Use for A/C ground deicing					
	TRL	9	9	9	9	2

Table 5.7: Qualitative comparison of Ice Protection Systems.

They also conducted a preliminary business case to evaluate the installation of graphene-based IPS in the Horizontal Tail Plane (HTP), which is not yet de-iced. However, ice accumulation on the leading edge has an impact on HTP aerodynamics and design. Aerodynamic studies suggest that a de-iced HTP on a Single Aisle Aircraft model can result in a 6-10% decrease in component size. Taking this important element into account, a preliminary estimate of savings was made,

demonstrating the prospect that graphene IPS might allow HTP weight, cost, and drag reductions, which are significant drivers for greener aeronautical structures. However, there are some risks that must be addressed, such as the interface of the graphene IPS with the on-board power and control network, robust electrical wiring and connections, reparability demonstration and long-term reliability, supply for high-rate production, and, last but not least, the demonstration of the solution's end-to-end Environmental, Health and Safety (EHS).

5.6 Conclusions

Thermoelectric ice protection systems (IPS) play a major role in next generation aeronautical products:

- Bleed-air-based IPS have a number of drawbacks, among which the incompatibility with polymer/composite structural components due to too high temperature of the air;
- Current thermoelectric IPS may suffer limitations to adapt to power density requirements or for integration into complex 3D-shaped components;
- For next-gen aircraft components like wings, rudder, rotor blades, air inlets, antennae, windshield, new easy to integrate and flexible ice protection technologies are urgently needed; flexible relates to the ability to adapt to the requirements in terms of geometry, generated power density and available on-board voltage supply;
- Environmental aspects (lower power consumption and emissions – CO_2/NO_x) are a key driver, too.

In this work, a graphene-based multilayer IPS with CFRP layers, insulating layer (GFRP), and graphene serpentine was designed and developed for industrialization and compatibility with aviation composite component manufacture.

This graphene solution's feasibility and proof of concept were demonstrated through major manufacturing experiments, as well several test as heating and homogeneity test and finally de-icing and anti-icing. It has been demonstrated that graphene serpentines may be used as an effective de-icing system by applying approximately 60V and achieving 4 kW/m^2 of heat flow. Additionally, its performance would be even better and could reach higher heat flux if more aircraft electrical capacities were used, since only 60V out of maximum 540V, which are expected in future more electrical aircrafts, were tested. Knowing that, due to its intrinsic properties of thermal and chemical stability, graphene would not be affected, then, it would be only necessary to protect the

insulating layers, which are applied in-between CFRP and graphene and on-top of graphene paper, as well as of the connections, which need to be improved. The test with the panel within the climatic chamber at high voltage, 60V, is the most indicative of the functionality sought, demonstrating that graphene serpentine can be utilized as an effective electrical heater to melt ice on the panel surface in less than one minute, 45 seconds. In terms of future industrialization, graphene heater design, integration inside the CFRP part, as well as electrodes and connections, must be further improved and refined to satisfy the criteria with greater efficiency and safety while consuming less power. Other critical issues, including as durability, system aging, and improved insulation layer selection to minimize weight, must be examined and studied in subsequent phases. Furthermore, for future TRLs, more representative anti-/de-icing testing capabilities and facilities, such as ice tunnel experiments, should be employed.

5.7 References

[1] X. Yao et al. “An advanced anti-icing/de-icing system utilizing highly aligned carbon nanotube webs” *Carbon*, vol. 136 (2018) pp. 130-138, doi:10.1016/j.carbon.2018.04.039

[2] O. Redondo et al. “Anti-icing and de-icing coatings based Joule's heating of graphene nanoplatelets” *Composites Science and Technology* vol. 164 (2018) pp. 65–73, doi:10.1016/j.compscitech.2018.05.031

[3] Karim et al. “Graphene-based surface heater for de-icing applications” *RSC Advances*, vol.8, (2018), 16815, doi:10.1039/c8ra02567c

[4] T. Blanco et al. “Graphene for Anti-icing” *Materiales Compuestos* vol. 12, 4, (2019) pp. 1-4

[5] L. Vertuccio et al. “Effective de-icing skin using graphene-based flexible heater” *Composites Part B* vol. 162 (2019) pp. 600–610, doi: 10.1016/j.compositesb.2019.01.045

[6] Chakraborty et al. “An integrated approach to vehicle and subsystem sizing and analysis for novel subsystem architectures” *Journal of Aerospace Engineering*. (2016), vol. 230, pp. 496-514. doi:10.1177/0954410015594399

[7] https://chemicals.cabro.it/

6. GRM for Out of Oven curing of composites

Advanced composite materials based on carbon fiber-reinforced polymers (CFRP) are now widely used in major aircraft structures, as well as high-performance sports goods, automotive, marine and wind energy constructions [1-3]. A remarkable example of the use of CFRP is the aircraft A350 XWB made by Airbus where the composite materials are more than half in percentage of the structural weight [1-4].

As the quantity, size, and complexity of these composite components increase, the demand for quicker, more cost-effective, and more flexible production collides with the constraints of existing processing methods. Traditionally, thermoset-based fiber reinforced polymers (FRP) have been manufactured utilizing autoclave methods which consolidate composite materials by controlled heat (typical 2-3 °C/min) and pressure (usually around 7 Bars) avoiding the formation of bubbles and obtaining high quality parts but, on the other side, they have many drawbacks such as significant acquisition and operation costs, massive energy consumption, limit on the size and design and low production rate [2-8].

With the recent development of out-of-autoclave prepregs it could be possible to realize as well high-performance composite materials with lower energy and costs combining the technology of vacuum bag with oven curing although some of the mentioned above limitations still remain [9]. In order to overcome these challenges, there has been an increasing interest in the development of out-of-autoclave (OoA) and out-of-oven (OoO) techniques.

A promising way to cure FRP can be seen in the realization of tailored molds incorporating electrothermal heaters that transform electric energy into heat through Joule effect, which potentially provides great energy saving and quicker manufacturing time without compromising the quality [2-4, 6].

In particular, the recent interest in nanomaterials, especially carbon based nano-fillers like graphene related materials (GRM) have enabled the development of many high performance multifunctional composites, demonstrating its potential as a Joule heating source to efficiently cure composite laminates [2,3, 5, 8]. They show other advantages over standard metal like copper used as resistive heater like i) high chemical and thermal stability, ii) flexibility and lightweight, iii) easy, scalable and environmentally friendly manufacturing process [9].

For example, Lee et all [5] reported an out-of-oven curing technique that cures a composite laminate via resistive heating of a carbon nanotube film and found that that the physical and

mechanical properties of OoO-cured laminates are equivalent to those of oven-cured laminates. Moreover, the OoO curing developed reduces energy consumption by over two orders of magnitude, thus providing great energy savings.

Liu et all [6] developed nanocomposite film based on graphene nanoplatelets (GNPs) and high density polyethylene that possesses self-regulating Joule heating capabilities, which can be used to cure epoxy based composites leading to great reduction of consumed energy and no detrimental effect on mechanical performance and glass transition temperature (Tg) of the final composite.

In this work, an OoO method is presented that employs a carbon fiber lay-up mold with a GRM-based heater embedded in the laminate surface, eliminating the need for a heating vessel or convective medium during curing. The physical and thermal characteristics of OoO-cured composites were then investigated and compared to those of oven-cured composites.

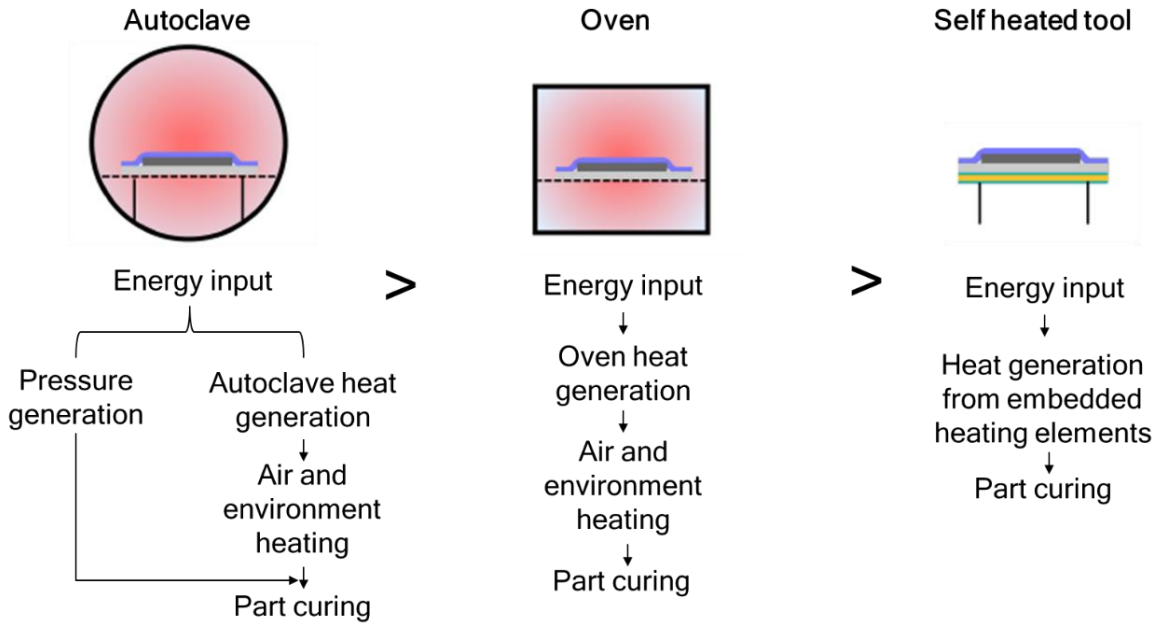

Figure 6.1: An illustration of the energy required to cure composite parts using various manufacturing techniques (autoclave, oven and self-heated tool) [6].

6.1 Manufacturing of GRM heating mold

The graphene paper (GS50 produced by Nanesa) was patterned by laser plotting in order to obtain the GRM heating element with a suitable electrical resistance (R=11,4 Ω) for our power supply instrumentation (TDK LAMBA GEN 40 V-38 A in direct current). Electrical connections with graphene paper were made using copper and silver paint.

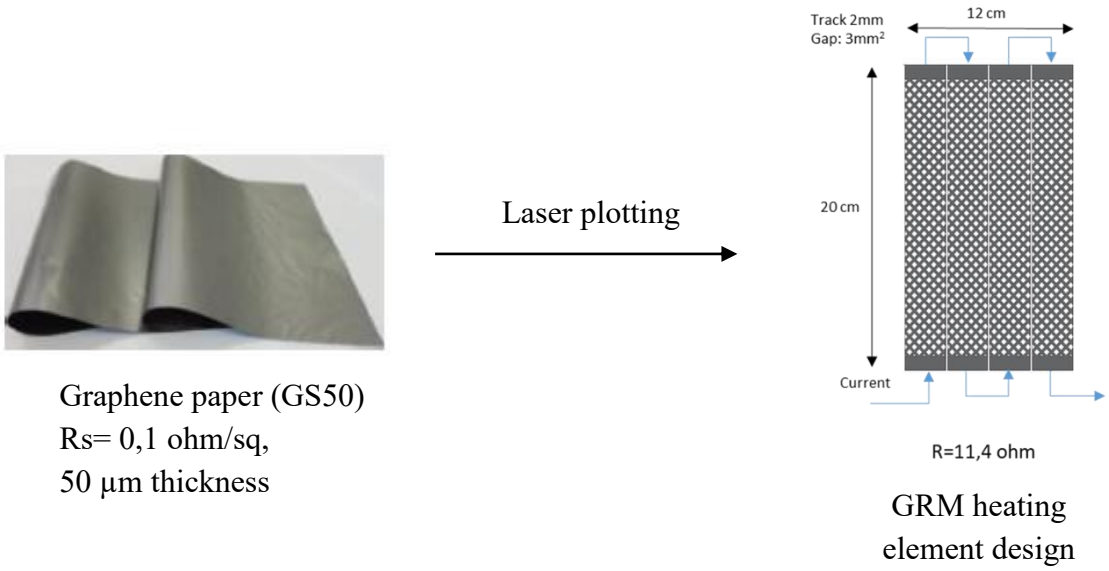

Figure 6.2: Production of the GRM heating element.

To minimize short circuits within the overall composite construction, the GRM heating element was placed between two insulating glass fiber (GF) prepreg layers (VV300S-DT190-38 supplied by Deltatech), while the lower half of the mold is made up of multiple layers of carbon fiber prepreg (GG200T-DT195N-42-MS supplied by Deltatech). The entire panel was then cured in a hot press at 135° for 90 minutes, according to the manufacturer's instructions. The stratification of the layers and the finished heating panel may be seen in figure 6.3.

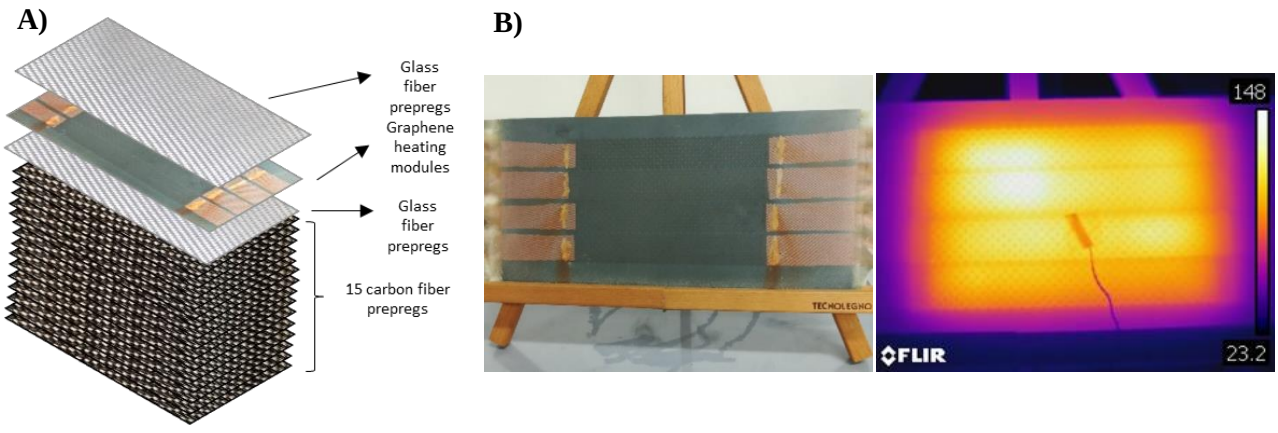

Figure 6.3: A) GRM heating mold scheme production, and its B) optical and thermal image.

6.2 Heating tests of GRM heating mold

Preliminary heating experiments at room temperature were performed to assess the temperature uniformity on the GRM heating mold surface when operated at various voltages. Figure 6.4 depicts the setup used for the test.

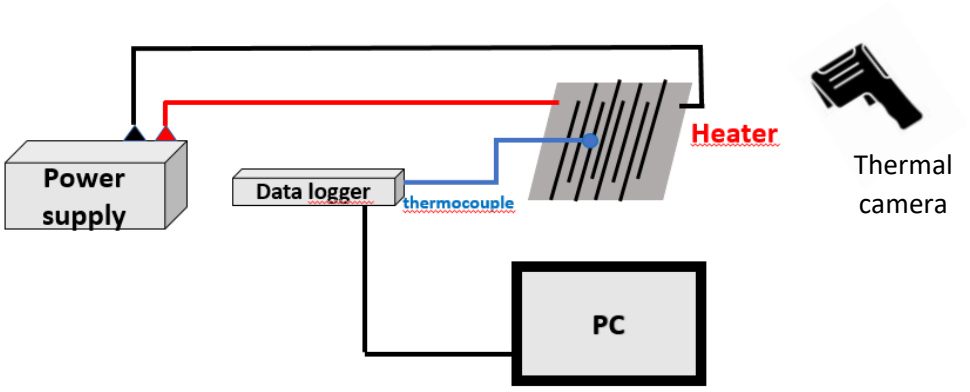

Figure 6.4: Measurement system for heating test of GRM heating mold.

The GRM heating mold (R= 11,4 Ω) was powered up with increasing voltage (11, 16, 22, and 27 V and 1, 1.4, 1.9 and 2,4 A respectively) while measuring the temperature recorded by the thermocouple put in the middle of the mold for each power. Thermal movies were also collected from during the experimentfrom the start till a stable temperature was achieved (plateau after the first ramp). The uniformity of the tempearature was quantified computing the standard deviation over the surface of the thermocouple temperature measured.

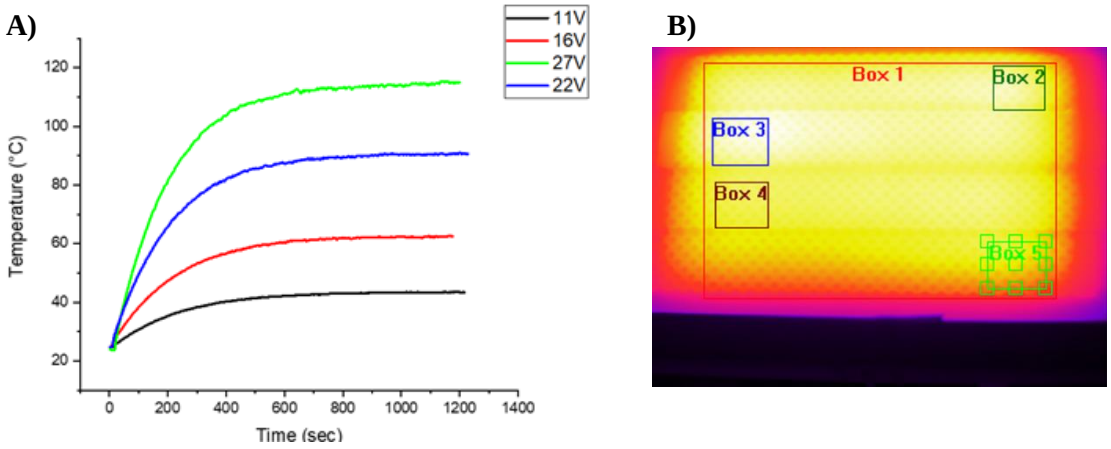

Figure 6.5: A) Temperature recorded by thermocouple at different voltages, B) example of thermal image used for the calculation of the std.

Results show that at the voltages utilized, the temperature on the surface of the GRM is relatively uniform, and increasing the power raises the T throughout the surface. The insulating material used for the vacuum bag required for curing might mitigate this issue by acting as a cage for the heat generated.

Voltage (V)	$T_{mean\ by\ thermocouple}$	Std IR camera
11	42	2
16	59	4
22	87	7
27	111	9

Table 6.2: Results of heating tests of GRM heating mold.

6.3 OoO setup for composite curing

GRM heating mold was connected to a temperature controlling device developed by CNR in order to perform the manufacturer's curing cycle (figure 6.6). The temperature controller unit operates on the basis of a temperature sensor (thermocouple) positioned on the uncured material's top surface. The power supply was set at 31,6 V during the procedure, and the temperature controller turns on/off the power supply as needed to reach and maintain the set temperature.

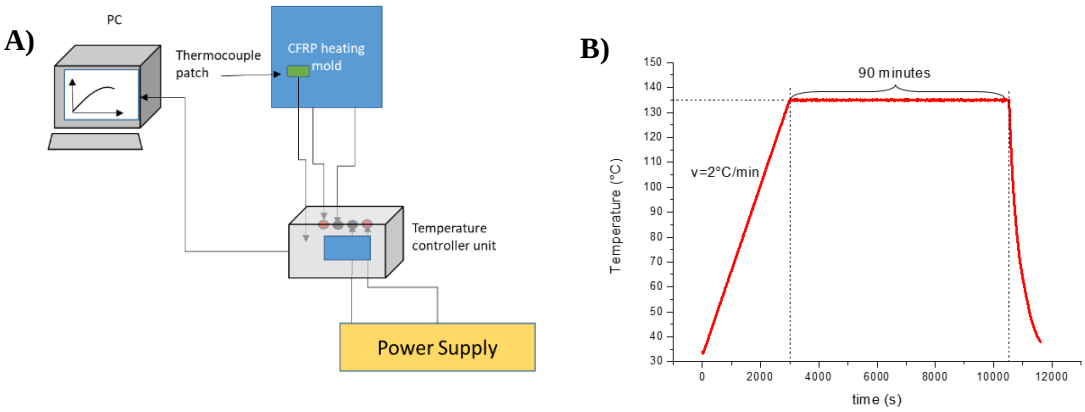

Figure 6.6: A) Temperature controller, B) curing cycle followed by the GRM mold.

GRM heating mold was used to cure 10 plies (sizes 7x15 cm) of carbon fiber prepreg (GG200T-DT195N-42-MS provided by Deltatech) using the "vacuum bag" technique, (figure 6.7). Vacuum bagging is a method of applying mechanical pressure to a laminate during its curing cycle. The pressurization of a composite laminate has numerous purposes. It begins by removing trapped air between layers. Second, it compacts the fiber layers to allow for efficient force transmission among fiber bundles and to prevent fiber orientation from shifting during cure. Third, it lowers humidity. Finally, and most importantly, the vacuum bagging procedure optimizes the composite part's fiber-to-resin ratio. For many years, these benefits have allowed the aerospace and racing sectors to exploit the physical qualities of sophisticated composite materials like carbon, aramid, and epoxy. Thanks to the controller unit and a pump, it was possible to complete a controlled curing process with a pressure of 1 Bar (vacuum), a ramp temperature rate of 2°C/min, and a temperature of 135°C for 90 minutes.

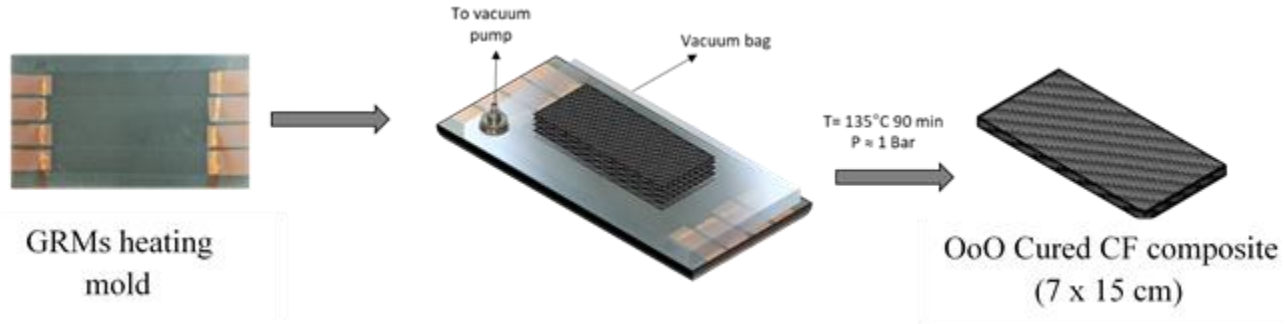

Figure 6.7: CF prepreg curing by GRM heating mold.

For comparison sake, we also cured similar samples using a classic oven. To this aim, the samples followed the same curing cycle of 135°C for 90 minutes using the vacuum bag in oven (model TCF 120, ArgoLab).

6.4 Characterization techniques for OoO and oven cured samples

To compare the mechanical and thermal properties of OoO-cured composites with those of oven-cured composites, degree of cure analysis, tensile and flexural testing and dynamic mechanical were performed.

6.4.1 Degree of curing analysis

In our case, after the curing using the oven and OoO methods, differential scanning calorimetry (DSC) was conducted using a DSC 8000 (Perkin Elmer) to evaluate the degree of cure of the laminate. The DSC run was carried out by scanning the heat flow from 30°C to 300°C at a ramp rate of 5°C/min. The degree of cure was calculated by comparing the area of the exothermic peak detected in the DSC curve of the heat-processed laminate to that of an uncured laminate. Two samples of each kind (OoO, oven, and uncured) were sliced and examined using the DSC technique.

6.4.2 Tensile and flexural test

Mechanical and physical testing of polymers and their composites is essential for determining material attributes for use in product design and analysis, quality control, application performance requirements, and the manufacturing process. Mechanical and physical testing guarantee that the material meets the performance requirements of industrial specifications, particularly in the aerospace and automotive. Mechanical testing of polymer composites entails determining mechanical characteristics such as strength and stiffness in order to evaluate their use in the design of a composite's structure. Tensile and flexural testing are the most frequent standardized mechanical tests for fiber reinforced polymer composites [10].

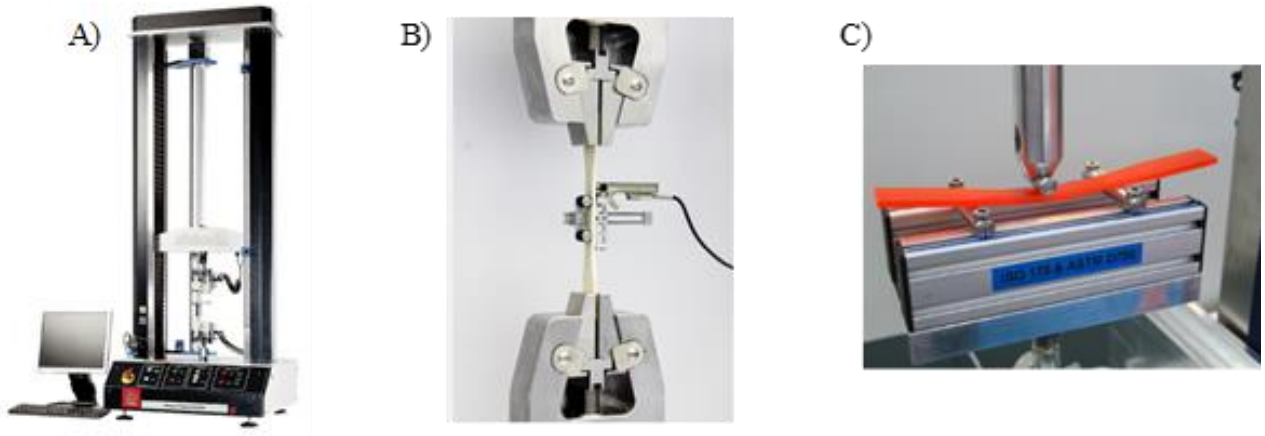

Figure 6.8: A) Universal testing machine used, B) tensile and C) flexural test.

Five samples (sizes 100 x 10 x 2 mm) of each type were cut and tested by a universal machine tensor check profile (Gibitre) equipped with a load cell of 2000 N to analyze the mechanical characteristics (tensile and flexural) of OoO and oven cured composites. The generated graphs were used to extrapolate tensile and flexural modulus and flexural strength.

6.4.3 Dynamic mechanical analysis (DMA)

The Dynamic Mechanical Analyzer employed for the composite laminate characterization was DMA model 242E Artemis (Netzsch, Germany) available at the University of Bologna. All DMA testing were performed with a 40 mm three-point bending fixture. Four 50x10x2 mm specimens from each oven-cured and OoO-cured laminate were tested in the temperature range of 40 °C to 300 °C at a heating rate of 2 °C/min and frequency of 1 Hz. The DMA test yielded the storage modulus, tanδ and the glass transition temperature was calculated from the peaks of the tan curves.

6.5 Results and discussion

Thermophysical and mechanical testing results are discussed for both curing methods (OoO and Oven).

6.5.1 Thermophysical analysis

DSC was utilized to evaluate the thermophysical properties of the OoO to oven curing vs the uncured starting material. As showed in figure 6.9, no exothermic peak could be identified in any scenario for both OoO (red line) and oven (blue line) cured samples, indicating that both composite materials were completely cured. Glassy transition temperature could not be precisely identified due to the high degree of curing achieved by composites samples, thus a DMA investigation was also performed.

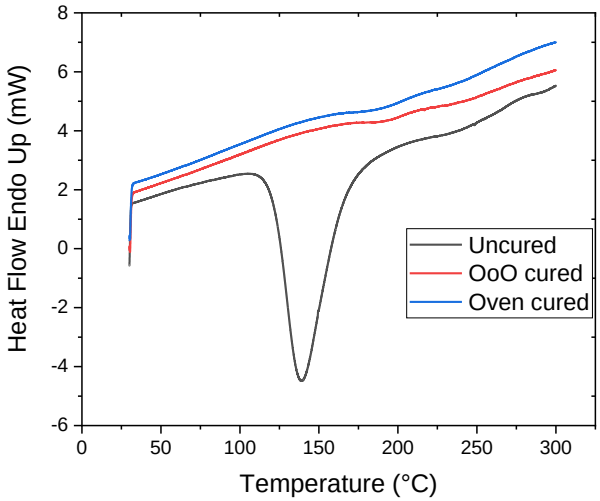

Figure 6.9: DSC curves of uncured, OoO and oven cured samples.

The storage modulus and tanδ data from DMA curves all point to oven and OoO-cured specimens having the identical dynamic mechanical responses. The representative storage modulus and tanδ curves from DMA measurements on the specimens at 1 Hz are shown in figure 6.10.

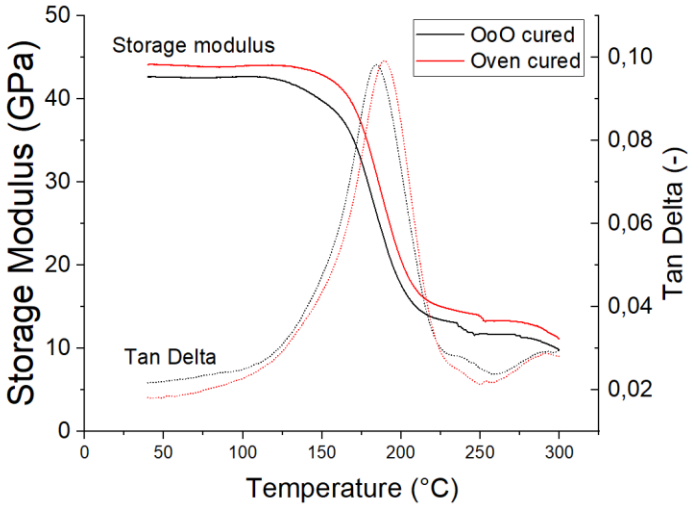

E' (Gpa) (OoO)	43,9 ± 2,8
E' (Gpa) (Oven)	42,3 ± 3,0
Tanδ (°C) (OoO)	184,3 ± 0,3
Tanδ (°C) (Oven)	188,9 ± 0,3

Figure 6.10 and Table 6.3: DMA curves and torage modulus and Tan δ peaks of OoO and oven cured samples.

Tan delta peak and the storage modulus at 1 Hz frequency are summarized in table 6.3. The oven-cured and the OoO-cured specimens exhibit almost the same Tg from the tan delta curves. Therefore, the DMA tests indicate that the oven and OoO curing provide the comparable dynamic properties of the polymer.

6.5.2 Mechanical analysis

The mechanical characteristics of composites manufactured using various methods are described and compared. The tensile modulus of these composites is shown in figure 6.11A, whereas the flexural modulus and strength are shown in figure 6.11B.

The average tensile modulus of these composites is determined to be 65,4-67,8 GPa, while the average flexural modulus is 47,5-48.9 GPa and the flexural strength is 800-850 MPa for OoO and oven samples, respectively. This means that the mechanical characteristics of OoO-processed composites are equivalent to those of oven-cured composites.

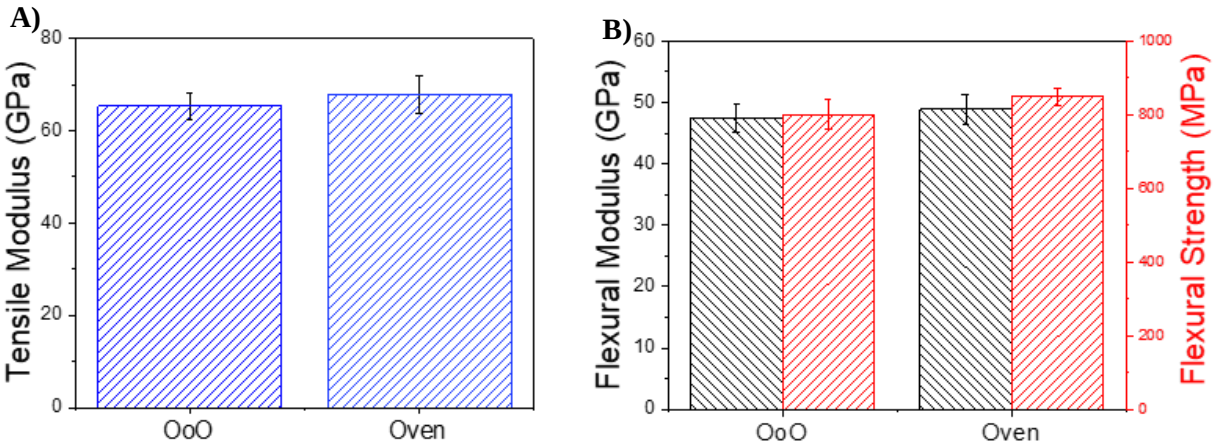

Figure 6.11: A) tensile and B) flexural properties comparison of OoO and oven curing specimens.

6.6 Conclusions

In summary, we compared the features of an out-of-oven curing method for a carbon fiber advanced composite prepreg system employing a GRM element as a heating element incorporated in a CFRP mold to that of a standard oven composite curing process. The thermophysical and mechanical characteristics of the treated out-of-autoclave composites were also examined. In the degree of cure analysis, dynamic mechanical analysis, and tensile and flexural tests, the results show that there is no significant difference between out-of-oven curing and oven curing; thus, out-of-oven curing can achieve the equivalent thermal and mechanical properties of out-of-oven composites as the conventional curing method.

Further work will be directed at using these new GRM heating element also in flexible structures, incorporating them in PDMS (stable until 250°C) layers which can be put directly into the vacuum bag stratification as a heating tool, delivering the following benefits: (1) Removal of size and form

constraints on composite components by the use of a scalable conductive heating element, (2) increased accessibility to composite manufacturing facilities, and (3) manufacturing cost reductions through efficient thermal processing.

6.7 References

[1] Valorosi et al, Composites Science and Technology 185 (2020) 107848

[2] Xia et al, Composites Science and Technology 164 (2018) 304–312

[3] Xu et al, Composites Science and Technology 149 (2017) 20-27

[4] Jayasree et al, Sci Eng Compos Mater (2020) 27:325–334

[5] Lee et al, Composites Science and Technology 166 (2018) 150-159

[6] Liu et al, Composites Science and Technology 190 (2020) 108032

[7] Nguyen et al, Advanced Engineering Materials, 18 (2016) 11:1906-1912

[8] Prolongo et al, Journal of Polymer Research, (2016) 23:189

[9] Scidà et al. "Application of graphene-based flexible antennas in consumer electronic devices", (2018) Materials Today Volume 21, Number 3

[10] Saba et al, Woodhead Publishing Series in Composites Science and Engineering (2019), 1-12

Conclusions and perspectives

The utilization and advantages of GRM in composites for a number of applications have been examined in this PhD thesis. In summary, these are the outcomes of the research topic:

- Benchmarking of commercial GRM-based master batches produced by industrial companies revealed a general trend regarding the addition of GRM in the neat polymer: increasing the degree of crystallinity and crystallization temperature while greatly improving thermal stability, particularly in one case (PC+5% GRM). Depending on the quality and dispersion efficiency of GRM inside the polymer matrix, a conductive network within the insulating matrix for anti-static or electric conductive applications is also feasible;
- GRM-coatings for water uptake reduction: results show that with GRM-coating is possible to reduce greatly the diffusion coefficient providing a delay in the water uptake, and thus the loss of T_g is shifted to longer conditioning times, especially with the coating G2Nan/RTM6. In this case, the coefficient of diffusion is reduced by 62% compared to the reference samples (uncoated);
- GRM as thermo-electrical anti-icing /de-icing system: it was designed and produced a graphene-based multilayer IPS with CFRP layers, an insulating layer (GFRP), and graphene serpentine. It has been proved that graphene serpentines may be utilized as an effective anti/de-icing system by applying 60V and creating a heat flow of 4 kW/m2. The test with the panel within the climatic chamber at high voltage, 60V, is the most representative of the desired functionality, indicating that graphene serpentine can be used as an effective electrical heater to melt ice on the panel surface in less than one minute, 45 seconds;
- GRM for Out of Oven curing of composites: we compared the characteristics of an out-of-oven curing technique for a carbon fiber advanced composite prepreg system that uses a GRM element as a heating element inserted in a CFRP mold to those of a typical oven composite curing procedure. The results demonstrate that there is no significant difference in the characteristics of cured between out-of-oven curing and oven curing; consequently, out-of-oven curing may achieve the comparable thermal and mechanical properties of out-of-oven composites as the traditional curing technique.

Acknowledgements

A conclusione di questo lavoro di tesi, vorrei fare miei più sentiti ringraziamenti alle persone che ho avuto modo di conoscere in questo importante periodo della mia vita e che mi hanno aiutato a crescere sia dal punto di vista professionale ma soprattutto umano.

Ringrazio il Prof. Loris Giorgini per la sua disponibilità e per avermi accompagnato durante il percorso di dottorato. Ripensando a quando l'ho conosciuta durante la mia laurea magistrale e anche durante il master, riconosco con piacere che mi ha trasmesso l'interesse e la passione per il mondo dei polimeri e dei compositi in particolare che hanno guidato questo lavoro.

Ringrazio tutta la mia famiglia che mi ha sempre sostenuto e incoraggiato nelle scelte che ho preso, consigliandomi e spronandomi nei momenti difficili.

Ringrazio il mio gruppo a ISOF e ringrazio Enzo per l'opportunità che mi ha dato. Vorrei ringraziare Emanuele, che mi ha insegnato molto in questi anni di lavoro spingendomi oltre limiti che difficilmente avrei superato. Ringrazio anche Alessandra, Andrea C., Andrea L., Roberta, Ilaria, Derek, Massimo, Giorgio e Silvano.

Ringrazio tutti i "*colleghi*" che ho conosciuto in questo periodo: Marco, Cecilia, Claudio, Giada, Alex, Alessandro K., Maria, Vitaliy, Vasia, Agata, Sara K., Alessandro P. e Matteo. Non basteranno queste poche righe per raccontare tutto quello che avrei da dire: semplicemente voglio ringraziarvi dal profondo per tutte le avventure passate insieme, dai momenti felici a quelli tristi che abbiamo trascorso, dentro e soprattutto fuori al CNR.

Ringrazio i miei amici di sempre e non più solo del "*mare*": Fax e Adri, Timo e Chiara, Jag e Ceci, Paolo, Ambro, Luca, Potter, Ale, Davide, Vale e Costy. Vi ringrazio per la vostra presenza e il vostro aiuto, ciascuno a proprio modo, che mi avete dato in questi anni.

Vorrei ringraziare Rachele, un'amica veramente "speciale" che mi ha accompagnato in questo ultimo periodo, così breve ma allo stesso tempo così intenso: grazie davvero per le lunghe chiacchierate e il supporto datomi in un momento veramente difficile per me, ho avuto modo di crescere davvero parecchio!

Infine dedico questa tesi a me stesso, ai miei sacrifici, alla mia tenacia e soprattutto alla mia pazienza che mi hanno permesso di arrivare fin qui.